UDK 66:54(05) CODEN HMIDA 8 ISSN 0367–598X

3

Hemijska industrija

Vol. 79

Časopis Saveza hemijskih inženjera Srbije

Chemical Industry

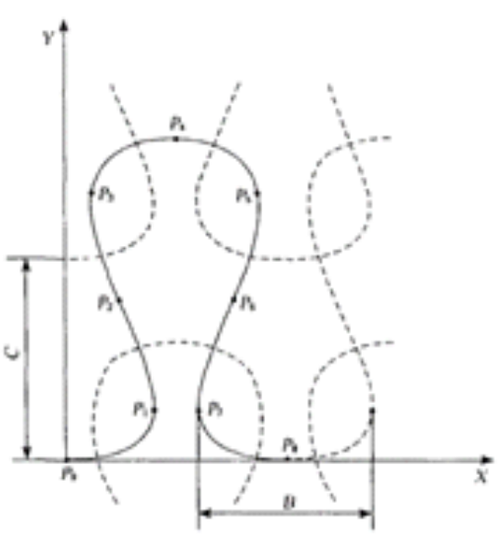

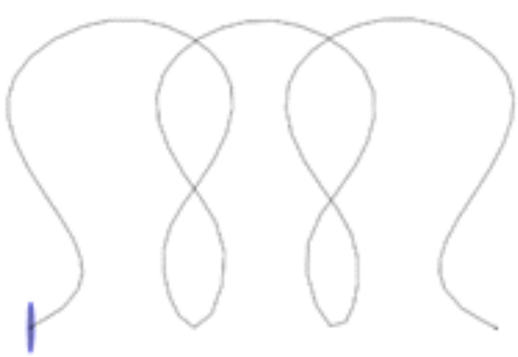

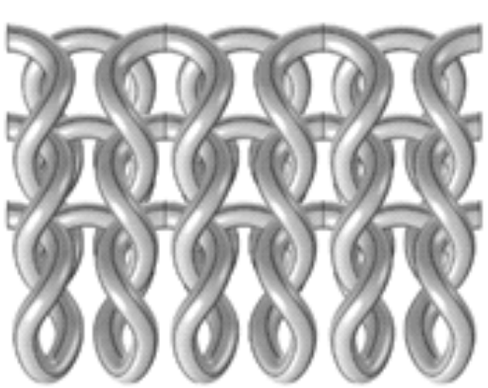

BEOGRAD, JUL-SEPTEMBAR 2025. HMIDA 8, 79(3) 127-189 (2025)

Aktivnosti Saveza hemijskih inženjera Srbije pomažu:

**MINISTARSTVO NAUKE,
TEHNOLOŠKOG RAZVOJA
I INOVACIJA
REPUBLIKE SRBIJE**

Tehnološko-metalurški fakultet
Univerziteta u Beogradu

Prirodno-matematički fakultet
Univerziteta u Novom Sadu

Institut za tehnologiju nuklearnih i
drugih mineralnih sirovina, Beograd

Tehnološki fakultet
Univerziteta u Novom Sadu

Institut za hemiju, tehnologiju i metalurgiju
Univerziteta u Beogradu

Fakultet tehničkih nauka
Univerziteta u Novom Sadu

Tehnološki fakultet
Univerziteta u Nišu, Leskovac

Fakultet tehničkih nauka
Univerziteta u Prištini
Kosovska Mitrovica

Institut IMS, Beograd

DCP HEMIGAL
Leskovac

Barič

Elixir Prahovo

Chemical Industry
Химическая промышленность

Hemijska industrija

Časopis Saveza hemijskih inženjera Srbije
Journal of the Association of Chemical Engineers of Serbia
Журнал Союза химических инженеров Сербии

VOL. 79 **Beograd, juli – septembar 2025.** **Broj 3**

Izdavač
Savez hemijskih inženjera Srbije
Beograd, Kneza Miloša 9/I

Redakcija
11000 Beograd, Kneza Miloša 9/I
Tel/fax: 011/3240-018
E-pošta: shi@ache.org.rs
www.ache.org.rs

Izlazi kvartalno, rukopisi se ne vraćaju

Za izdavača: Ivana T. Drvenica

Sekretar redakcije: Slavica Desnica

Izdavanje časopisa pomaže
Republika Srbija, Ministarstvo nauke, tehnološkog razvoja i inovacija

Uplata pretplate i oglasnog prostora vrši se na tekući račun Saveza hemijskih inženjera Srbije, Beograd, broj 205-2172-71, Komercijalna banka a.d., Beograd

Menadžer časopisa i kompjuterska priprema
Aleksandar Dekanski

Štampa
Razvojno-istraživački centar grafičkog inženjerstva, Tehnološko-metalurški fakultet, Univerzitet u Beogradu, Karnegijeva 4, 11000 Beograd

Indeksiranje

Radovi koji se publikuju u časopisu *Hemijska Industrija* ideksiraju se preko *Clarivate* servisa *Science Citation Index - Expanded™* i *Journal Citation Reports™ (JCR)*, kao i *Scopus* servisa *CiteScore™*

SADRŽAJ/CONTENTS

Valorization of soybean meal to produce high-protein animal feed and value-added products using a new strain of *Aureobasidium pullulans*

Slađana Z. Davidović[1], Miona G. Miljković[1], Nevena Ilić[2], Milica Veljković[2] and Suzana Dimitrijević-Branković[1]

[1]*University of Belgrade, Faculty of Technology and Metallurgy, Belgrade, Serbia*
[2]*Innovation Centre of the Faculty of Technology and Metallurgy, Belgrade, Serbia*

Abstract

Soybean meal (SBM) is a by-product of soybean oil production. It is a high-quality protein supplement for animal feed. However, it is rich in anti-nutritive factors and indigestible components, among which the special attention is focused on galacto-oligosaccharides, due to the lack of α-galactosidase in monogastric animals. The main goal of this study was to apply fermentation using a selected strain of black yeast-like fungus of the SBM to obtain a high-protein, low-oligosaccharide soy-based product. Screening for an appropriate strain of *Aureobasidium* spp. among natural isolates from grapes has been performed. The highest α-galactosidase activity of 0.89 U cm^{-3} was produced by the strain identified as *A. pullulans* P8. It was applied in SBM submerged (SmF) and solid-state fermentations (SSF). Maximal crude protein yield (~61 % based on dry weight) and the lowest galacto-oligosaccharides content were obtained after 3 days of SmF at 30 °C and 10 % of dry matter. SSF produced ~58 % crude protein after 7 days of incubation at 30 °C with substrate containing 30 % of dry matter. Extracellular enzymatic activities of cellulase, pectinase, amylase, xylanase, and α-galactosidase were detected in the supernatant after SmF, indicating its potential for hydrolysis of various lignocellulosic biomass substrates.

Keywords: Black yeast-like fungus; solid-state fermentation; submerged fermentation; α-galactosidase; extracellular hydrolytic enzymes; grape

Available on-line at the Journal web address: http://www.ache.org.rs/HI/

ORIGINAL SCIENTIFIC PAPER

UDC: 636.087:582.736.308:663.15

Hem. Ind. **79(3)** 127-139 (2025)

1. INTRODUCTION

Soybean (*Glycine max* (L.) Merril) is an important oilseed crop with a global production of 389 million metric tons estimated in 2026 [1]. Soybean meal (SBM) is a co-product of soybean oil production. It is rich in high-quality proteins thus representing a cost-effective and vastly available food source for livestock, poultry, and fish [2-4]. SBM is also rich in carbohydrates, which comprise about 35 to 40 % of its dry matter [5]. Nonstructural soybean carbohydrates are represented by low molecular weight sugars (among which the most abundant is sucrose), oligosaccharides, and starch. Structural polysaccharides include cellulose, pectin, and hemicellulose, together with mannans, galactans, and xyloglucans.

Although highly wholesome, consumption of soybeans is limited by various anti-nutritional factors, including nondigestible oligosaccharides and polysaccharides. The most prevalent oligosaccharide in soybean is stachyose, followed by raffinose, while only a trace amount of verbascose is found [3]. These are galacto-oligosaccharides (also referred to as raffinose family oligosaccharides (RFOs)) sharing the common feature represented by 1, 2 or 3 galactose residues in raffinose, stachyose and verbascose, respectively, linked to a sucrose unit. Terminal galactose moiety is linked by an α-1-6 glycosidic bond that is cleaved by the enzyme α-galactosidase [6]. Due to the lack of α-galactosidase these oligosaccharides are indigestible for monogastric animals. Although they are degraded by intestinal microbiota, flatulence and diarrhea occur. Young animals are especially susceptible to anti-nutritional factors, as their digestive system is not fully developed [7,8]. The effective removal of indigestible RFOs is achieved by adding exogenous α-galactosidase into animal feed [6]. This treatment showed enhanced nutrient digestibility, improved average daily gain, and reduced diarrhea rate in weaned piglets [9].

Corresponding authors: Slađana Z. Davidović, University of Belgrade, Faculty of Technology and Metallurgy, Belgrade, Serbia
E-mail: sdavidovic@tmf.bg.ac.rs
Paper received: 15. March 2024; Paper accepted: 28 May 2025; Paper published: 5 August 2025.
https://doi.org/10.2298/HEMIND240315009D

The other approach to improve the nutritional quality of food and food ingredients is fermentation, which could be applied as the only treatment, or together with enzymatic hydrolysis [10-13]. Importantly, fermentation eliminates not only RFOs but also other anti-nutrition factors presented in soybeans [14]. Fermented SBM has lower contents of oligosaccharides and higher crude protein (CP) than the unfermented SBM, so that it has been shown as highly nutritious for weanling pigs [15]. However, not all microorganisms can use complex soybean carbohydrates, thus additional treatments are required before soybean can be used as fermentation feedstock [16]. To overcome this issue different microorganisms were applied to obtain double-fermented SBM [4]. Adding double-fermented SBM in broiler food resulted in better feed efficiency, nutrient digestibility, and ultimately higher quality of breast meat. Additional health-promoting effects could be obtained by choosing probiotic microorganisms for fermentation [8]. Nevertheless, fermentation could also exert negative effects, depending on the microorganism used [17]. Therefore, exploring for new adequate strains is of crucial importance.

Yeast-like black fungi are ubiquitous polymorphic microorganisms primarily recognized as pullulan producers [18-20]. Other biotechnological applications include also single cell protein, melanin source, siderophores, biosurfactants, and different industrially important enzymes [21-23]. We hypothesized that microorganisms with such versatile properties could be suitable candidates for fermented SBM production. To test this hypothesis, we have performed screening for an appropriate strain of yeast-like black fungi among natural isolates from grapes. The highest α-galactosidase producer was applied in solid-state (SSF) and submerged fermentation (SmF) of SBM with the final aim of obtaining a high-protein, low-oligosaccharide product. Moreover, the extracellular hydrolytic enzyme potential of the new isolate *Aureobasidium pullulans* P8 has been explored.

2. EXPERIMENTAL

2. 1. Materials

The working microorganism was isolated from grapes. The grapes of the autochthonous varieties were picked at the moment of full ripeness from the organically certified vineyards of the sample estate "Sremski Karlovci", Faculty of Agriculture in Novi Sad, Serbia. SBM was kindly obtained from Bankom doo., Belgrade, Serbia. Microbiological media (malt extract broth, yeast extract, casein hydrolysate, and agar) were purchased from Torlak, Serbia. Raffinose was purchased from Fluka (Germany), carboxymethyl cellulose (CMC), pectin, and xylan were purchased from Sigma-Aldrich (USA), and soluble starch and microcrystalline cellulose (Avicel) were purchased from Merck (Germany). All other chemicals were of analytical grade and purchased from Merck (Germany) and Lach-Ner (Czech Republic).

2. 2. Isolation and characterization of yeast-like black fungi from grapes

Three different organic grapes (*Vitis vinifera* L.) were used for isolation of black yeast-like fungi, two white varieties (Panonija and Morava) and one black (Dionis). A few grapes of each variety were separately soaked in a sterile physiological solution and vigorously vortexed for 5 min. Serial dilutions were made and plated on sterile malt extract agar (MEA) plates. Seeded plates were incubated at 30 °C for 3 days. Afterward, a few colonies were picked from each group, inoculated in malt extract broth (MEB), and incubated at 30 °C at 130 rpm for two days. To ensure that strains are purified they were re-streaked on MEA plates.

2. 2. 1. Quantitative determination of α-galactosidase activity

Erlenmeyer flasks (100 cm^3) containing 30 cm^3 of malt extract broth supplemented with 20 g dm^{-3} raffinose were inoculated with 1.5 cm^3 of black yeast-like fungi isolates fresh cultures and incubated in an orbital shaker (Ikka, Germany) at 30 °C and 130 rpm. After two days, the fermentation medium was centrifuged at 6000 *g* for 15 min and α-galactosidase activity was determined in the supernatant by using raffinose as substrate according to the procedure described by Carević *et al.* [24]. Concentration of released galactose was determined by the 3,5-dinitro-salicylic acid (DNS) method [25]. Absorbance was read using a UV/visible spectrophotometer (Ultrospec 3300 pro, Amersham Bioscience, Sweden). One unit (U) of α-galactosidase activity was defined as the amount of enzyme that

released 1 μmol of galactose equivalents per minute. The isolate with maximal determined α-galactosidase activity was selected for further experiments.

2. 2. 2. Identification of the selected strain

DNA extraction was carried out from a 4-day-old yeast culture grown in a liquid ISP1 (5.0 g L^{-1} of casen hydrolysate, 3.0 g L^{-1} of yeast extract) medium. Detailed procedure of DNA extraction and molecular identification of yeast by PCR method using ITS1/ITS4 primer pair (ITS1: 5'-TCC GTA GGTGAA CCT GCG G-3', ITS4: 5'-TCC TCC GCT TAT TGA TAT GC-3'), is described in our previous study [26]. Macrogen double-sequenced amplified PCR products, quality verified and aligned them. The obtained sequences, which represented a partial sequence of the ITS region were deposited in the NCBI GenBank database.

2. 2. 3. Examination of the enzymatic potential of the selected yeast-like black fungi strain

To explore the enzymatic potential of the selected strain, a qualitative test on a selective agar medium was performed as described earlier [26]. The activity of α-galactosidase was detected on MEA with added raffinose by the same procedure.

2. 2. 4. Determination of optimal growth conditions for the selected strain

To determine the optimal temperature for growth, the selected strain of yeast-like black fungus was incubated in MEB at different temperatures in the range of 4 to 37 °C for 48 h. To determine the optimal acidity for growth, the selected strain of yeast-like black fungus was incubated in MEB, whose pH value was previously adjusted in the range from 3 to 10. The number of viable cells was determined for each tested condition on MEA plates after incubation for 48 h at 30 °C

2. 3. Solid-state fermentation of soybean meal

The SBM was weighed in 300 cm^3 Erlenmeyer flasks and wetted with distilled water or ammonium sulfate solution (2.4 mg g^{-1} of SBM dry matter) to obtain a final moisture content of 70 %. After autoclaving (121 °C, 30 min) and cooling, the flasks were inoculated with a selected strain of yeast-like black fungus fresh culture (approximately 10 % of inoculum). Incubation was carried out at 30 °C for 1 to 7 days. For each sampling day, three Erlenmeyer flasks were prepared and analysed. Additional three Erlenmeyer flasks were prepared for control, which underwent all the steps as samples except for inoculation. For the biomass analysis, 1 g of the sample was aseptically transferred to 9 cm^3 saline and vigorously vortexed for 5 min. Afterward, serial dilutions were made and plated on sterile MEA plates. Colonies were counted after 3 days of incubation at 30 °C. The rest of the fermentation medium was analysed for carbohydrate and protein contents. The same procedure was performed with the control samples.

2. 4. Submerged fermentation of soybean meal

For SmF 10 % SBM in water was prepared in Erlenmeyer flasks of 300 cm^3, autoclaved (121 °C, 20 min), and after cooling seeded with a selected strain of yeast-like black fungus fresh culture and incubated at 30 °C and 130 rpm for 3 days. For each sampling day, three Erlenmeyer flasks were prepared and analysed. An additional three Erlenmeyer flasks were prepared for control, which underwent all the steps as samples except for inoculation. For the biomass analysis, an aliquot of 1 cm^3 was aseptically transferred to 9 cm^3 saline and the rest of the fermentation medium was centrifuged for 15 min at 6000*g*. Pellets were subjected to protein and carbohydrate analyses and supernatants were analysed for hydrolytic enzyme activities.

2. 5. Protein analysis

Fermented soybean samples (and unfermented controls) were dried at 45 °C overnight and CP content was determined by the Kjeldahl method [27].

2. 6. Carbohydrate analysis

To analyse the carbohydrate content the dried SBM samples (fermented and unfermented controls) were extracted with 50 cm^3 of 40 % ethanol per gram of dry mass at 40 °C and 120 rpm for 2 h. The procedure was repeated three times and collected extracts were combined and then evaporated using a rotary evaporator (Büchi, Switzerland). The evaporated residue (from 3 g of dry product) was dissolved in 10 cm^3 of HPLC-grade water, and the resulting solution was analysed by using high-performance liquid chromatography (HPLC). Analyses were performed using a Dionex Ultimate 3000 HPLC device (Thermo Scientific, USA) with a Hi-Plex Ca^{2+} column (Agilent, USA) for carbohydrates (300 × 7.7 mm, 8 µm) at 80 °C. HPLC-grade water at a flow rate of 0.6 cm^3 min^{-1} was used as the mobile phase. Product detection was performed using an RI detector RefractoMax 520 (ERC, Germany) set at 40 °C. Data collection and further processing were performed using Chromeleon 7.2. software [28].

2. 7. Determination of hydrolytic enzyme activities

The supernatant obtained after SmF was used as a source of extracellular hydrolytic enzymes, *i.e.* α-galactosidase, amylase, xylanase, pectinase, and cellulase. The enzymatic activities were determined as previously described [24,26].

2. 8. Statistical analysis

All results are presented as mean values of three replicates ± standard deviation. Statistical analysis was performed by Origin Lab software (OriginPro 9.0) [29]. The significance of difference of experimental data was analysed by analysis of variance (ANOVA), followed by Tukey's test, and a confidence level of 95 % was chosen.

3. RESULTS AND DISCUSSION

3. 1. Isolation of yeast-like black fungi from grapes and screening for a high α-galactosidase producer

In this study over 30 microorganisms, natural inhabitants of grapes, have been isolated and preliminary characterrized. The isolates were designated as P, M or D, followed by a number, based on the grape variety from which the strain was isolated, *i.e.* Panonija, Morava and Dionis. After first screening based on the morphology of their cells on MEA and microscopic observation (Fig. 1), ten isolates with an appearance typical for *Aureobasidium* spp. [30], were selected for further work.

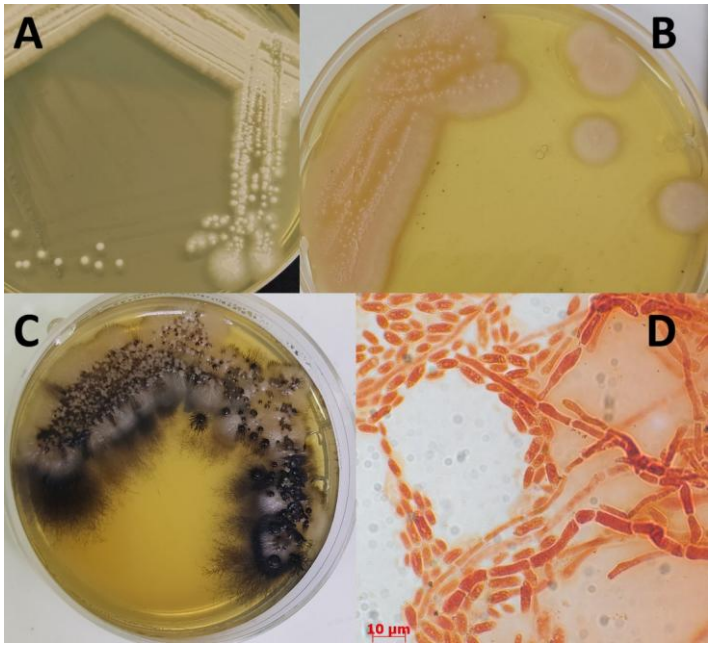

Figure 1. Appearance of black yeast isolates on an MEA plate incubated at 25 °C: strain M12 (A), strain P8 (B), and strain D3 (C), and optical micrograph of P8 cells (D)

The macroscopic morphology of isolates was characterized by pale yellow to pinkish colonies with smooth surfaces and aerial mycelium (Fig. 1a). Individual colonies increased in size over time reaching 5 to 20 mm diameter (Fig. 1b). Over time the colony surface became slimy and turned black due to melanin synthesis (Fig. 1c). Microscopic observation of the cultures from MEA plates revealed typical spherical yeast-like cells as well as conidiogenous cells and blastoconidia (Fig. 1d). These properties indicated that isolated strains belonged to black yeast-like fungi, and they were screened for α-galactosidase activity.

The α-galactosidase activity was detected in all tested strains and was in the range of 0.13 to 0.89 U cm^{-3}, significantly (p <0.05) differing among isolates (data not shown). However, the isolate P8 was selected as the most potent producer for further work.

3. 2. Identification and characterization of the new yeast-like black fungus strain

Based on morphological properties, the strain P8 was classified under the phylum Ascomycota. It was anticipated that the new isolate belongs to the genus *Aureobasidium*. Through the examination of a sequence that contained the internal transcribed spacer region (ITS), the novel strain P8 was specifically identified as *Aureobasidium pullulans* P8. The obtained sequence has been deposited in the NCBI-GenBank database and assigned the following accession number: OR921445.

Utilization of complex polysaccharides prevailing in soybeans is possible only for microorganisms capable of producing enzymes for their degradation. Therefore, the new isolate was cultivated with different polysaccharides as a sole carbon source under qualitative test for enzymatic potential examination. Besides already determined α-galactosidase activity, extracellular activities of amylase, pectinase, cellulase (degradation of CMC and avicel), and xylanase were detected (Fig. 2). Namely, halo zones appeared on selective agar plates around growth regions indicating the area of the substrate hydrolysis [26]. This result was expected since *Aureobasidium* spp. are well recognized for producing versatile enzymes [21]. However, not all strains produced cellulase [31,32], while the others lacked xylanase [33], suggesting that the ability for the desired enzyme synthesis is strain-specific.

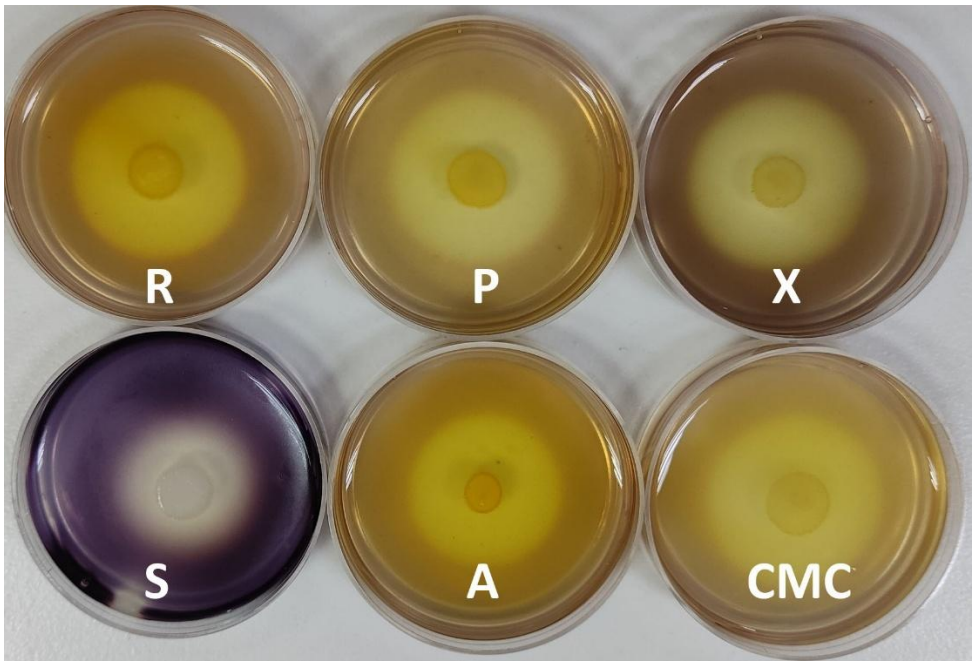

Fig. 2. Qualitative detection of extracellular enzymatic activities (α-galactosidase, pectinase, xylanase, amylase, exoglucanase, and endoglucanase, respectively) of novel strain A. pullulans P8 on selective agar medium plates containing: raffinose (R), pectin (P), xylan (X), starch (S), avicel (A) and carboxymethyl cellulose (CMC), respectively

Testing the growth possibility under different conditions (temperatures in the range of 4 to 37 °C and pH values ranging from 3 to 10) showed that *A. pullulans* P8 can grow under all examined conditions (Fig. 3). However, the

temperature optimum was found to be in the range of 25 to 30 °C. Temperatures lower than the optimal supported growth more than those higher than the optimal ones. These results are in accordance with the literature data reporting mesophilic nature of *Aureobasidium* spp. [23,34]. Considering the medium acidity, neither one of pH values could be chosen as optimal as high growth was observed at all tested pH values. *Aureobasidium* spp. are ubiquitous organisms resistant to various stress conditions [23]. It has been reported that different cell forms are prevalent at specific pH values, enabling its survival. However, growth inhibition was observed for *A. pullulans* Cau 19 at pH 9.5 [32]. From the aspect of technological application, the ability of *A. pullulans* P8 to grow at a wide range of pH values is a very favorable feature, enabling its application for fermentation utilizing versatile substrates.

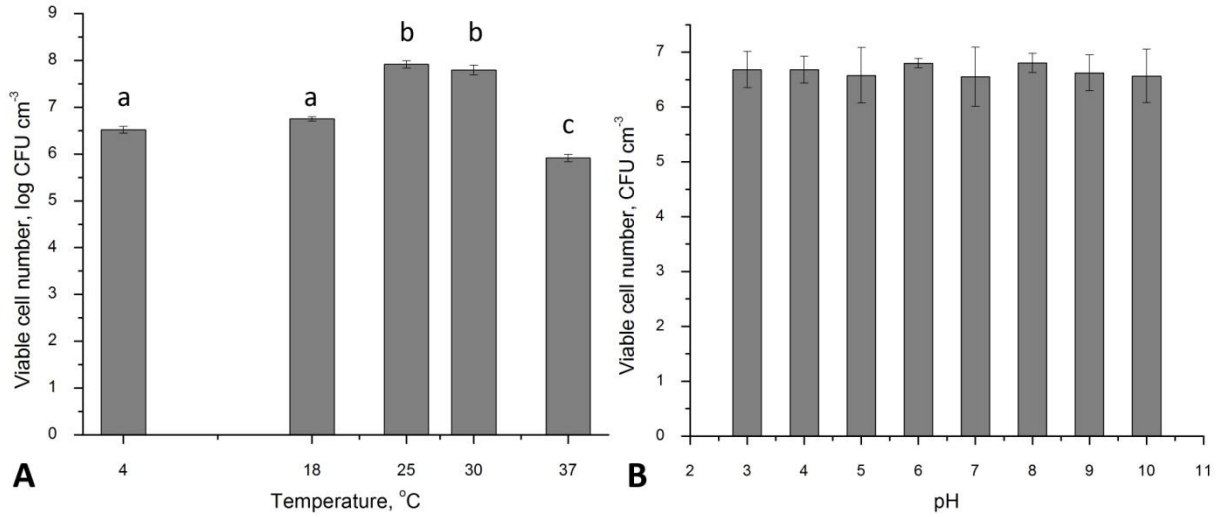

Figure 3. Effects of temperature (A) and pH (B) on A. pullulans P8 growth. The results are presented as mean values of three independent experiments ± standard deviations. Values having the same letters are not significantly different from each other.

3. 3. Fermentation of soybean meal

3. 3. 1 Crude protein content analysis

SBM is an attractive component of animal feed primarily due to its high protein content that can be additionally improved by fermentation. During fermentation microorganisms use carbohydrates and lipids remaining after oil extraction from soybean as carbon sources to enlarge the biomass, thus an increase in the proportion of CP in fermented SBM occurs [4]. In this study, the potential of new isolate *A. pullulans* P8 for high protein SBM production was exploited under two types of fermentation. The CP content had an increasing trend during both SSF and SmF (Tables 1 and 2, respectively). The lowest increment in the CP content was observed after 24 h of SSF when the least viable cells were detected as well. After 72 h of SSF, the microorganism entered the stationary growth phase. However, prolonged fermentation time resulted in higher CP content, finally reaching 57.78±0.49 % based on dry matter (dm) after 168 h. Compared to unfermented control an increase in the CP content by 20.8 % was achieved.

Table 1. Crude protein content and viable cell number in SBM fermented by A. pullulans P8 during SSF

Fermentation time, h	Crude protein content, % dm		Viable cell number, log CFU g^{-1} dm	
	Water	AS	Water	AS
0 (unfermented control)	47.83±0.25		0	0
24	48.94±0.70*	48.48±0.43*	6.92±0.13	6.44±0.31
72	52.42±0.60	48.59±0.48	8.65±0.17	7.58±0.30
120	55.59±0.86	51.39±0.83	8.58±0.32	8.03±0.11
168	57.78±0.49	56.42±0.43	8.69±0.23	7.95±0.27

The results are presented as mean values of three independent experiments ± standard deviations
Water -fermented control; AS - ammonium-sulfate supplemented. *Values within rows that do not differ from each other (p >0.05)

The slow growth rate observed during SSF on SBM may have been caused by low availability of free nitrogen. Namely, nonprotein nitrogen content in SBM is usually less than 1 % [35]. To enhance the metabolic activity of *A. pullulans* P8, SBM was supplemented with ammonium sulfate (AS) as the preferable source of inorganic N among *Aureobasidium* spp. [20,36,37]. However, the addition of AS to SBM significantly slowed down the fungal growth and negatively influenced the CP content (Table 3). This result might have been a consequence of the already low C:N ratio in SBM [16] that was further lowered by the addition of the inorganic N source and ultimately became unfavorable for *A. pullulans* P8 growth. Therefore, the inorganic N source was not added to SBM during SmF.

Table 2. Protein content and viable cell number in SBM fermented by A. pullulans P8 during SmF

Fermentation time, h	Crude protein content, % dm	Viable cell number, log CFU cm^{-3}
0 (unfermented control)	49.02±0.19	0
24	54.98±0.25	6.45±0.20
48	60.03±0.25	8.08±0.71
72	61.11±0.11	8.38±0.53

The results are presented as mean values of three independent experiments ± standard deviations

Contrary to SSF, the increase in the CP content during SmF was accompanied by the fungal growth (Table 2). After 48 h of incubation the CP content reached 60 % (dm basis) and significantly increased up to 61 %, observed after 72 h of incubation. Compared to the unfermented control, an increase in the CP content of 24.7% was achieved.

The crude protein content in fermented SBM obtained in this study was higher than those reported in the literature. For example, SBM with 55.71 % CP (9.8 % enhancement) was obtained by solid-state fermentation using *Bacillus subtilis natto* [38]. Although this value is achieved in a shorter time (62.3 h compared to 168 h in this study) it was obtained after optimization, while optimization has not been performed during our study. In another study the protein content increased by 16.6 % in SBM fermented by *Bacillus subtilis* E20 after 96 h of SSF [2]. When two-stage fermentation of SBM was applied with *Aspergillus oryzae* and *Bacillus subtilis* an increase in the CP content by only 3.7 % was obtained [4], while simultaneous fermentation with *Lactobacillus plantarum*, *B. subtilis*, and *Saccharomyces cerevisiae* raised the CP content by 13.3 % [8].

By comparing the highest protein yields obtained by SSF and SmF using *A. pullulans* P8, it is evident that ~5.8 % more protein is produced in the latter case. Moreover, it was obtained after 3 days of fermentation, while SSF lasted for 7 days. The prolonged time of fermentation required for SSF is probably a consequence of slow aeration and reduced mass transfer that are generally recognized and reported as drawbacks of this type of fermentation [39]. During SmF, water-soluble sugars are readily available, while mixing enables their uniform distribution enhancing microbial growth. However, submerged processes are generally unfavorable for industrial applications since they require more equipment and higher energy consumption than SSF. To make SmF more economically acceptable, but also following circular economy principles, the liquid obtained after centrifugation could be further applied as a source of industrially important enzymes.

3. 3. 2 Carbohydrate content analysis

Besides high protein content, another important goal of the present study was to reduce RFOs content in SBM. Fermented SBM samples with the highest CP contents were analysed for carbohydrate content using HPLC. Comparing chromatograms of the control sample and fermented samples (solid-state), two main features could be observed (Fig. 4a). Peaks corresponding to sucrose, raffinose, and stachyose have decreased, while peaks of galactose and higher oligosaccharides have increased. That indicated the activity of α-galactosidase. Namely, during its growth, *A. pullulans* P8 synthesized α-galactosidase that cleaved terminal galactose residues from galacto-oligosaccharides and galactomananas present in SBM. Raffinose was formed as a product of stachyose hydrolysis. It was further hydrolysed to sucrose and galactose that were consumed by microorganism, supporting its growth. However, more sugars were produced than consumed. On the other hand, released galactose served also as a substrate for α-galactosidase in transglycosylation reaction [6] that increased the content of higher oligosaccharides, compared to the control. Moreover, differences among samples were detected as well. More stachyose and raffinose were noticed in the sample

obtained after 7 days of SSF when AS was added to SBM, than in SBM wetted with water. There was a negligible difference in galactose contents among these two samples, while the content of higher oligosaccharides was lower in AS-supplemented SBM, implying that the addition of AS had a negative effect on α-galactosidase production and/or activity. This result corresponds well with already discussed results obtained in this study *i.e.,* the protein content was significantly lower, and weaker growth was observed in samples with AS. Finally, analysis of the chromatogram of the sample obtained after 3 days of submerged fermentation (Fig. 4b) shows the absence of peaks corresponding to raffinose and stachyose. Also, the galactose content was lower than that in the control, while the content of higher oligosaccharides was the same as in the control. According to results obtained by the HPLC analysis, it could be concluded that SBM obtained after 3 days of submerged fermentation has the lowest content of indigestible carbohydrates, which makes it the most suitable for animal feed.

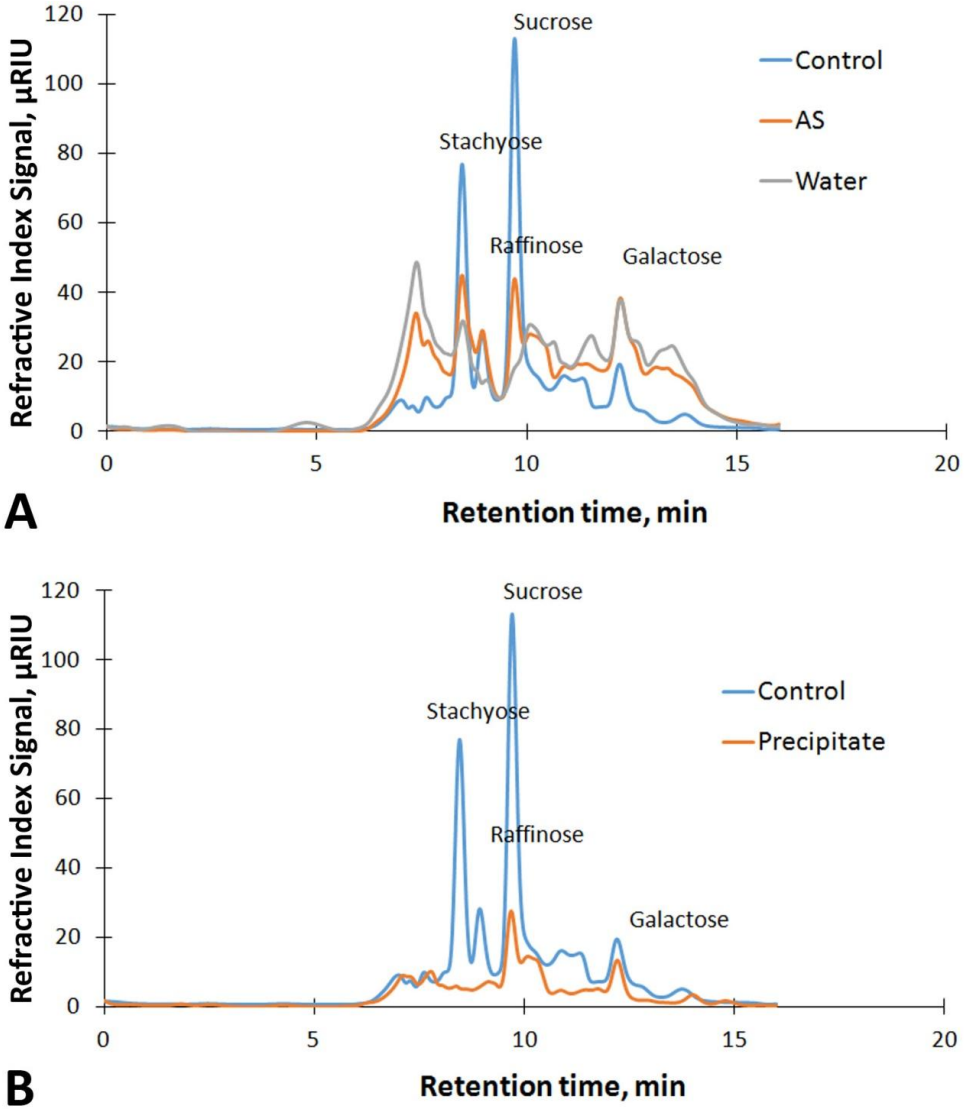

Figure 4. Residual sugars of SBM: (A) after 7 days of SSF with A. pullulans P8 in unfermented control, fermented control (water), and ammonium-sulfate supplemented SBM (AS); (B) after 3 days of SmF with A. pullulans P8 in unfermented control and precipitate obtained after centrifugation

3. 4. Determination of extracellular hydrolytic enzyme activities produced by *A. pullulans* P8 during SmF of SBM

In recent years production of many different enzymes using biomass and by-products from the food industry has been intensively studied [26,40-43]. In the current study, we showed that the new isolate *A. pullulans* P8 could produce amylase, cellulase, xylanase, pectinase, and α-galactosidase during SmF using SBM as a sole nutrient source.

The common feature for all extracellular enzymes examined during the current study is the lowest activity observed in the supernatant obtained after 24 h of SmF (Fig. 5). During the first 24 h of incubation, *A. pullulans* P8 used readily available monosaccharides to increase its biomass. When this source is depleted, extracellular enzymatic activities are required to hydrolyse complex carbohydrates. Significantly higher activities of all examined enzymes were detected after 48 h of incubation, which further increased for cellulase, pectinase, and xylanase, or stayed at the same level to the end of fermentation in the case of amylase and α-galactosidase.

Investigations of genomes of *Aureobasidium* spp. have shown an abundance of genes encoding most of the enzyme families involved in carbohydrate degradation [44]. For a high level of desired enzyme biosynthesis, however, selection of the appropriate substrate is crucial [43,45]. Another approach for obtaining enhanced enzymatic activities is optimization of the substrate concentration, but also of other factors that affect enzyme synthesis by microorganisms, such as the C:N ratio, temperature, aeration, pH, incubation time, *etc.* [40,41,43].

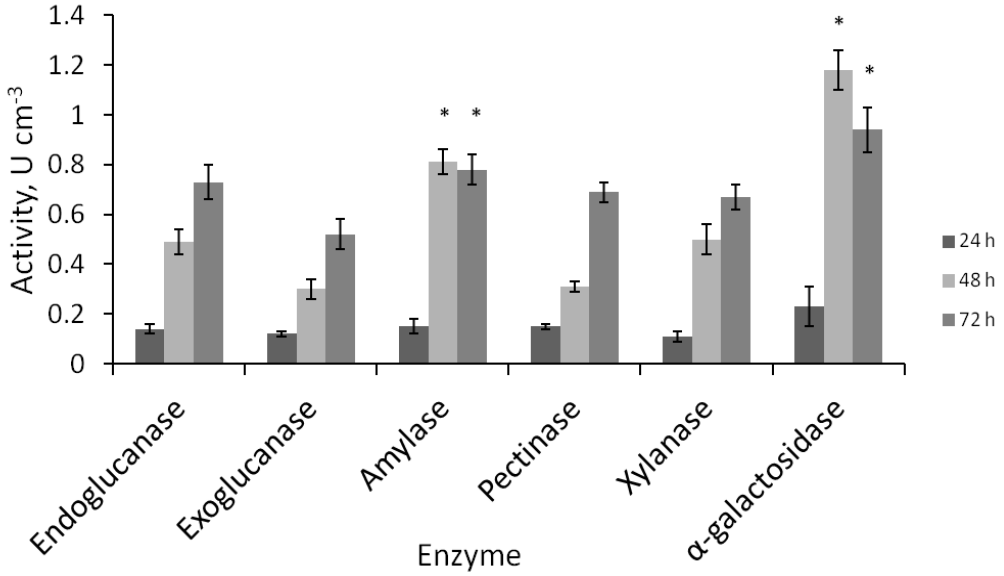

*Figure 5. Extracellular enzymatic activities in supernatant obtained during SmF of SBM using A. pullulans P8. The results are presented as mean values of three independent experiments ± standard deviations. *Values within the same group that do not differ from each other (p >0.05)*

Testing the possibility of different waste substrates to induce the production of xylanase in *A. pullulans* has shown the activity of 0.51 U cm^{-3} on hazelnut skin [45], which was lower than the maximal xylanase activity observed in our study (0.67 U cm^{-3}). However, ten times higher xylanase activity than in our study (67.44 U cm^{-3}) was obtained by the same fungal strain on wheat bran as substrate.

Unexpectedly, high amylase activity of 0.78 U cm^{-3} was determined in the supernatant after 48 h of SmF by *A. pullulans* P8, although the starch content in SBM is very low compared to other polysaccharides [3]. *A. pullulans* Cau 19 produced 0.456 U cm^{-3} after 5 days of growth in medium containing 1 % of starch [32]. After optimization, the amylase activity reached 0.8 U cm^{-3}, a level comparable to the result obtained in our study. This implies that *A. pullulans* P8 is a high amylase producer.

The activity of α-galactosidase obtained after 48 h of SmF using SBM exceeded that obtained in raffinose-supplemented MEB (1.18 *vs.* 0.89 U cm^{-3}), suggesting the potency of SBM to support α-galactosidase biosynthesis by *A. pullulans* P8. This effect could be explained by the ability of different SBM constituents to stimulate α-galactosidase production. Namely, besides RFOs, galactose, glucose, pectin, and galactomannans have been reported as potent carbon sources for the induction of α-galactosidase production by different microorganisms [6].

In our previous study [26], SBM has been shown as the best substrate for inducing pectinase production by *Bjerkandera adusta* TMF1 and *Schizophillum commune* TMF3. In the current study pectinase activity produced by *A. pullulans* P8 was 0.69±0.04 U cm^{-3}. A higher activity (3.8 U cm^{-3}) was reported in the study conducted by Bennamoun *et al.* [46] for a high pectinase-producing strain of *A. pullulans*, using 4 % tomato pomace as substrate.

Both endo and exoglucanase activities were detected in the supernatant after SmF by *A. pullulans* P8. Higher activities, by approximately 3 to 10-fold, for *Aureobasidium* spp. endoglucanase were reported in the literature than those obtained in the present study (0.73±0.07 U cm^{-3}). For example, *A. pullulans* NRRL-Y-2311-1 endoglucanase activity obtained after 120 h of SmF using differently processed canola meal was in the range of 2.27 to 3.17 U cm^{-3} [47]. *A. pullulans* LB83 produced 6.86 U cm^{-3} on SBM during 60 h of SmF [48], while the same strain produced 7.42 U cm^{-3} on sugarcane bagasse. On the other hand, in the study of Leite *et al.* [34] exoglucanase activity was not detected regardless of the substrate used for fermentation. In the current study, exoglucanase activity of 0.52±0.06 U cm^{-3} was obtained, and it was the lowest among all the tested enzyme activities.

Relatively low endoglucanase activities obtained in our study compared to literature data could be a result of activities of proteases produced by *A. pullulans* P8 during fermentation [47]. Although proteases were not the focus of this research, it is reasonable to expect they had been secreted. The effect of protease activity was more pronounced when complex substrates were used as nitrogen sources compared to ammonium sulfate [49]. Likewise, it was observed that different nitrogen sources significantly influenced amylase activity [32]. Since SBM was the only nutrient source in the current study, future experimental work will consider the effect of its supplementation with different inorganic nitrogen sources.

Although the activity of neither enzyme was optimized during the present study, it was shown that *A. pullulans* P8 has the potential to produce carbohydrate-degrading enzymes. Further research will focus on isolating, purifying, and applying these enzymes. Importantly, the crude enzyme mixture obtained in the present study could be used for bioethanol production without the need for time-consuming and expensive purification steps [26]. Additionally, it could be used for SBM hydrolysis for animal food production, as well as other complex lignocellulosic substrates that require the use of various enzymes to be degraded [17,26,43].

4. CONCLUSION

This study has shown the immense potential of a new strain of *A. pullulans* P8 isolated from grapes for producing high protein, low oligosaccharide soybean-based feed. The CP content in fermented SBM was increased by 20.8 and 24.7 % compared to control during SSF and SmF, respectively. The highest CP content of ~~61 % (dry matter basis) was achieved after three days of submerged fermentation using *A. pullulans* P8. This sample also exhibited the lowest galacto-oligosaccharide content, making it the most suitable for animal feed. Furthermore, the study revealed extracellular activities of different carbohydrate degrading enzymes in supernatant obtained after submerged fermentation. It is important to note that this study is only the first screening that elucidated the wide application potential of new strain *A. pullulans* P8. Therefore, subsequent research endeavors will focus on optimization of the fermentation process aiming to further enhance the content of crude protein and hydrolytic enzyme activities and to shorten the incubation time. Scaling-up experiments also need to be conducted. Finally, an animal feeding trial should be performed to verify the real beneficial effect of the new fermented soybean-based product *in vivo*.

Acknowledgement: *This study was supported by the Ministry of Science, Technological Development and Innovation of the Republic of Serbia (Contract numbers 451-03-136/2025-03/200135 and 451-03-136/2025-03/200287) and the Innovation Fund of the Republic of Serbia through the program Innovation Vouchers (Voucher number 1076). The authors are thankful to Bankom d.o.o. for providing the material for research and performing crude protein analysis.*

Data availability: The obtained sequences, which represented a partial sequence of the ITS region were deposited in the NCBI GenBank database: https://www.ncbi.nlm.nih.gov/nuccore/OR921445

REFERENCES

[1] ReportLinker. https://www.reportlinker.com/clp/global/3685. Accessed June 26, 2025.

[2] Shiu YL, Wong SL, Guei WC, Shin YC, Liu CH. Increase in the plant protein ratio in the diet of white shrimp, Litopenaeus vannamei (Boone), using Bacillus subtilis E20-fermented soybean meal as a replacement. *Aquac Res.* 2015; 46(2): 382-394. https://doi.org/10.1111/are.12186

[3] Karr-Lilienthal LK, Kadzere CT, Grieshop CM, Fahey GC. Chemical and nutritional properties of soybean carbohydrates as related to nonruminants. *Livest Prod Sci.* 2005; 97(1): 1-12. https://doi.org/10.1016/j.livprodsci.2005.01.015

[4] Abdel-Raheem SM, Mohammed ESY, Mahmoud RE, Gamal MFE, Nada HS, El-Ghareeb WR, Marzok M, Meligy AMA, Abdulmohsen M, Ismail H, Ibrahim D, Kishawy ATY. Double-Fermented Soybean Meal Totally Replaces Soybean Meal in Broiler Rations with Favorable Impact on Performance, Digestibility, Amino Acids Transporters and Meat Nutritional Value. *Animals.* 2023; 13(6): 1030. https://doi.org/10.3390/ani13061030

[5] Middelbos IS, Fahey GC. Soybean Carbohydrates. In: Johnson LA, White PJ, Galloway R, eds. Soybeans Chemistry, Production, Processing, and Utilization. Urbana, IL: AOCS Press; 2008. p. 269-296. https://doi.org/10.1016/B978-1-893997-64-6.50012-3

[6] Anisha GS. Microbial α-galactosidases: Efficient biocatalysts for bioprocess technology. *Bioresour Technol* 2022; 344: 126293. https://doi.org/10.1016/j.biortech.2021.126293

[7] Celi P, Cowieson AJ, Fru-Nji F, Steinert RE, Kluenter A-M, Verlhac V. Gastrointestinal functionality in animal nutrition and health: New opportunities for sustainable animal production. *Anim Feed Sci Technol.* 2017; 234: 88-100. https://doi.org/10.1016/j.anifeedsci.2017.09.012

[8] Zhu J, Gao M, Zhang R, *et al.* Effects of soybean meal fermented by L. plantarum, B. subtilis and S. cerevisieae on growth, immune function and intestinal morphology in weaned piglets. *Microb Cell Fact.* 2017; 16(1): 191. https://doi.org/10.1186/s12934-017-0809-3

[9] Shang QH, Ma XK, Li M, Zhang LH, Hu JX, Piao XS. Effects of α-galactosidase supplementation on nutrient digestibility, growth performance, intestinal morphology and digestive enzyme activities in weaned piglets. *Anim Feed Sci Technol.* 2018; 236: 48-56. https://doi.org/10.1016/j.anifeedsci.2017.11.008

[10] Milić MD, Buntić A V., Mihajlovski KR, Ilić N V., Davidović SZ, Dimitrijević-Branković SI. The development of a combined enzymatic and microbial fermentation as a viable technology for the spent coffee ground full utilization. *Biomass Convers Biorefinery.* 2023; 13(8): 6747-6759. https://doi.org/10.1007/s13399-021-01605-8

[11] Jakobsen G V., Jensen BB, Bach Knudsen KE, Canibe N. Impact of fermentation and addition of non-starch polysaccharide-degrading enzymes on microbial population and on digestibility of dried distillers grains with solubles in pigs. *Livest Sci.* 2015; 178: 216-227. https://doi.org/10.1016/j.livsci.2015.05.028

[12] Senanayake D, Torley PJ, Chandrapala J, Terefe NS. Microbial Fermentation for Improving the Sensory, Nutritional and Functional Attributes of Legumes. *Fermentation.* 2023;.9(7): 635. https://doi.org/10.3390/fermentation9070635

[13] Tang J, Li W, Zhou Q, *et al.* Effect of heating, microbial fermentation, and enzymatic hydrolysis of soybean meal on growth performance, nutrient digestibility, and intestinal microbiota of weaned piglets. *J Anim Sci.* 2023; 101: skad384. https://doi.org/10.1093/jas/skad384

[14] Xue J, Wu J, Ji Y, *et al.* Effect of microbial fermentation on the quality of soybean meal. *Int J Food Sci Technol.* 2024; 59(1): 72-83. https://doi.org/10.1111/ijfs.16817

[15] Baker KM, Liu Y, Stein HH. Nutritional value of soybean meal produced from high protein, low oligosaccharide, or conventional varieties of soybeans and fed to weanling pigs. *Anim Feed Sci Technol.* 2014; 188: 64-73. https://doi.org/10.1016/j.anifeedsci.2013.10.018

[16] Loman A Al, Ju LK. Soybean carbohydrate as fermentation feedstock for production of biofuels and value-added chemicals. *Process Biochem.* 2016; 51(8): 1046-1057. https://doi.org/10.1016/j.procbio.2016.04.011

[17] Deng Z, Duarte ME, Kim SY, Hwang Y, Kim SW. Comparative effects of soy protein concentrate, enzyme-treated soybean meal, and fermented soybean meal replacing animal protein supplements in feeds on growth performance and intestinal health of nursery pigs. *J Anim Sci Biotechnol.* 2023; 14(1): 89. https://doi.org/10.1186/s40104-023-00888-3

[18] Chen S, Zheng H, Gao J, Song H, Bai W. High-level production of pullulan and its biosynthesis regulation in Aureobasidium pullulans BL06. *Front Bioeng Biotechnol.* 2023; 11. https://doi.org/10.3389/fbioe.2023.1131875

[19] Cruz-Santos MM, Antunes FAF, Arruda GL, *Shibukawa VP, Prado, CA, Ortiz-Silos N, Castro-Alonso MJ, Marcelino PRF, Santos JC.* Production and applications of pullulan from lignocellulosic biomass: Challenges and perspectives. *Bioresour Technol.* 2023; 385: 129460. https://doi.org/10.1016/j.biortech.2023.129460

[20] Thirumavalavan K, Manikkadan TR, Dhanasekar R. Pullulan production from coconut by-products by Aureobasidium pullulans. *African J Biotechnol.* 2009; 8(2): 254-258

[21] Wang P, Jia S-L, Liu G-L, Chi Z, Chi Z-M. Aureobasidium spp. and their applications in biotechnology. *Process Biochem.* 2022; 116: 72-83. https://doi.org/10.1016/j.procbio.2022.03.006

[22] Di Francesco A, Sciubba L, Bencivenni M, Marzadori C, Baraldi E. Application of Aureobasidium pullulans in iron-poor soil. Can the production of siderophores improve iron bioavailability and yeast antagonistic activity? *Ann Appl Biol.* 2022; 180(3): 398-406. https://doi.org/10.1111/aab.12742

[23] Rensink S, van Nieuwenhuijzen EJ, Sailer MF, Struck C, Wösten HAB. Use of Aureobasidium in a sustainable economy. *Appl Microbiol Biotechnol.* 2024; 108(1): 202. https://doi.org/10.1007/s00253-024-13025-5

[24] Carević M, Banjanac K, Ćorović M, *et al.* Selection of lactic acid bacteria strain for simultaneous production of α- and β-galactosidases. *Zast Mater.* 2016; 57(2): 265-273. https://doi.org/10.5937/zasmat1602265c

[25] Miller GL. Use of Dinitrosalicylic Acid Reagent for Determination of Reducing Sugar. *Anal Chem.* 1959; 31(3): 426-428. https://doi.org/10.1021/ac60147a030

[26] Ilić N, Davidović S, Milić M, *et al.* Valorization of lignocellulosic wastes for extracellular enzyme production by novel Basidiomycetes: screening, hydrolysis, and bioethanol production. *Biomass Convers Biorefinery.* 2022; 13: 17175-17186. https://doi.org/10.1007/s13399-021-02145-x

[27] ISO 5983-1:2005; Animal feeding stuffs: Determination of nitrogen content and calculation of crude protein content. Part 1: Kjeldahl method, International Standard Organization. Technical Committee: Geneva, Switzerland, 2005; ISO/TC 34/SC 10. https://www.iso.org/standard/39145.html

[28] Thermo Fisher Scientific. Chromeleon (Version 7.2) [Computer Software]. Thermo Fisher Scientific, 2018. https://www.thermofisher.com/order/catalog/product/CHROMELEON7

[29] OriginLab Corporation. OriginPro (Version 9.0) [Computer Software]. OriginLab Corporation, 2012. https://www.originlab.com/

[30] van Nieuwenhuijzen EJ. Aureobasidium. *Encycl Food Microbiol Second Ed* 2014; 1: 105-109. https://doi.org/10.1016/B978-0-12-384730-0.00017-3

[31] Bankeeree W, Lotrakul P, Prasongsuk S, Kim SW, Punnapayak H. Enhanced Production of Cellulase-Free Thermoactive Xylanase Using Corncob by a Black Yeast, Aureobasidium pullulans CBS 135684. *Korean Chem Eng Res.* 2016; 54(6): 822-829. https://doi.org/10.9713/kcer.2016.54.6.822

[32] Mulay YR, Deopurkar RL. Production of amylase from indigenously isolated strain of Aureobasidium Pullulans and its hyper producing mutant. *J Microbiol Biotechnol Food Sci.* 2017; 7(3): 287-293. https://doi.org/10.15414/jmbfs.2017/18.7.3.287-293

[33] Zajc J, Černoša A, Francesco A Di, *et al.* Fungal Genomics & Biology Characterization of Aureobasidium pullulans Isolates Selected as Biocontrol Agents Against Fruit Decay Pathogens. *Fungal Genom Biol.* 2020; 10(1): 163. https://doi.org/10.35248/2165-8056.20.10.163

[34] Leite RSR, Bocchini DA, Martins EDS, Silva D, Gomes E, Da Silva R. Production of cellulolytic and hemicellulolytic enzymes from Aureobasidium pulluans on solid state fermentation. *Appl Biochem Biotechnol.* 2007; 137-140(1-12): 281-288. https://doi.org/10.1007/s12010-007-9058-y

[35] Thakur M, Hurburgh CR. Quality of US soybean meal compared to the quality of soybean meal from other origins. *JAOCS, J Am Oil Chem Soc.* 2007; 84(9): 835-843. https://doi.org/10.1007/s11746-007-1107-8

[36] Badr-Eldin SM, El-Tayeb OM, El-Masry HG, Mohamad FHA, El-Rahman OAA. Polysaccharide production by Aureobasidium pullulans: factors affecting polysaccharide formation. *World J Microbiol Biotechnol.* 1994; 10(4): 423-426. https://doi.org/10.1007/BF00144465

[37] Lotrakul P, Unhapattaratitikul P, Seelanan T, Prasongsuk S, Punnapayak H. An aubasidan-like β-glucan produced by Aureobasidium pullulans in Thailand. *ScienceAsia.* 2013; 39(4): 363. https://doi.org/10.2306/scienceasia1513-1874.2013.39.363

[38] Zhang Y, Ishikawa M, Koshio S, *et al.* Optimization of soybean meal fermentation for aqua-feed with bacillus subtilis natto using the response surface methodology. *Fermentation.* 2021; 7(4): 306. https://doi.org/10.3390/fermentation7040306

[39] Ilić N, Milić M, Beluhan S, Dimitrijević-Branković S. Cellulases: From Lignocellulosic Biomass to Improved Production. *Energies.* 2023; 16(8): 3598. https://doi.org/10.3390/en16083598

[40] Miljkovic M, Davidovic S, Djukic-Vukovic A, *et al.* Utilization of agro-industrial by-products as substrates for dextransucrase production by Leuconostoc mesenteroides T3: Process optimization using response surface methodology. *Hem Ind.* 2021; 75(3): 135-146. https://doi.org/10.2298/HEMIND200710015M

[41] Mihajlovski K, Davidovic S, Veljovic D, Carevic M, Lazic V, Dimitrijevic-Brankovic S. Effective valorization of barley bran for simultaneous cellulase and β-amylase production by Paenibacillus chitinolyticus CKS1: Statistical optimization and enzymes application. *J Serbian Chem Soc.* 2017; 82(11): 1223-1236. https://doi.org/10.2298/JSC170514092M

[42] Salim AA, Grbavčić S, Šekuljica N, *et al.* Enzyme production by solid-state fermentation on soybean meal: A comparative study of conventional and ultrasound-assisted extraction methods. *Biotechnol Appl Biochem.* 2019; 66(3): 361-368. https://doi.org/10.1002/bab.1732

[43] Ademakinwa AN, Agboola FK. Kinetic and thermodynamic investigations of cell-wall degrading enzymes produced by Aureobasidium pullulans via induction with orange peels: application in lycopene extraction. *Prep Biochem Biotechnol.* 2019; 49(10): 949-60. https://doi.org/10.1080/10826068.2019.1650375

[44] Gostinčar C, Ohm RA, Kogej T, *et al.* Genome sequencing of four Aureobasidium pullulans varieties: Biotechnological potential, stress tolerance, and description of new species. *BMC Genomics.* 2014;.15(1): 549 . https://doi.org/10.1186/1471-2164-15-549

[45] Yegin S, Buyukkileci AO, Sargin S, Goksungur Y. Exploitation of Agricultural Wastes and By-Products for Production of Aureobasidium pullulans Y-2311-1 Xylanase: Screening, Bioprocess Optimization and Scale Up. *Waste and Biomass Valorization.* 2017; 8(3): 999-1010. https://doi.org/10.1007/s12649-016-9646-6

[46] Bennamoun L, Hiligsmann S, Dakhmouche S, *et al.* Production and Properties of a Thermostable, pH—Stable Exo-Polygalacturonase Using Aureobasidium pullulans Isolated from Saharan Soil of Algeria Grown on Tomato Pomace. *Foods.* 2016; 5(4): 72. https://doi.org/10.3390/foods5040072

[47] Alhomodi AF, Gibbons WR, Karki B. Estimation of cellulase production by Aureobasidium pullulans, Neurospora crassa, and Trichoderma reesei during solid and submerged state fermentation of raw and processed canola meal. *Bioresour Technol Reports.* 2022; 18: 101063. https://doi.org/10.1016/j.biteb.2022.101063

[48] Vieira MM, Kadoguchi E, Segato F, da Silva SS, Chandel AK. Production of cellulases by Aureobasidium pullulans LB83: optimization, characterization, and hydrolytic potential for the production of cellulosic sugars. *Prep Biochem Biotechnol* 2021; 51(2): 153-163. https://doi.org/10.1080/10826068.2020.1799393

[49] Qian Y, Zhong L, Sun Y, *et al.* Enhancement of Cellulase Production in Trichoderma reesei via Disruption of Multiple Protease Genes Identified by Comparative Secretomics. *Front Microbiol.* 2019; 10. https://doi.org/10.3389/fmicb.2019.02784

Valorizacija sojine sačme za proizvodnju visokoproteinske stočne hrane i proizvoda sa dodatom vrednošću korišćenjem novog soja *Aureobasidium pullulans*

Slađana Z. Davidović[1], Miona G. Miljković[1], Nevena Ilić[2], Milica Veljković[2] i Suzana Dimitrijević-Branković[1]

[1]*Univerzitet Beogradu, Tehnološko-metalurški fakultet Beograd, Srbija*
[2]*Inovacioni centar Tehnološko-metalurškog fakulteta, Beograd, Srbija*

(Naučni rad)

Izvod

Sojina sačma je nusproizvod koji nastaje nakon ekstrakcije ulja iz zrna soje. S obzirom na to da je bogata visokokvalitetnim proteinima, sojina sačma se koristi kao dodatak za stočnu hranu. Međutim, bogata je takođe i antinutritivnim faktorima i nesvarljivim komponentama, među kojima je posebna pažnja usmerena na galaktooligosaharide, zbog nedostatka α-galaktozidaze kod monogastričnih životinja. Osnovni cilj ovog istraživanja bio je da se odabere pogodan soj crne gljivice nalik kvascu (*Aureobasidium* spp.) među deset prirodnih izolata iz grožđa, koji bi tokom fermentacije sojine sačme dao proizvod sa velikim sadržajem proteina i malim sadržajem oligosaharida. Sa tim ciljem odabran je izolat P8 koji je pokazao najveću aktivnost α-galaktozidaze od 0,89 U cm^{-3}. Odabrani soj je identifikovan kao *A. pullulans* P8. Maksimalni prinos sirovih proteina u fermentisanoj sojinoj sačmi (61 % računato na suvu materiju) i najmanji sadržaj galaktooligosaharida dobijeni su nakon 3 dana inkubacije na 30 °C potopnom fermentacijom pri sadržaju 10 % suve materije sojine sačme. Fermentacijom na čvrstom supstratu dobijeno je ~58 % sirovih proteina nakon 7 dana inkubacije na 30 °C pri sadržaju suve materije od 30 %. U supernatantu dobijenom nakon potopne fermentacije izmerene su aktivnosti ekstracelularnih enzima (celulaze, pektinaze, amilaze, ksilanaze i α-galaktozidaze), što ukazuje na potencijal ovog pomoćnog proizvoda za hidrolizu različitih lignoceluloznih supstrata.

Ključne reči: crna gljivica nalik kvascu; fermentacija na čvrstoj podlozi; potopna fermentacija; α-galaktozidaza; ekstracelularni hidrolitički enzimi; grožđe

Human pluripotent NT2/D1 cells immobilized in alginate microfibers: a 3D system for testing the effects of bioactive compounds

Jelena Lj. Pejić[1], Milena C. Milivojević[1], Marija L. Schwirtlich[1], Jelena S. Petrović[2,3], Jasmina J. Stojkovska[2], Milena J. Stevanović[1,4,5] and Marija M. Mojsin[1]

[1]*University of Belgrade, Institute of Molecular Genetics and Genetic Engineering, Belgrade, Serbia*
[2]*University of Belgrade, Faculty of Technology and Metallurgy, Belgrade, Serbia*
[3]*Innovation Centre of the Faculty of Technology and Metallurgy, Belgrade, Serbia*
[4]*University of Belgrade, Faculty of Biology, Belgrade, Serbia*
[5]*Serbian Academy of Sciences and Arts, Belgrade, Serbia*

Abstract

Extensive consumption of energy drinks (ED) and alcohol mixed with energy drinks (AmED) has become a prevalent practice among young people. Marked as enhancers of physical and mental performance due to their high levels of stimulant ingredients, such as caffeine and taurine, ED and AmED consumption can potentially cause adverse effects on the central nervous system (CNS) and cardiovascular system. Despite the role of stem cells in development and tissue renewal, studies examining the potential effects of consumption on these cells are lacking. In this study, we established a 3D system based on alginate microfibers to test the effects of bioactive compounds on human NT2/D1 embryonal carcinoma cells, a widely used malignant counterpart of human stem cells. We also assessed the effects of simulated acute ED and AmED consumption on the viability of pluripotent cells and evaluated the efficiency of mass transport to the cells using mathematical modeling. The obtained results show that the 3D system enables undisturbed growth and proliferation of NT2/D1 cells and uniform distribution of the tested compounds to all cells within the microfiber. Simulated acute ED and AmED consumption in the 3D culture did not affect the viability of NT2/D1 cells, compared to a 2D culture, where caffeine induced a significant, yet small, decrease in cell viability.

Keywords: Human embryonal carcinoma cells; alginate hydrogels; cell viability; mass transport; energy drinks; caffeine.

Available on-line at the Journal web address: http://www.ache.org.rs/HI/

ORIGINAL SCIENTIFIC PAPER

UDC: 616-089.22:677.469:576.5

Hem. Ind. **79(3)** 141-155 (2025)

1. INTRODUCTION

Energy drinks (ED) are non-alcoholic beverages widely consumed by children, adolescents, and young people [1,2]. The major constituents of ED, caffeine and taurine, present in high concentrations, have been shown to enhance mental and physical performance [1]. On the other hand, excessive consumption of ED can cause significant health issues, primarily in the cardiovascular and neurological systems, raising health concerns and the necessity for regulatory guidelines addressing the safe consumption of ED [3,4]. Consumption of ED in combination with alcohol (alcohol mixed with energy drinks - AmED), an increasingly popular trend among adolescents, leads to altered and risk-taking behavior and makes them more prone to intoxication than consuming ED alone [5]. Studies addressing this issue were mainly focused on the effects of ED on mature cells of neural and cardiovascular origins [6-8]. Research, which analyzed the impact of ED constituents on human induced pluripotent stem cell (iPSC)-derived cardiomyocytes, shed light on the potential adverse effects these components may exert on the cardiovascular system [6]. The negative effect of caffeine and taurine, used in concentrations labeled on ED, was also confirmed in immature oligodendrocytes and hippocampal neurons derived from P0-P1 Wistar rats, causing a disturbance in the development capacity of oligodendrocytes and in the morphology of neurons [7]. In addition, research on human neuronal cell line SH-SY5Y showed that major ED constituents, caffeine, taurine, and guarana, caused the excessive removal of antioxidant species in cells, thus causing antioxidative stress, which disrupts cellular homeostasis [8]. Despite the importance of stem cells and progenitor cells in both embryonal and adult development,

Corresponding author: Marija M. Mojsin, Institute of Molecular Genetics and Genetic Engineering, University of Belgrade
E-mail: mojsin@imgge.bg.ac.rs
Paper received: 24 July 2024; Paper accepted: 30 July 2025; Paper published: 5 September 2025.
https://doi.org/10.2298/HEMIND240724011P

research regarding the effects of ED on these cell types is missing. Therefore, there is a need for the development of adequate and relevant models based on stem cells and progenitor cells.

NT2/D1 cell line, a pluripotent embryonal carcinoma (EC) cells [9], could be used to create such models since it is considered the malignant counterpart of human embryonic stem (ES) cells [10]. Previous studies demonstrated that human EC cells and human ES cells share significant genetic similarities. Microarray analysis identified 330 genes as highly expressed in both cell types, particularly pluripotency-related genes such as POU5F1 (Oct4), suggesting a common molecular basis underlying their pluripotent phenotype [11]. Additionally, it was shown that EC cells and ES cells exhibit genetic similarities in the expression of pluripotency markers such as SSEA3, SSEA4, and Oct4, also in class 1 MHC antigens and Thy1, reflecting their common embryonic origins [9]. EC cells, such as NT2/D1 cell line, despite originating from tumors, offer a simplified model compared to ES cells, thus facilitating the study of the effect of diverse compounds on the developmental mechanisms of humans without ethical concerns and providing complementary insights alongside ES cells [9].

2D cell culture is the most suitable, cost-effective, and widely used approach for *in vitro* monitoring of cell growth and analyzing the cell response upon drug treatment [12,13]. Despite being the effective approach for the first step in drug screening, it has many limitations due to the absence or changed cell morphology, polarity, cell-to-cell, and cell-to-ECM interactions present in native tissues in the human body, important for maintaining a physiologically relevant microenvironment [13,14]. These limitations could be addressed using experimental animals as *in vivo* models. Although widely used in research, significant differences between animals and humans prevent the extrapolation of results obtained in animal models to clinical trials [15]. Studies also showed large differences between human and mouse embryonic stem cells in morphology, tempo of differentiation, expression profiles of genes involved in the regulation of cell cycle, cell death, differentiation, etc [15-18]. Consequently, certain stimuli, e.g, signaling molecules, compounds, that affect some biological processes in mouse cells could have either negligible effect or the opposite effect in human cells. Therefore, 3D cell culture models emerged as necessary to bridge the gap between two widely used approaches for drug screening - 2D cell culture and animal models [13].These challenges are recognised by EU Directive 2010/63, which encourages the 3Rs principle (refine, reduce and replace) to develop alternative three-dimensional (3D) models that can mimic human tissues and disease complexity for research and drug testing [19]. NT2/D1 cells were successfully differentiated into mature neurons in a 3D model of sphere formation [20] and alginate hydrogels [21]. Cell immobilization in alginate hydrogels shows great potential due to the natural origin of alginate, enabling cells to grow and interact within, and allowing the exchange of metabolites, oxygen, and stimuli between cells in fibers and the surrounding medium [22,23].

The aim of this research was to establish a 3D model system of pluripotent NT2/D1 cells immobilized in alginate microfibers and analyze the potential effects of ED and AmED consumption on the viability of human pluripotent cells.

2. EXPERIMENTAL

2. 1. Cell culture

NT2/D1 cells, a kind gift from Prof. Peter W. Andrews (University of Sheffield, UK), were grown in Dulbecco's Modified Eagle Medium (DMEM) High Glucose (4.5 g dm^{-3} glucose) supplemented with 10 % Fetal Bovine Serum (FBS) and Antibiotic-Antimycotic solution (10,000 units cm^{-3} of penicillin, 10,000 μg cm^{-3} of streptomycin, and 25 μg cm^{-3} of Amphotericin B), all purchased from Thermo Fisher Scientific (MA, USD). Cells were maintained in cell incubators at 37 °C, 10 % CO_2 and high humidity atmosphere. A 2D model system of NT2/D1 cells was maintained by propagating cells in standard adherent culture dishes where these cells grow in a monolayer. A 3D culture system was obtained by immobilization of NT2/D1 cells in alginate microfibers as previously described [22]. Briefly, sodium alginate (A3249, low viscosity, AppliChem, Germany) solution (1.5 wt.%) with cells (5×10^6 cells cm^{-3} alginate) was manually extruded through a blunt edge stainless steel needle (25 gauge, Small Parts Inc., USA) into a gelling bath containing 0.18 M Ca^{2+} ions ($CaCl_2\cdot2H_2O$, Sigma-Aldrich, USA). After complete gelling (15 min incubation in the gelling bath), microfibers were washed in a cell culture medium without FBS and finally maintained in the cell culture conditions described above. Alginate microfibers were visualized by light microscopy and diameters were measured using Leica LAS v4.12 Software. Measurements were performed in three biological replicates, with three independent average diameter calculations for each alginate microfiber.

2. 2. Cell recovery

Immobilized NT2/D1 cells were released by dissolving alginate microfibers in 2 % w/v sodium citrate ($Na_3C_6H_5O_7 \cdot 2H_2O$, Sigma-Aldrich, USA) solution (0.1 g of microfibers in 1 cm^3 of the solution) for 10 min at 37 °C. Cell suspension was pelleted by centrifugation at 1300 rpm for 5 min. The supernatant was discarded and the cell pellet was washed two times with the cell culture medium. Cell number was determined using the Trypan blue exclusion test of cell viability. Retrieved cells were cultivated in adherent culture dishes for 72 h and analyzed for viability, adhesion, and proliferative capacity.

2. 3. Cell treatments

NT2/D1 cells in 2D and 3D cell cultures were treated with the main components of energy drinks, caffeine (CAF) and taurine (TAU), individually, together (CAF+TAU) and in combination with alcohol (CAF+TAU+EtOH); energy drink alone (ED) or in combination with alcohol (ED+EtOH). Components were dissolved in a cell culture medium in concentrations corresponding to their actual amounts in the energy drink, *i.e.* 0.32 mg cm^{-3} caffeine and 4 mg cm^{-3} taurine. Energy drink samples (500 mm^3 each) were dried in a vacuum concentrator (Concentrator 5301, Eppendorf). Then, dry pellets were dissolved in initial volumes (500 mm^3) of cell culture medium to preserve the original concentrations of all components and pH was adjusted to 7.4 using 0.1 N NaOH/HCl [6]. Final concentrations of all components in the cell culture medium during treatments were ten times lower than the original concentrations in energy drinks to simulate the real consumption *in vivo* [6].

Ethanol, in a concentration of 20 mM, was used with caffeine and taurine or ED to simulate AmED consumption. This concentration corresponds to the physiologically relevant blood alcohol content in adults after quick consumption of a few drinks [24]. For treatments, NT2/D1 cells were cultured in 96-well plates, either seeded in 2D monolayer culture (10^4 cells per well) or in 3D culture immobilized in alginate microfibers (cut to 1 cm in length per well). Treatment was initiated 24 h after cell seeding in both cell culture conditions - 2D monolayer and 3D microfiber culture, and it lasted for 24 h to simulate acute consumption, as described previously [7,25]. Untreated NT2/D1 cells were used as a control since all components were dissolved in the cell culture medium.

2. 4. Fixation of NT2/D1 cells immobilized in alginate microfibers

NT2/D1 cells immobilized and propagated within alginate microfibers for 7 days were washed once in Phosphate Buffered Saline (PBS) and incubated in Fixative Solution (Cell Signaling Technology, Inc., Danvers, MA, USA) for 15 min at room temperature. After incubation, cells were rinsed two times in PBS and visually inspected using a Leica DM IL LED Inverted Microscope (Leica Microsystems, Leica Microsystems GmbH, Germany). During fixation and washing in PBS, alginate microfibers were disintegrated, but cell clusters remained intact.

2. 5. MTT assay

Viability of NT2/D1 cells was assessed using a colorimetric MTT test. This assay measures cell viability by assessment of the mitochondrial ability to metabolize MTT (3-(4,5-dimethyl-2-thiazolyl)-2,5-diphenyl-2H-tetrazolium bromide) (Merck & Co., Inc., USA). In viable, metabolically active cells, MTT is reduced into purple formazan crystals, which can be visually confirmed by light microscopy or spectrophotometrically measured upon solubilization in DMSO (dimethyl sulfoxide) [26]. For the visual inspection of NT2/D1 cells during the 7 day propagation in alginate microfibers, cells in 3D culture were incubated with MTT solution (MTT dissolved in cell culture medium at a concentration 0.5 mg cm^{-3}) for 24 h, at four time points – after 1, 2, 3 and 7 days at 37°C in cell incubator. Images were taken using a Leica DM IL LED Inverted Microscope (Leica Microsystems, Leica Microsystems GmbH, Germany). Colorimetric measurements were performed as previously described [26,27]. NT2/D1 cells grown in 96-well plates, in 2D and 3D cell cultures, were incubated with MTT solution (MTT dissolved in cell culture medium at a concentration of 0.5 mg cm^{-3}) for 4 h at 37 °C in a cell incubator. After incubation, the MTT solution was discarded, and water-insoluble formazan crystals were dissolved by incubation in DMSO for 5 min with agitation at room temperature. Solubilization of formazan was monitored by visual inspection of the alginate microfibers using light microscopy. Absorbances of the dissolved formazan solutions were measured at 570 nm using a microplate reader, Tecan Infinite 200 PRO (Tecan Group Ltd., Switzerland). Statistical analysis was performed with SPSS statistical

software package (SPSS Inc. Released 1999. SPSS for Windows, Version 10.0., USA). Cell viability was calculated and presented as a percentage of the corresponding untreated control NT2/D1 cells (either 2D or 3D) expressed as 100 %. Data were expressed as means ± SEM (Standard Error of the Means).

2. 6. Live/dead assay

Effects of ED and AmED treatments on the viability of NT2/D1 cells in alginate microfibers were evaluated using LIVE/DEAD™ Cell Imaging Kit (488/570) (Invitrogen, ThermoFisher Scientific, USA). Live/dead assay is based on two distinctive characteristics of live cells - membrane integrity and intracellular esterase activity. In this two-color assay, cells are simultaneously stained with green-fluorescent calcein-AM (indicating live cells with intracellular esterase activity) and red-fluorescent BOBO-3 Iodide (indicating dead cells that lost membrane integrity). NT2/D1 cells immobilized in alginate microfibers were propagated for 48 h in the cell culture (24 h without treatment and 24 h with/without treatment) and stained according to the manufacturer's instructions. Images of the stained NT2/D1 cells immobilized in alginate microfibers were taken using a Leica TCS SP7 confocal laser-scanning microscope (Leica Microsystems CMS GmbH, Wetzlar, Germany). Sequence of 40 cross section images (5 µm each) of alginate microfibers were analyzed. Z stacks were overlapped by Maximal intensity processing tool of LAS AF software (Leica Microsystems, Leica Microsystems GmbH, Germany).

3. RESULTS AND DISCUSSION

3. 1. Immobilization of NT2/D1 cells in alginate microfibers

NT2/D1 cells were successfully immobilized in alginate microfibers with consistent and uniform size (average diameter of 190 ± 10 µm, Fig. 1) using manual extrusion of cell/alginate suspension (5×10^6 cells cm^{-3}, 1.5 % w/w alginate) into the gelling bath containing Ca^{2+} ions. The obtained alginate microfibers with immobilized cells were further cultivated in standard cell culture conditions for up to 7 days.

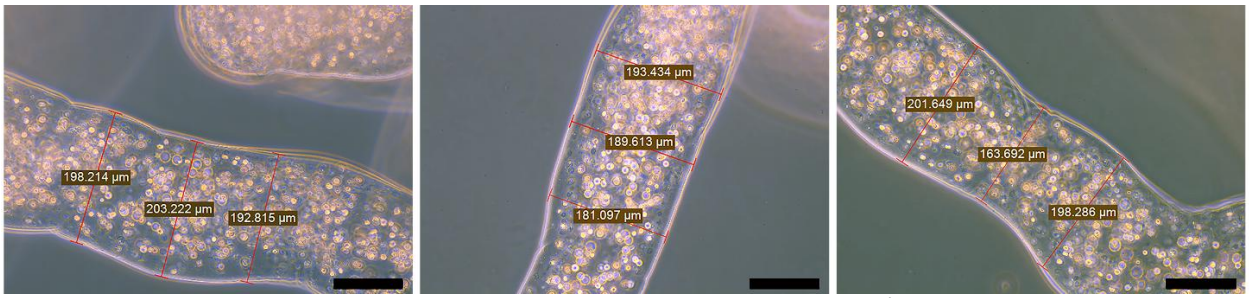

Figure 1. *Representative optical micrographs of alginate microfibers with immobilized NT2/D1 cells showing diameter measurements. Scale bar: 100µm*

Morphology of NT2/D1 cells and their growth in alginate microfibers were analyzed by light microscopy (Fig. 2, Panel A). Representative images of cells captured during the propagation have shown uniform cell distribution in microfibers, as well as a continuous increase in cell number during the 7-day course of cultivation (Fig. 2, Panel A). In addition, cells spontaneously form cellular aggregates and clusters of cells (large cellular aggregates) (Fig. 2, Panel A). At the first time point, day 1, we observed a high density of single cells within microfibers (Fig. 2, Panel A, day1), while increased number of cells during prolonged growth in alginate microfibers resulted in cell aggregation (Fig. 2, Panel A, days 2 and 3) and the formation of cell clusters at day 7 (Fig. 2, Panel A). To confirm cellular aggregation and clustering, we performed chemical fixation of the NT2/D1 cells after 7 days of propagation in alginate microfibers (Fig. 2, Panel B). Cell fixation ensured the preservation of the original state, shape and structures of cellular aggregates and clusters (Fig. 2, Panel B) and corroborate previous observation that NT2/D1 cells in alginate microfibers proliferate and establish cell-to-cell contacts to enhance cell viability and functionality within cellular aggregates [28].

These results were also confirmed using MTT assay for visualization of viable cells within alginate fibers. As presented in Figure 2, Panel C, the intensity of formazan dye, indicator of the presence of live cells, markedly increased during

7 days of propagation. MTT assay also showed cell aggregations at day 2 and 3 and cell cluster formation at day 7 (Fig. 2, Panel C, Images g-i).

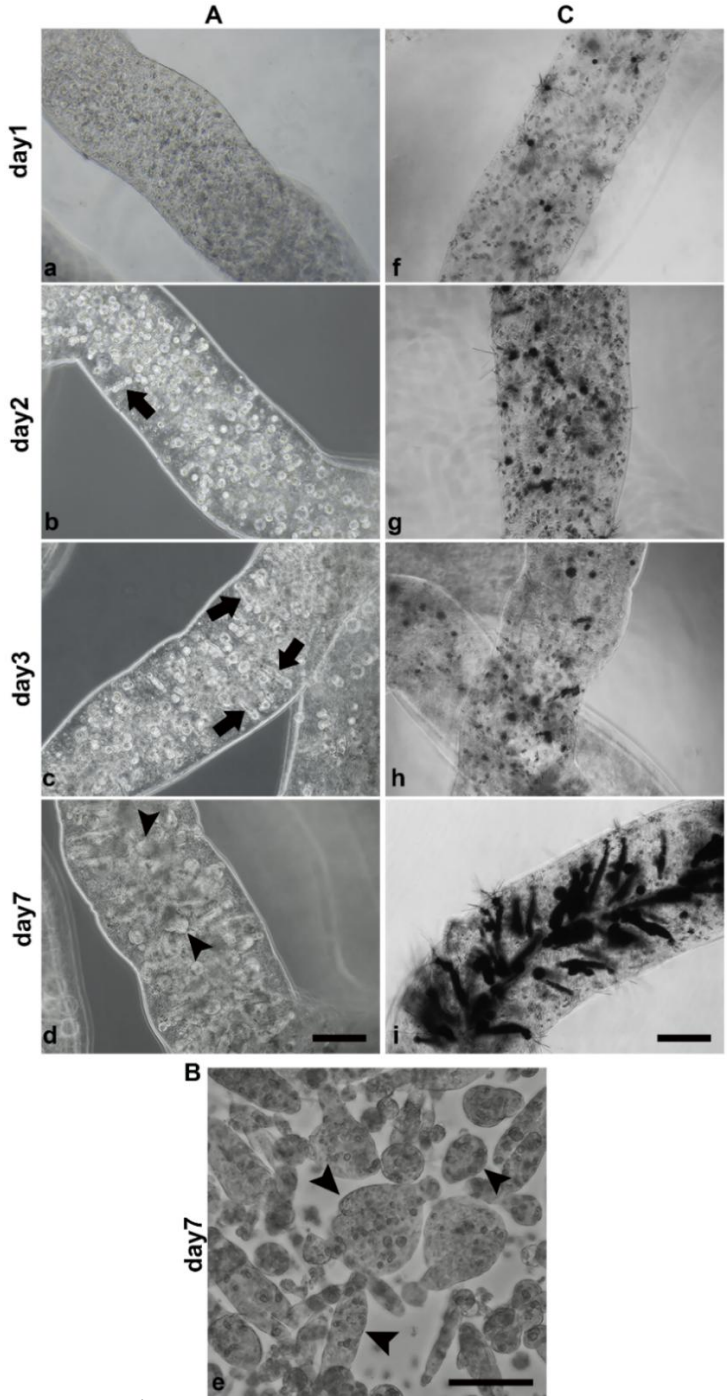

Figure 2. *NT2/D1 cells during a 7-day course of cells growing in alginate microfibers. Light microscopy of A) NT2/D1 cells in alginate microfibers at indicated time points. Black arrows indicate cell aggregates at days 2 and 3 and cell clusters at day 7. Scale bar: 100 µm. B) Fixation of NT2/D1 cells after 7 day propagation showing cellular clusters (black arrowheads) in alginate microfibers. Scale bar-50µm. C) Formazan dyed NT2/D1 cells in alginate microfibers at indicated time points. Scale bar: 100 µm.*

We also wanted to investigate the effect of cell retrieving procedure on the viability, proliferation capacity and adhesion potential of immobilized cells. Immobilized NT2/D1, cells were retrieved from microfibers 24 h after immobilization, counted and seeded in adherent culture dishes for growth in 2D culture, Figure 3. Concentration of

retrieved NT2/D1 cells was 1.5×10^6 cells per cm^3. Compared to $5x10^6$ cells per cm^3, initially immobilized in alginate microfibers, the observed cell loss was significant (~3 fold).

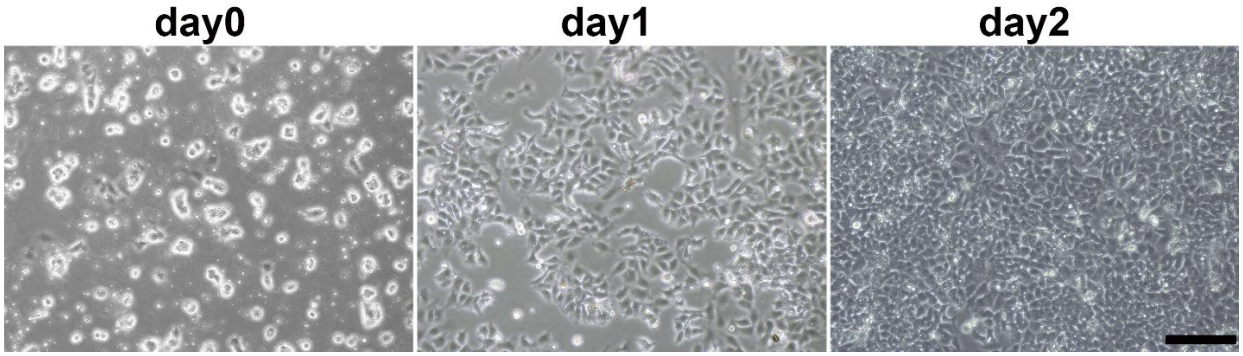

Figure 3. *Light microscopy of NT2/D1 cells retrieved from alginate microfibers and propagated in 2D cell culture for the indicated periods of time. Scale bar-100 µm*

The observed result is comparable to the cell number reduction during retrieval from alginate microfiber previously described in similar studies [29,30] and it is due to cytotoxicity of Na-citrate [31]. Sodium citrate inhibits proliferation and induces apoptosis of hepatocellular carcinoma cells [31,32]. In addition, increased sensitivity of NT2/D1 cells to cytotoxic agents was previously established [33]. Nevertheless, retrieved NT2/D1 cells seeded in monolayer 2D culture retained viability, ability to attach to a culture dish surface and capacity to proliferate (compare images at day 0, day 1, and day 2 in Figure 3).

NT2/D1 cells were previously maintained in both 2D (adherent monolayer culture) and 3D model systems (cultivation in non-adherent conditions that promote spheres formation) [34]. That study showed remarkable differences in NT2/D1 cells growth under 2D and 3D culturing conditions [34]. Cells in the 2D culture had 5 times higher proliferative capacity then spheroid culture that was limited by the gradual decrease in oxygen concentration from the periphery to the center of spheroid [34]. Hypoxic condition in the center of spheroid induced very low cell proliferation rate in that zone [34]. Limitations in oxygen and nutrients diffusion, accumulation of metabolic waste and consequent cell necrosis in spheroids [35,36] could be overcome using alginate 3D cell culture models. As a matter of fact, NT2/D1 cells were successfully encapsulated in alginate beads [21]. In order to create a 3D model for efficient differentiation of NT2/D1 cells in dopaminergic neurons authors tested optimal conditions (cell density and permeability of the beads) for encapsulation of cells in alginate beads [21].They showed that 1.0×10^6 cells cm^{-3} encapsulated in the highly permeable alginate beads (obtained by 0.1 M $CaCl_2$ in the gelling bath) promoted high exchange between cells and medium and consequently increased viability, proliferation, and metabolic activity of NT2/D1 cells [21]. Presented results confirm that biocompatible, immunogenic, and non-toxic alginate hydrogels are highly suitable for supporting the growth and propagation of human pluripotent NT2/D1 cells in a 3D environment.

We also detected differences in morphology of NT2/D1 cells grown in alginate microfibers and 2D monolayer cultures, which is in concordance with previous observations [37-39]. This result could be explained by the fact that cells in the 3D cell culture gained a round shape, due to a single growth direction and the absence of cell attachment to the cultureware. This is in contrast to the flattened shape of cells in a 2D monolayer, which is in agreement with results from previous studies. [40]

3. 2. The effects of ED and AmED treatments on the viability of NT2/D1 cells in 2D and 3D model systems

In order to assess the effects of treatments on cells in 2D and 3D cell cultures, the cells were exposed for 24 h to treatments that simulated the consumption of energy drinks and their major components (caffeine and taurine) alone or in combination with alcohol. Experimental settings, duration and concentrations of tested compounds were in concordance with the previously conducted studies [7,25]. Accordingly, the following treatments were applied: caffeine (CAF); taurine (TAU); the combination of caffeine and taurine (CAF+TAU); caffeine and taurine in combination with alcohol (CAF+TAU+EtOH); energy drink (ED); ED in combination with alcohol (ED+EtOH).

After 24 h of treatment, microfibers in all treated groups preserved their integrity, while NT2/D1 cells preserved their morphology compared to the untreated control (Fig. 4, Panel A). To assess the potential effects of ED and AmED treatments on the viability of NT2/D1 cells in 2D and 3D cell cultures MTT assay was used (Fig. 4, Panel B).

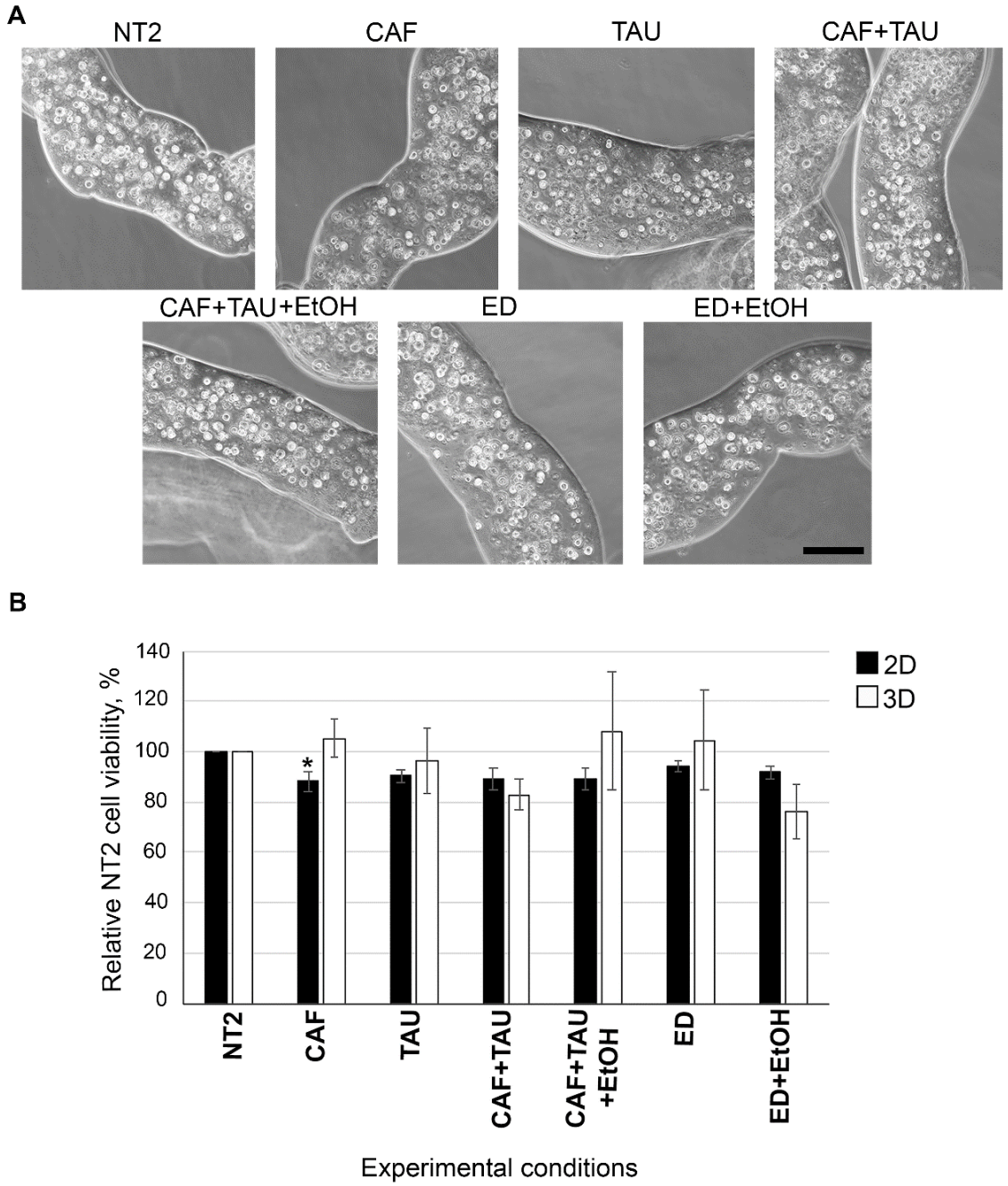

Figure 4: *NT2/D1 cells immobilized in alginate microfibers cultivated for 24 h and then treated for 24 h with the indicated treatments. A) Light microscopy of treated NT2/D1 cells in alginate microfibers. NT2-control untreated cells. Scale bar: 100 µm. B) Viability of NT2/D1 cells assessed by MTT assay. NT2/D1 cells were cultivated for 24 h in monolayer cultures (2D) or immobilized in alginate microfibers (3D) and then exposed for 24 h to the treatments listed above. Values are normalized to the values of corresponding controls, either 2D NT2/D1 or 3D NT2/D1, untreated cells expressed as 100 %. Data are represented as means ± SEM of three independent experiments performed in triplicate.* indicates $p < 0.05$. NT2-control untreated cells.*
SEM - standard error of the means.

The obtained results indicate a slight difference in cell viability between 2D and 3D cell cultures in response to treatments. The slight reduction in cell viability, although statistically nonsignificant, in response to all treatments in the 2D model system can be observed, except for caffeine, where a statistically significant but low decrease (12 %) in cell

viability is observed (Fig. 4, Panel B). On the other hand, none of the treatments significantly affect NT2/D1 cell viability in a 3D model system (Fig. 4, Panel B). Noticeable, although statistically insignificant, decrease in cell viability after treatments with caffeine/taurine and ED/EtOH in 3D probably reflects the fact that the 3D cell culture had higher deviations than 2D cultures (Fig. 4, Panel B). This is one of the well-established properties of 3D cultures, caused by the variation in the initial culture conditions, such as cell density and distribution in the 3D matrix [41-43].

In addition, cell viability after treatments with ED and AmED was evaluated by LIVE/DEAD assay (Fig. 5).

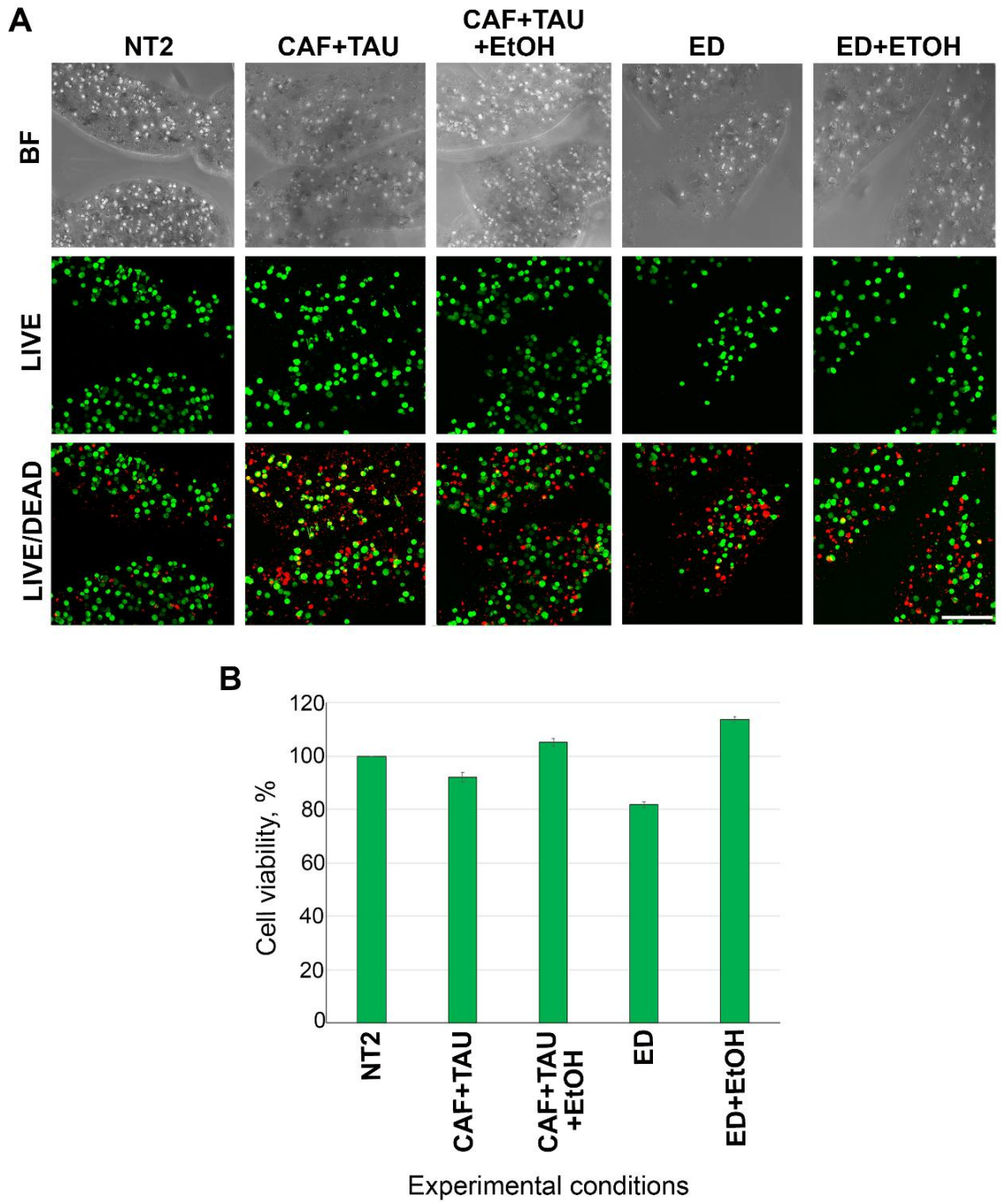

Figure 5. *Live/dead cell viability assay of NT2/D1 cells in alginate microfibers after ED and AmED treatments. A) Representative images of NT2/D1 cells in alginate microfibers after 24 h of indicated treatments. A representative Z stack of bright-field (BF), green fluorescence (LIVE), and merged fluorescence (LIVE/DEAD) that was overlapped (40 cross-sections, 5 µm each) by the Maximal intensity processing tool of LAS AF Software. Scale bar: 200 µm. B) Quantification of viable cells from the LIVE/DEAD assay using ImageJ software. Values are presented as a cell viability compared to control cells, which is set to 100 %. Data are presented as mean ± SEM, * indicates $p < 0.05$. SEM - standard error of the means*

This assay discriminates viable and non-viable cells using a green fluorescent dye, calcein-AM for live cells and red fluorescent BOBO-3 Iodide dye to visualize dead cells. As presented in Figure 5, Panel A, vast majority of cells entrapped in alginate microfibers retained viability with respect to the limited and moderate mortality. Viable cells maintained equal and uniform distribution within the microfiber (Fig. 5, Panel A). Apparently, the differences in distributions between central and peripheral regions of the microfibers could not be distinguished (Fig. 5, Panel A). Quantification of the LIVE/DEAD assay showed that indicated treatments did not significantly affect the NT2/D1 cell viability (Fig. 5, Panel B). Statistically insignificant but detectable decrease in cell viability after CAF/TAU and ED treatments is probably due to high deviations caused by the repeatability and reproducibility issues of 3D cultures [41-43].

The obtained results suggest that 24 h treatments that simulate ED and AmED consumption in both 2D and 3D cell culture models did not affect the viability of pluripotent NT2/D1 cells. In the case of treatments with ED components, caffeine induced a 12 % decrease in cell viability in the 2D model, while in the 3D model, the effect on NT2/D1 viability was non-detectable. We speculate that the alginate 3D system may provide a protective microenvironment for pluripotent cells with respect to the 2D monolayer culture. It has been shown previously that alginate oligosaccharides showed antioxidant and neuroprotective effects on NT2-derived mature neurons against H_2O_2-induced neurotoxicity [44]. The same protective effects were described in chromium-induced brain damage in rats and H_2O_2-induced senescence in H9C2 cardiomyocytes [45,46].

Effects of ED and AmED were extensively investigated in correlation with mental health and behavioral control in human volunteers and animal models [47,48]. Considering that ED and AmED primarily affect the CNS and cardiovascular system, physiological effects were mostly examined in animal models, animal primary cell cultures, and mature cells from these two organic systems [7,47,49,50]. Investigations of the effects of ED and AmED on pluripotent cells, stem cells and induced pluripotent stem cells (iPSc) are missing. Further studies should be focused on the effects of ED and AmED on the populations of stem cells and progenitor cells since consumption has increased among children, adolescents (vulnerable groups with ongoing neurodevelopment) and young people (potential association of ED intake before and during pregnancy with health risks) [4,7]. These results show, for the first time, that NT2/D1 cells immobilized in alginate microfibers represent a valuable 3D model system for studying the potential cytotoxic effects of bioactive compounds, components of food and beverages, on the pluripotent cells.

3. 3. Mathematical modeling of mass transport in 3D cell culture

In order to assess the efficiency of substance transport, specifically caffeine, taurine, and ethanol, within alginate microfibers, and to evaluate whether the hydrogel imposes any mass transport limitations, which could contribute to its protective effects, mathematical modeling was applied. Namely, the aim was to adopt a diffusion-reaction mass transport model previously developed [22] to predict concentration profiles of caffeine, taurine and ethanol within the single microfiber under cell culture conditions. Briefly, the model was based on the assumption that the external mass transfer resistance on the microfiber surface could be neglected and that the mass transport within the microfibers was the rate-limiting factor. Additionally, the following assumptions were made [22]: 1) the microfiber is cylindrical; 2) the diameter of the microfiber is constant; 3) the modeled substance is consumed at a constant rate per cell, following a zero-order chemical reaction; 4) the concentration of the modeled substance in the medium, and consequently at the microfiber surface, is constant; 5) mass transport occurs solely in the radial direction. Hence, the internal mass transport through the microfiber was described by the subsequent diffusion-reaction equation [22]:

$$\frac{\partial c}{\partial t} = \frac{D}{r}\frac{\partial}{\partial r}\left(r\frac{\partial c}{\partial r}\right) - \rho q \qquad (1)$$

where D represents the diffusion coefficient of the modeled substance, r denotes the radial coordinate from the center of the microfiber, q is the consumption rate of the substance per cell and ρ indicates the cell concentration per unit volume of the microfiber.

Solution of the partial differential Equation (1) was achieved numerically, by using the 'pdepe' function in MATLAB R2018a programming platform (MathWorks Inc.) [51].

3. 3. 1. Initial and boundary conditions

For all three modeled substances (caffeine, taurine and ethanol), the starting concentration in the microfiber was equal to zero, giving the following initial condition, Equation (2):

$$t = 0 \qquad 0 \le r \le R \qquad c = 0 \tag{2}$$

where R is the radius of the microfiber.

In accordance with the assumption about cylindrical geometry of the microfibers, the symmetry boundary condition was set along the microfiber axis, Equation (3):

$$r = 0 \qquad \frac{\partial c}{\partial r} = 0 \tag{3}$$

A constant concentration, equal to that in the medium (c_m), was assumed at the outer boundary of the microfiber, Equation (4):

$$r = R \qquad c = c_m \tag{4}$$

3. 3. 2. Model parameters

The diameter of the microfibers was specified as 190 μm, based on the average value obtained from at least 15 diameter measurements. The cell concentration per unit volume was specified as 5×10^6 cells cm^{-3}, based on the initial cell density.

3. 3. 3. Modeling of caffeine transport

The caffeine diffusion coefficient was adopted as 5.01×10^{-7} cm^2 s^{-1}, as reported in literature for caffeine diffusion in anionic hydrogels [52], while the caffeine concentration in the culture medium was 0.16 mol m^{-3} after treatment with either pure caffeine or the energy drink. It should be noted that in this study, NT2/D1 cells were used as *in vitro* models of embryonic neurogenesis and formation of different neuronal phenotypes, and it is well known that caffeine binds to the adenosine receptors of neurons and glial cells, as an antagonist, while it is metabolized in hepatocytes [53]. Therefore, the consumption term in Equation (1) was omitted. The mathematical model was solved using a spatial step size of Δr = 0.96 μm and a time step of Δt = 0.25 s.

The modeling results showed that the steady state was reached after 343 s with the caffeine concentration in the microfiber center reaching the concentration in the culture medium. This result implies efficient mass transport of caffeine throughout the whole microfiber under culture conditions.

3. 3. 4. Modeling of taurine transport

The taurine diffusion coefficient was adopted as 5.1×10^{-6} cm^2 s^{-1}, as reported in literature for glucose [54]. Glucose (M = 180.16 g mol^{-1}) is a small, polar molecule, with similar molecular weight to that of taurine (M=125.14 g mol^{-1}). The taurine concentration in the culture medium was 3.2 mol m^{-3} after treatment with either pure taurine or the energy drink. Additionally, the taurine consumption rate per cell for SF-295 human glioblastoma cell line, the most similar cell line with NT2/D1 cells, was reported to be 0.150 fmol $cell^{-1}$ h^{-1} (the mean value of two measurements: 0.097 and 0.203 fmol $cell^{-1}$ h^{-1}, taken from Supplement Database_S1, Jain *et al.* [55]. It is important to note that the assumption of a constant concentration of taurine in the medium was based on calculations demonstrating that the time required for complete consumption of taurine by the cells was vastly longer than the duration of the experiment, and thus the consumption was negligible within the experimental timeframe. The mathematical model was solved using a spatial step size of Δr = 0.96 μm and a time step of Δt = 0.25 s. The taurine concentration profile was plotted as a function of normalized radial distance (Fig. 6).

The simulation demonstrates that the steady state is reached after 33 s with the taurine concentration in the center of the microfiber practically reaching the value of taurine concentration in the culture medium. Further modeling of taurine transport, taking into account the experimental setup and the 24-hour exposure period, demonstrated that after 24 h, the taurine concentration throughout the entire microfiber remained equal to that in the surrounding medium.

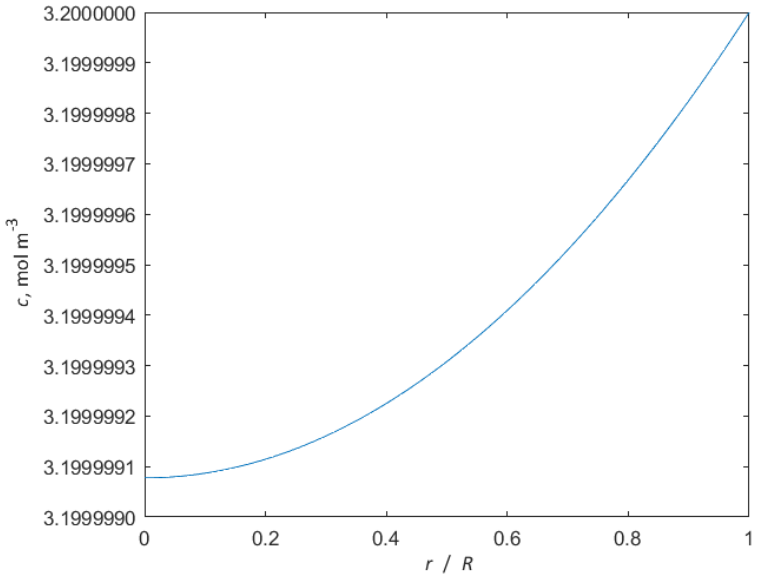

Figure 6: *Taurine concentration is represented in relation to the normalized radial distance within a microfiber (r/R) at steady state (R represents the microfiber radius, r/R=0 indicates the central axis of the microfiber and r/R=1 indicates its outer surface).*

3. 3. 5. Modeling of ethanol transport

For modeling of ethanol transport through the alginate microfibers, the diffusion coefficient was set to 9.6×10^{-6} cm^2 s^{-1}, as reported in literature for ethanol in 2 wt.% alginate hydrogel [54]. The ethanol concentration was 20 mol m^{-3} in the culture medium after addition of ethanol in the combination with caffeine and taurine, as well as in the combination with the energy drink. On the other hand, there is a significant lack of literature data regarding ethanol consumption by stem cells. Therefore, we adopted the highest calculated value of consumption rate of oxygen by human mesenchymal stem cells (hMSC) as 0.012 µmol 10^{-6} cells^{-1} h^{-1}, reported in literature [56]. As in the case of taurine, the assumption of a constant ethanol concentration in the medium was based on calculations demonstrating that the time required for complete consumption by the cells was significantly longer than the duration of the experiment. The mathematical model was solved using a spatial step size of Δr = 0.96 µm and a time step of Δt = 0.25 s. The ethanol concentration profile in the microfiber was plotted as a function of normalized radial distance (Fig. 7).

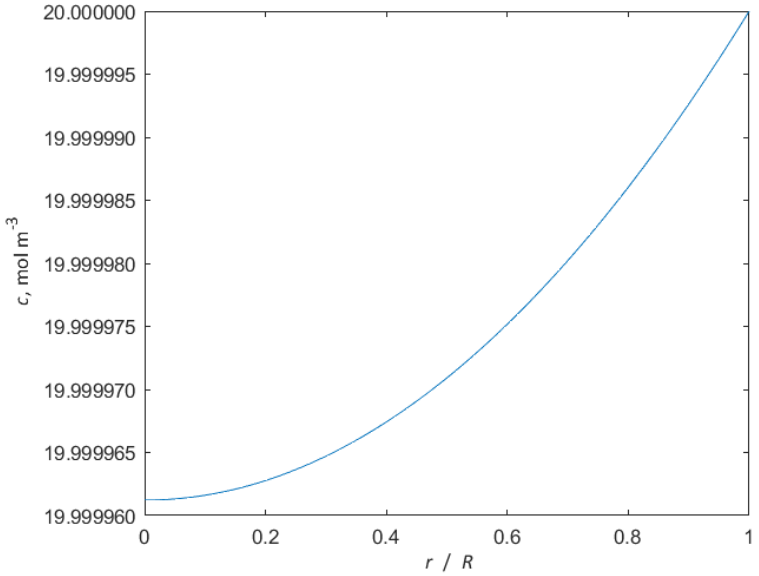

Figure 7: *The profile of ethanol concentration is represented in relation to the normalized radial distance within a microfiber (r/R) at a steady state (R represents the microfiber radius, r/R=0 indicates the central axis of the microfiber and r/R=1 indicates its outer surface)*

The ethanol concentration in the center of the microfiber reaches that in the medium in only 22 s, demonstrating highly efficient transport of ethanol throughout the whole microfiber. The steady state is achieved almost immediately, with the ethanol concentration in the centre of the microfiber equal to that in the culture medium. Upon modeling ethanol transport over a 24-hour period, it was found that the concentration within the microfiber closely matched that of the surrounding medium.

Overall, the modeling results demonstrated efficient mass transport of all three investigated substances within the 3D cell culture model. The model supported growth and proliferation of pluripotent NT2/D1 cells making it possible to mimic the certain behavior and structure characteristics of cells *in vivo* - round shaped single cells that form 3D aggregates with efficient supply of nutrients and active molecules throughout the microfibers. This 3D model could be used for the evaluation of substance effects on individual cells at the beginning of cultivation, as well as on cell aggregates at day 2, and on multilayered cell cluster at day 7. It is anticipated that cellular responses to a given substance may differ between single cells and those within aggregates, highlighting the importance of considering cell organization during experimental data analysis. In contrast to 2D models, 3D models provide gradients of nutrients, oxygen, metabolites, and tested compounds to cells which make them more accurate and physiologically relevant [57].

Retinoic acid induced neural differentiation of NT2/D1 cells in 2D culture is a widely used model of human neurogenesis [58]. After four weeks of induction NT2/D1 cells differentiate into mature neurons and astrocytes [58]. In addition, NT2/D1 cells encapsulation in alginate microbeads enabled low-rate spontaneous dopaminergic neuronal differentiation in a 3-week period [21]. Our future goal will be to establish 3D culture of alginate microfibers for 4 weeks long RA-induced neural differentiation of NT2/D1 cells to test the effects of acute and chronic consumption of ED and AmED on different stages of human neurogenesis.

4. CONCLUSION

In this study, we established a 3D model of human pluripotent NT2/D1 cells immobilized in alginate microfibers. The immobilized NT2/D1 cells preserved viability, proliferative capacity and potential to form aggregates during a 7-day course of propagation. To validate the 3D NT2/D1 cell model system for bioactive compounds testing, we performed mathematical modeling of mass transport in the 3D cell cultures. Obtained results showed that all tested compounds were uniformly distributed to all cells inside the microfiber, similar to the uniform distribution of compounds to cells growing in a monolayer. Acute 24-hour treatment with ED and the contained compounds, alone or in combination with alcohol, did not affect the viability of immobilized NT2/D1 cells in the 3D model. Correlation with the same treatments in 2D culture showed differences in the effect of caffeine on cell viability. The caffeine treatment resulted in a low but statistically significant decrease in cell viability of 12 % in 2D monolayer culture. NT2/D1 cells immobilized in alginate microfibers represent a potential 3D platform for testing the effects of different compounds from food and beverages on human pluripotent cells.

Acknowledgement: This study was supported by the Ministry of Science, Technological Development and Innovation of the Republic of Serbia (contract numbers: 451-03-66/2024-03/200042; 451-03-65/2024-03/200135; 451-03-66/2024-03/200287).

REFERENCES

[1] Alsunni AA. Energy Drink Consumption: Beneficial and Adverse Health Effects. *Int J Health Sci (Qassim)*. 2015; 9(4): 468-474. https://ijhs.qu.edu.sa/index.php/journal/article/view/1244

[2] Nadeem IM, Shanmugaraj A, Sakha S, Horner NS, Ayeni OR, Khan M. Energy Drinks and Their Adverse Health Effects: A Systematic Review and Meta-analysis. *Sports Health*. 2021; 13(3): 265-277. https://doi.org/10.1177/1941738120949181PMC8083152

[3] De Sanctis V, Soliman N, Soliman AT, Elsedfy H, Di Maio S, El Kholy M, Fiscina B. Caffeinated energy drink consumption among adolescents and potential health consequences associated with their use: a significant public health hazard. *Acta Biomed*. 2017; 88(2): 222-231. https://doi.org/10.23750/abm.v88i2.6664PMC6166148

[4] Ding M, Markon AO, Jones-Dominic OE, Purdue-Smithe AC, Rich-Edwards JW, Wolpert BJ, Chavarro JE. Intake of Energy Drinks Before and During Pregnancy and Adverse Pregnancy Outcomes. *JAMA Netw Open*. 2023; 6(11): e2344023. https://doi.org/10.1001/jamanetworkopen.2023.44023PMC10660164

[5] Oteri A, Salvo F, Caputi AP, Calapai G. Intake of energy drinks in association with alcoholic beverages in a cohort of students of the School of Medicine of the University of Messina. *Alcohol Clin Exp Res*. 2007; 31(10): 1677-1680. https://doi.org/10.1111/j.1530-0277.2007.00464.x

[6] Luo YS, Chen Z, Blanchette AD, Zhou YH, Wright FA, Baker ES, Chiu WA, Rusyn I. Relationships between constituents of energy drinks and beating parameters in human induced pluripotent stem cell (iPSC)-Derived cardiomyocytes. *Food Chem Toxicol*. 2021; 149: 111979. https://doi.org/10.1016/j.fct.2021.111979PMC8286543

[7] Serdar M, Mordelt A, Müser K, Kempe K, Felderhoff-Müser U, Herz J, Bendix I. Detrimental Impact of Energy Drink Compounds on Developing Oligodendrocytes and Neurons. *Cells*. 2019; 8(11): 1381. https://doi.org/10.3390/cells8111381PMC6912672

[8] Zeidán-Chuliá F, Gelain DP, Kolling EA, Rybarczyk-Filho JL, Ambrosi P, Terra SR, Pires AS, da Rocha JB, Behr GA, Moreira JC. Major components of energy drinks (caffeine, taurine, and guarana) exert cytotoxic effects on human neuronal SH-SY5Y cells by decreasing reactive oxygen species production. *Oxid Med Cell Longev*. 2013; 2013: 791795. https://doi.org/10.1155/2013/791795PMC3674721

[9] Andrews PW. From teratocarcinomas to embryonic stem cells. *Philos Trans R Soc Lond B Biol Sci*. 2002; 357(1420): 405-417. https://doi.org/10.1098/rstb.2002.1058PMC1692959

[10] Andrews PW, Damjanov I, Simon D, Banting GS, Carlin C, Dracopoli NC, Føgh J. Pluripotent embryonal carcinoma clones derived from the human teratocarcinoma cell line Tera-2. Differentiation *in vivo* and *in vitro*. *Lab Invest*. 1984; 50(2): 147-162. https://pubmed.ncbi.nlm.nih.gov/6694356/

[11] Sperger JM, Chen X, Draper JS, Antosiewicz JE, Chon CH, Jones SB, Brooks JD, Andrews PW, Brown PO, Thomson JA. Gene expression patterns in human embryonic stem cells and human pluripotent germ cell tumors. *Proc Natl Acad Sci U S A*. 2003; 100(23): 13350-13355. https://doi.org/10.1073/pnas.2235735100PMC263817

[12] Foglizzo V, Cocco E, Marchiò S. Advanced Cellular Models for Preclinical Drug Testing: From 2D Cultures to Organ-on-a-Chip Technology. *Cancers (Basel)*. 2022; 14(15): 3692. https://doi.org/10.3390/cancers14153692PMC9367322

[13] Kapałczyńska M, Kolenda T, Przybyła W, Zajączkowska M, Teresiak A, Filas V, Ibbs M, Bliźniak R, Łuczewski Ł, Lamperska K. 2D and 3D cell cultures - a comparison of different types of cancer cell cultures. *Arch Med Sci*. 2018; 14(4): 910-919. https://doi.org/10.5114/aoms.2016.63743PMC6040128

[14] Habanjar O, Diab-Assaf M, Caldefie-Chezet F, Delort L. 3D Cell Culture Systems: Tumor Application, Advantages, and Disadvantages. *Int J Mol Sci*. 2021; 22(22): 12200. https://doi.org/10.3390/ijms222212200PMC8618305

[15] Zhao X, Bhattacharyya A. Human Models Are Needed for Studying Human Neurodevelopmental Disorders. *Am J Hum Genet*. 2018; 103(6): 829-857. https://doi.org/10.1016/j.ajhg.2018.10.009PMC6288051

[16] Ginis I, Luo Y, Miura T, Thies S, Brandenberger R, Gerecht-Nir S, Amit M, Hoke A, Carpenter MK, Itskovitz-Eldor J, Rao MS. Differences between human and mouse embryonic stem cells. *Dev Biol*. 2004; 269(2): 360-380. https://doi.org/10.1016/j.ydbio.2003.12.034

[17] Greber B, Wu G, Bernemann C, Joo JY, Han DW, Ko K, Tapia N, Sabour D, Sterneckert J, Tesar P, Schöler HR. Conserved and divergent roles of FGF signaling in mouse epiblast stem cells and human embryonic stem cells. *Cell Stem Cell*. 2010; 6(3): 215-226. https://doi.org/10.1016/j.stem.2010.01.003

[18] Matsuda M, Hayashi H, Garcia-Ojalvo J, Yoshioka-Kobayashi K, Kageyama R, Yamanaka Y, Ikeya M, Toguchida J, Alev C, Ebisuya M. Species-specific segmentation clock periods are due to differential biochemical reaction speeds. *Science*. 2020; 369(6510): 1450-1455. https://doi.org/doi:10.1126/science.aba7668

[19] European Parliament and of the Council. Consolidated text: Directive 2010/63/EU of the European Parliament and of the Council of 22 September 2010 on the protection of animals used for scientific purposes. Off J Eur Union. 2010; L 276: 233–279. Available from: https://eur-lex.europa.eu/legal-content/EN/TXT/?uri=CELEX:02010L0063-20190626

[20] Hill EJ, Woehrling EK, Prince M, Coleman MD. Differentiating human NT2/D1 neurospheres as a versatile in vitro 3D model system for developmental neurotoxicity testing. *Toxicology*. 2008; 249 (2-3): 243-250. https://doi.org/10.1016/j.tox.2008.05.014

[21] Cacciotti I, Ceci C, Bianco A, Pistritto G. Neuro-differentiated Ntera2 cancer stem cells encapsulated in alginate beads: First evidence of biological functionality. *Mater Sci Eng C Mater Biol Appl*. 2017; 81: 32-38. https://doi.org/10.1016/j.msec.2017.07.033

[22] Radonjić M, Petrović J, Milivojević M, Stevanović M, Stojkovska J, Obradović B. Chemical engineering methods in analyses of 3D cancer cell cultures: Hydrodinamic and mass transport considerations. *Chem Ind Chem Eng Q*. 2022; 28(3): 211-223. https://doi.org/10.2298/CICEQ210607033R

[23] Sun J, Tan H. Alginate-Based Biomaterials for Regenerative Medicine Applications. *Materials (Basel)*. 2013; 6(4): 1285-1309. https://doi.org/10.3390/ma6041285PMC5452316

[24] Mead EA, Wang Y, Patel S, Thekkumthala AP, Kepich R, Benn-Hirsch E, Lee V, Basaly A, Bergeson S, Siegelmann HT, Pietrzykowski AZ. miR-9 utilizes precursor pathways in adaptation to alcohol in mouse striatal neurons. *Adv Drug Alcohol Res*. 2023; 3: 11323. https://doi.org/10.3389/adar.2023.11323PMC10730111

[25] Doyle W, Shide E, Thapa S, Chandrasekaran V. The effects of energy beverages on cultured cells. *Food Chem Toxicol*. 2012; 50(10): 3759-3768. https://doi.org/10.1016/j.fct.2012.07.008

[26] Mosmann T. Rapid colorimetric assay for cellular growth and survival: application to proliferation and cytotoxicity assays. *J Immunol Methods*. 1983; 65(1-2): 55-63. https://doi.org/10.1016/0022-1759(83)90303-4

[27] Stojkovska JJ, Zvicer J, Milivojevic M, Petrovic I, Stevanovic M, Obradovic B. Validation of a novel perfusion bioreactor system in cancer research. *Hem Ind*. 2020; 74(3): 187-196. https://doi.org/10.2298/HEMIND200329015S

[28] Saltzman WM, Kyriakides TR. Cell interactions with polymers. In: Lanza R, Langer R, Vacanti JP, Atala A, eds. *Principles of Tissue Engineering* 5th ed. Cambridge, MA: Academic Press; 2020: 275-293. https://doi.org/10.1016/B978-0-12-818422-6.00017-4

[29] Nebel S, Lux M, Kuth S, Bider F, Dietrich W, Egger D, Boccaccini AR, Kasper C. Alginate Core-Shell Capsules for 3D Cultivation of Adipose-Derived Mesenchymal Stem Cells. *Bioengineering (Basel)*. 2022; 9(2): 66. https://doi.org/10.3390/bioengineering9020066PMC8869374

[30] Rodriguez S, Lau H, Corrales N, Heng J, Lee S, Stiner R, Alexander M, Lakey JRT. Characterization of chelator-mediated recovery of pancreatic islets from barium-stabilized alginate microcapsules. *Xenotransplantation*. 2020; 27(1): e12554. https://doi.org/10.1111/xen.12554

[31] Vo P, Nguyen S, Minh Do N, Truong K, Pham P. Sodium citrate inhibits proliferation and induces apoptosis of hepatocellular carcinoma cells. *Biomed Res Ther*. 2020; 7: 3659-3666. https://doi.org/10.15419/bmrat.v7i3.592

[32] Wu Y, Jia C, Liu W, Zhan W, Chen Y, Lu J, Bao Y, Wang S, Yu C, Zheng L, Sun L, Song Z. Sodium citrate targeting Ca(2+)/CAMKK2 pathway exhibits anti-tumor activity through inducing apoptosis and ferroptosis in ovarian cancer. *J Adv Res*. 2024; 65: 89-104. https://doi.org/10.1016/j.jare.2024.04.033PMC11518946

[33] Burger H, Nooter K, Boersma AW, Kortland CJ, Stoter G. Expression of p53, Bcl-2 and Bax in cisplatin-induced apoptosis in testicular germ cell tumour cell lines. *Br J Cancer*. 1998; 77(10): 1562-1567. https://doi.org/10.1038/bjc.1998.257PMC2150079

[34] Kitano O, Nakazawa K. Neuronal Differentiation of NT2 Cells in Monolayer and Spheroid Cultures. *MATEC Web Conf*. 2021; 333: 07008. https://doi.org/10.1051/matecconf/202133307008

[35] Hirschhaeuser F, Menne H, Dittfeld C, West J, Mueller-Klieser W, Kunz-Schughart LA. Multicellular tumor spheroids: an underestimated tool is catching up again. *J Biotechnol*. 2010; 148(1): 3-15. https://doi.org/10.1016/j.jbiotec.2010.01.012

[36] Pinto B, Henriques AC, Silva PMA, Bousbaa H. Three-Dimensional Spheroids as In Vitro Preclinical Models for Cancer Research. *Pharmaceutics*. 2020; 12(12): 1186. https://doi.org/10.3390/pharmaceutics12121186PMC7762220

[37] Han YL, Wang S, Zhang X, Li Y, Huang G, Qi H, Pingguan-Murphy B, Li Y, Lu TJ, Xu F. Engineering physical microenvironment for stem cell based regenerative medicine. *Drug Discov Today*. 2014; 19(6): 763-773. https://doi.org/10.1016/j.drudis.2014.01.015

[38] Nicodemus GD, Bryant SJ. Cell encapsulation in biodegradable hydrogels for tissue engineering applications. *Tissue Eng Part B Rev*. 2008; 14(2): 149-165. https://doi.org/10.1089/ten.teb.2007.0332PMC2962861

[39] Tibbitt MW, Anseth KS. Hydrogels as extracellular matrix mimics for 3D cell culture. *Biotechnol Bioeng*. 2009; 103(4): 655-663. https://doi.org/10.1002/bit.22361PMC2997742

[40] Vergani L, Grattarola M, Nicolini C. Modifications of chromatin structure and gene expression following induced alterations of cellular shape. *Int J Biochem Cell Biol*. 2004; 36(8): 1447-1461. https://doi.org/10.1016/j.biocel.2003.11.015

[41] Demircan Yalcin Y, Luttge R. Electrical monitoring approaches in 3-dimensional cell culture systems: Toward label-free, high spatiotemporal resolution, and high-content data collection in vitro. *Organs-on-a-Chip*. 2021; 3: 100006. https://doi.org/https://doi.org/10.1016/j.ooc.2021.100006

[42] Hagiwara M, Nobata R, Kawahara T. High repeatability from 3D experimental platform for quantitative analysis of cellular branch pattern formations. *Integr Biol (Camb)*. 2018; 10(5): 306-312. https://doi.org/10.1039/c8ib00032h

[43] Jensen C, Teng Y. Is It Time to Start Transitioning From 2D to 3D Cell Culture? *Front Mol Biosci*. 2020; 7: 33. https://doi.org/10.3389/fmolb.2020.00033PMC7067892

[44] Eftekharzadeh B, Khodagholi F, Abdi A, Maghsoudi N. Alginate protects NT2 neurons against H2O2-induced neurotoxicity. *Carbohydr Polym*. 2010; 79(4): 1063-1072. https://doi.org/https://doi.org/10.1016/j.carbpol.2009.10.040

[45] Feng WJ, Mou J, Liao PP, Zhou J, Zhang NN, Hu T, Wang S, Zhang SY, Mao YJ. Alginate oligosaccharides exert protective effects on hydrogen peroxide-induced senescence in H9C2 cardiomyocytes by regulating the redox state of cells. *Food Sci Biotechnol*. 2024; 33(12): 2835-2844. https://doi.org/10.1007/s10068-024-01534-yPMC11339193

[46] Saleh EM, Hamdy GM, Hassan RE. Neuroprotective effect of sodium alginate against chromium-induced brain damage in rats. *PLoS One*. 2022; 17(4): e0266898. https://doi.org/10.1371/journal.pone.0266898PMC9009676

[47] Krahe TE, Filgueiras CC, da Silva Quaresma R, Schibuola HG, Abreu-Villaça Y, Manhães AC, Ribeiro-Carvalho A. Energy drink enhances the behavioral effects of alcohol in adolescent mice. *Neurosci Lett*. 2017; 651: 102-108. https://doi.org/https://doi.org/10.1016/j.neulet.2017.04.050

[48] Richards G, Smith AP. A Review of Energy Drinks and Mental Health, with a Focus on Stress, Anxiety, and Depression. *J Caffeine Res*. 2016; 6(2): 49-63. https://doi.org/10.1089/jcr.2015.0033PMC4892220

[49] Graneri L, Lam V, D'Alonzo Z, Nesbit M, Mamo JCL, Takechi R. The Consumption of Energy Drinks Induces Blood-Brain Barrier Dysfunction in Wild-Type Mice. *Front Nutr*. 2021; 8: 668514. https://doi.org/10.3389/fnut.2021.668514PMC8126614

[50] Petribu BN, Abrahao KP, Souza-Formigoni MLO. Ethanol combined with energy drinks: Two decades of research in rodents. *Front Behav Neurosci*. 2022; 16: 1100608. https://doi.org/10.3389/fnbeh.2022.1100608PMC10017554

[51] *MATLAB Release 2018a* [computer program]. Natick, MA: The MathWorks, Inc.; 2018. https://www.mathworks.com/

[52] Chern J-M, Lee W-F, Hsieh M-Y. Absorption Isotherm of Caffeine and Release Kinetics from Swollen NIPAAm Hydrogels: Experiments and Modeling. *Ind Eng Chem Res*. 2004; 43(19): 6150-6156. https://doi.org/10.1021/ie049616d
[53] Rodak K, Kokot I, Kratz EM. Caffeine as a Factor Influencing the Functioning of the Human Body-Friend or Foe? *Nutrients*. 2021; 13(9): 3088. https://doi.org/10.3390/nu13093088PMC8467199
[54] Estapé D, Gòdia F, Solà C. Determination of glucose and ethanol effective diffusion coefficients in Ca-alginate gel. *Enzyme Microb Technol*. 1992; 14(5): 396-401. https://doi.org/10.1016/0141-0229(92)90009-d
[55] Jain M, Nilsson R, Sharma S, Madhusudhan N, Kitami T, Souza AL, Kafri R, Kirschner MW, Clish CB, Mootha VK. Metabolite profiling identifies a key role for glycine in rapid cancer cell proliferation. *Science*. 2012; 336(6084): 1040-1044. https://doi.org/10.1126/science.1218595PMC3526189
[56] Zhao F, Pathi P, Grayson W, Xing Q, Locke BR, Ma T. Effects of oxygen transport on 3-d human mesenchymal stem cell metabolic activity in perfusion and static cultures: experiments and mathematical model. *Biotechnol Prog*. 2005; 21(4): 1269-1280. https://doi.org/10.1021/bp0500664
[57] Urzì O, Gasparro R, Costanzo E, De Luca A, Giavaresi G, Fontana S, Alessandro R. Three-Dimensional Cell Cultures: The Bridge between In Vitro and In Vivo Models. *Int J Mol Sci*. 2023; 24(15): 12046. https://doi.org/10.3390/ijms241512046PMC10419178
[58] Andrews PW. Retinoic acid induces neuronal differentiation of a cloned human embryonal carcinoma cell line in vitro. *Dev Biol*. 1984; 103(2): 285-293. https://doi.org/10.1016/0012-1606(84)90316-6

Humane pluripotentne NT2/D1 ćelije imobilizovane u alginatnim mikrovlaknima: 3D sistem za testiranje uticaja bioaktivnih jedinjenja

Jelena Lj. Pejić[1], Milena C. Milivojević[1], Marija L. Schwirtlich[1], Jelena S. Petrović[2,3], Jasmina J. Stojkovska[2], Milena J. Stevanović[1,4,5] i Marija M. Mojsin[1]

[1]Univerzitet u Beogradu, Institut za molekularnu genetiku i genetičko inženjerstvo, Beograd, Srbija
[2]Univerzitet u Beogradu, Tehnološko-metalurški fakultet, Beograd, Srbija
[3]Inovacioni centar Tehnološko-metalurškog fakulteta, Beograd, Srbija
[4]Univerzitet u Beogradu, Biološki fakultet, Beograd, Srbija
[5]Srpska akademija nauka i umetnosti, Beograd, Srbija

(Naučni rad)

Izvod

Učestala konzumacija energetskih pića (engl. *energy drinks-ED*) i njihova kombinacija sa alkoholom (engl. *energy drinks mixed with alcohol-AmED*) postala je rastući trend među mladim ljudima. Proklamovano povećanje psihičkih i fizičkih performansi usled konzumiranja ED, koji u svom sastavu sadrže visoke doze stimulativnih sastojka - kofeina i taurina, može dovesti do neželjenih posledica, prvenstveno na funkcije centralnog nervnog sistema (CNS) i kardiovaskularnog sistema. Uprkos ključnoj ulozi u razviću i adultnoj homeostazi, istraživanja o potencijalnom efektu konzumacije ED i AmED na matične i progenitorske ćelije su malobrojne. U radu je predstavljena optimizacija 3D model sistema na bazi alginatnih mikrovlakana za testiranje uticaja bioaktivnih jedinjenja na humane NT2/D1 embrionalne karcinomske ćelije, široko korišćeni model sistem kao pandan humanim matičnim ćelijama. Ispitan je uticaj akutne konzumacije ED i AmED na vijabilnost ovih ćelija i uz pomoć matematičkog modelovanja evaluirana je efikasnost prenosa mase ispitivanih komponenti do imobilisanih ćelija. Dobijeni rezultati pokazuju da ovaj model sistem omogućava optimalan rast i proliferaciju NT2/D1 pluripotentnih ćelija i uniformnu distribuciju ispitivanih komponenti kroz alginatna mikrovlakna. Simulirana akutna konzumacija ED i AmED nije uticala na vijabilnost NT2/D1 ćelija u 3D sistemu, za razliku od 2D modela gde je kofein doveo do malog ali statistički značajnog pada vijabilnosti.

Ključne reči: humane embrionalne karcinomske ćelije; alginatni hidrogel; ćelijska vijabilnost; prenos mase; energetska pića; kofein

Effect of pretreatment, lyophilization parameters and different cryoprotectants on the efficiency of probiotic freeze-drying immobilization

Tanja Ž. Krunić[1] and Andrea M. Osmokrović[2]

[1]*Innovation Centre of the Faculty of Technology and Metallurgy, Belgrade, Serbia*
[2]*University of Belgrade, Faculty of Technology and Metallurgy, Belgrade, Serbia*

Abstract

Lyophilization is an excellent process to increase the shelf life of food products or preserve probiotics. Living cells prefer mild conditions, and any deviation (vacuum, high or low temperatures) leads to cell damage. This paper examined the influence of different freeze-drying process parameters on the survival of probiotic *Lactobacillus plantarum* immobilized on the activated charcoal pad. In specific, the process included several phases in which different pretreatments, freezing temperatures, cryoprotectants and phase durations were investigated. Activation of *L. plantarum* in De Man, Rogosa and Sharpe (MRS) broth before freezing, resulted in the increased initial number of living cells, but also positively affected the cell survival after the lyophilization process. Freezing the culture in liquid nitrogen did not significantly affect cell viability after lyophilization compared to deep freezing at -80 °C, while incubation of the culture in a refrigerator for 2 h before lyophilization increased the probiotic viability. Also, the prolonged duration of lyophilization from 5 to 48 h had a slight impact on probiotic viability. The use of milk showed a significant increase in culture survival, while sucrose, maltose, and trehalose showed cryoprotectant ability, but significantly lower than that of milk. The best lyophilization protocol resulting in the highest viability of *L. plantarum* included the culture activation by MRS incubation, followed by either deep freezing in liquid nitrogen or by precooling for 2 h at 7 °C and then deep freezing at -80 °C in milk, and ending with lyophilization for 5 h.

Keywords: Lactobacillus plantarum; viability; milk; liquid nitrogen; preservation

Available on-line at the Journal web address: http://www.ache.org.rs/HI/

ORIGINAL SCIENTIFIC PAPER

UDC: 664.8.047+579.864

Hem. Ind. **79(3)** 157-165 (2025)

1. INTRODUCTION

Cell preservation is one of the main challenges in the development of efficient probiotic systems aimed at different applications, such as pharmaceuticals, functional foods, *etc*. The primary goal of preserving cells is to maintain their viability while ensuring that their biochemical, morphological, physiological, and genetic characteristics are not altered [1]. Even though there are several efficient cell preservation strategies, lyophilization or freeze-drying is considered the gold standard in the biopharmaceutical sector, especially when the goal is to preserve sensitive microbial cells. During the process of freeze-drying, bacterial cells are exposed to low temperatures and consequent removal of water within the cells. However, the freezing step may lead to cellular damage due to the formation of ice crystals and osmotic stresses. To protect cells against such damage, different protectants may be added to the drying media. The role of protectants is to stabilize the cells during water removal and to provide a good matrix that allows shape maintenance of the entire sample during and after processing. In this way, protectants conserve viability of the cells and allow their stability and easy rehydration. Many different substances have been used for testing protective ability, including skimmed milk, polyols, polysaccharides, disaccharides, amino acids, proteins, minerals, salts of organic acids, vitamins, *etc*. [2-4]. However, sensitive microorganisms like lactic acid bacteria (LAB), even in the presence of effective protectants, can lose viability and stability [5] since the microbial cell survival during this process is dependent on other

Corresponding authors: Tanja Ž. Krunić, Innovation Center of the Faculty of Technology and Metallurgy, Karnegijeva 4, 11000 Belgrade
E-mail: tkrunic@tmf.bg.ac.rs
Paper received: 2. April 2025; Paper accepted: 7 June 2025; Paper published: 26 June 2025.
https://doi.org/10.2298/HEMIND250402010K

factors as well, such as the initial microorganism concentration, growth conditions, freezing rate, rehydration conditions, *etc.* [6,7].

To overcome these limitations, novel methodologies have been sought, and one of the simple approaches is immobilization of microorganisms on different carriers *via* physical or chemical methods [8]. Unlike free cells, immobilized microorganisms exhibit higher cell density and biological activity as well as higher resistance to environmental influences [9]. However, viability and function of the immobilized microorganisms are affected by the type of carrier used [10]; therefore, selecting an appropriate carrier for immobilization of microorganisms is crucial. Carbon materials such as granular activated charcoal, biochar, carbon nanotubes, graphene, and their derivatives are widely used for adsorbing pathogenic microorganisms in wastewater treatment and purification. Their high mechanical strength, well-developed porosity, large specific surface area, and tunable surface chemistry make them particularly suitable for microbial attachment [9]. Moreover, these materials are shown to support the stability and viability of immobilized microorganisms [11-14], which have been extensively investigated for biodegradation of different contaminants in water and soil. To a much lesser extent, carbonaceous materials have been used in other fields, including biomedical applications. For example, activated carbon fabric (ACF) has been examined for cell therapy and stem cell culture support [15] which shows that these materials are not just excellent carriers for prokaryotic but for eukaryotic cells as well. In addition, immobilized bacteria have been observed to continue to multiply on activated charcoal and, over time, release into the surrounding solution [16] which suggests that carbon materials hold significant potential for broader biomedical applications, including the development of efficient delivery systems for live biological agents.

The aim of this study was to investigate functionalization of ACF with probiotic microorganisms and to evaluate the influence of various factors on the survival rate of immobilized cells during freeze-drying. Precisely, the aim was to immobilize probiotics by simple adsorption onto ACF, freeze-dry produced biocomposites, and afterwards investigate the cell viability in physiologically relevant solutions. In addition, the aim was also to examine different factors that influence the survival rate of freeze-dried immobilized microbes, such as initial growth conditions, different freezing temperatures, duration of the freeze-drying process, efficacy of different protective agents, as well as modification of the environmental factors e.g. temperature. In this study, we used the bacteria strain *Lactobacillus plantarum* 299v (*Lp*299v) as a model microorganism, a typical representative of probiotic bacteria which has been extensively characterized in the literature and widely used in medicine.

2. EXPERIMENTAL

2. 1. Bacterial strain

Lactobacillus plantarum (LAB *Lp299v* DSM 9843) stabilized with starch (Flobian®, Abela Pharm, Croatia) in the form of lyophilized powder was directly dissolved in 10 mL of normal saline solution (NS) (0.9 % w/v NaCl), diluted 1:100 and further used either for immobilization or for preparation of frozen stock as described previously [17]. Bacteria from the frozen stock were later incubated under anaerobic conditions in De Man, Rogosa and Sharpe (MRS) broth (Torlak, Serbia) at 37 °C for 18 h two times consecutively and then washed in 10 mL of NS 3 times. The obtained cultures, non-activated (directly from lyophilized powder) and activated ones (from frozen stock), respectively, were then centrifuged at 4000 rpm for 5 min, and bacterial pellets were further re-suspended in 1 ml of different freeze-drying media with/without protectant ability.

2. 2. Freeze-drying medium

Four different variants of freeze-drying medium with protectant ability were used: 10 % w/v skimmed milk (Imlek, Serbia), 10 % w/v sucrose (Centrohem, Serbia), 10 % w/v trehalose dehydrate (Carl Roth, Germany), and 30 % w/v maltose monohydrate (Carl Roth, Germany). Suspensions of freeze-drying media with disaccharides (sucrose, trehalose, and maltose) were prepared in NS. Two freeze-drying media were used as controls: NS, which does not exhibit protectant ability, and formulation Reagent 18 (R18) recommended by the American Type Culture Collection (ATCC), which generates samples that freeze dry well and are very effectively preserved. Precisely, R18 is prepared by mixing 0.75 g trypticase

soy (TS) broth (Torlak, Serbia), 10 g sucrose, and 5 g bovine serum albumin fraction V (Sigma, USA) to 100 mL deionized water [17]. All freeze-drying media were filter-sterilized through a 0.2 µm filter before mixing with cells.

2. 3. Immobilization of bacterial cells on activated carbon pads

Activated carbon (AC) pads were prepared in a circular shape (12 mm in diameter, 0.5 mm thick) by punching from ACF (ConvaTec, USA). The obtained pads were placed in a glass Petri dish, sterilized by hot air at 160 °C for 2 h, and then used for immobilization of bacterial cells. Concretely, 100 µl of a freeze-drying medium mixed with cells (concentration 10^7 and 10^{10} for non-activated and activated cultures, respectively) was aseptically added on top of each pad and left to settle for 15 min at room temperature.

2. 4. Freeze-drying

The samples were put in a plastic Petri dish and freeze-dried using a freeze dryer, Beta 2-8 LD plus (Christ, Germany). The freeze-drying parameters and the influence of pretreatments were investigated in three experimental series.

In the first experimental series, AC pads with immobilized non-activated probiotics with different protectants (skimmed milk, R18, or 10 % sucrose) or without (NS only) were frozen at -80 °C and then freeze-dried for either 5 h or 48 h (-40 °C, 12 Pa).

In the second experimental series, AC pads with immobilized activated probiotics with different protectants (skimmed milk, R18, 10 % trehalose, or 30 % maltose) or without (NS only) were frozen in liquid nitrogen and then freeze-dried for 5 h (-40 °C, 12 Pa)

In the third experimental series, AC pads with immobilized activated probiotics with a protectant (skimmed milk) or without (NS only) were precooled at 7°C for either 2 h or 10 h, followed by freezing at -80 °C and then freeze-dried for 5 h (- 40 °C, 12 Pa).

The design of all three experimental series is presented in Figure 1. AC pads with immobilized cells after freeze-drying were gold-coated and visualized by a MIRA 3 XMU Field Emission Scanning Electron Microscope (Tescan USA Inc., Cranberry Twp, PA).

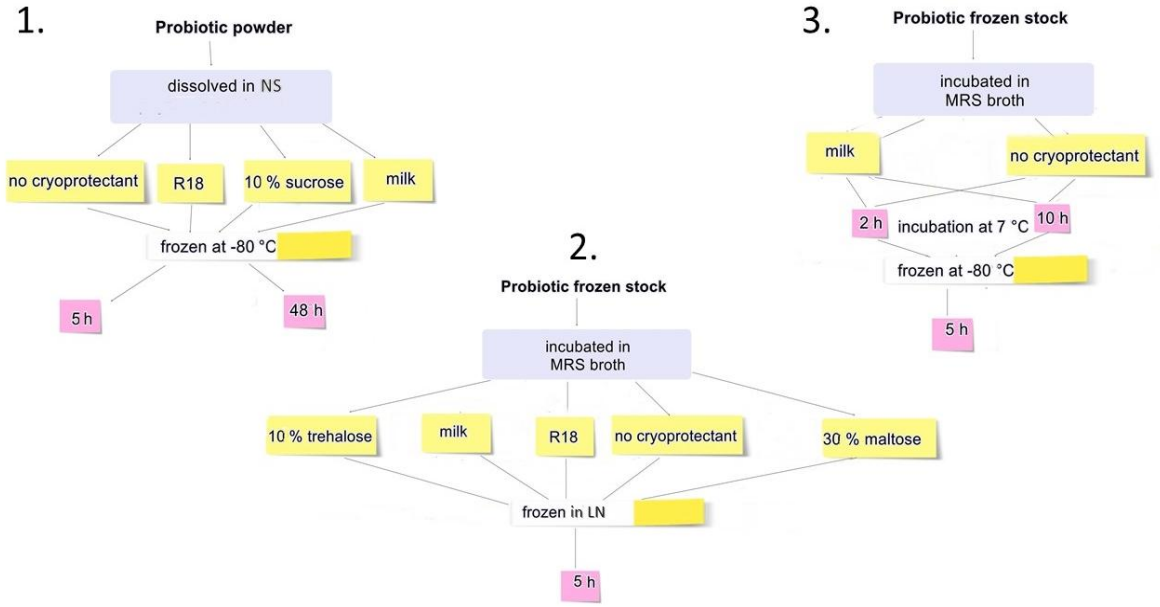

Figure 1. Scheme of the study, divided into three phases (NS is normal saline solution and LN is liquid nitrogen)

2. 5. Determination of cell viability after the freeze-drying process

The pads with the immobilized probiotic after freeze-drying were incubated in 2 ml of NS each at 37 °C for 10 min and then examined for live cells. The cell number was determined by the pour plate counting method and was expressed in $\log_{10}$ CFU/ml.

2. 6. Statistical analysis

Experiments were performed in triplicate. All values are expressed as a mean ± standard deviation. Mean values were analyzed using one-way ANOVA. The Tukey post hoc test was performed for means comparison (Origin Pro 8 software package) [18]. Data was considered significantly different when p <0.05.

3. RESULTS AND DISCUSSION

AC pads made by punching were approximately 12 mm in diameter (Fig. 2) and weighed 0.017 ± 0.001 g. Immobilization was achieved by simple seeding of bacterial cell suspensions with/without protectants on each AC pad (100 µl). Immobilized cells without protectants were visualized after freeze-drying by field emission scanning electron microscopy (FE-SEM, Fig. 2).

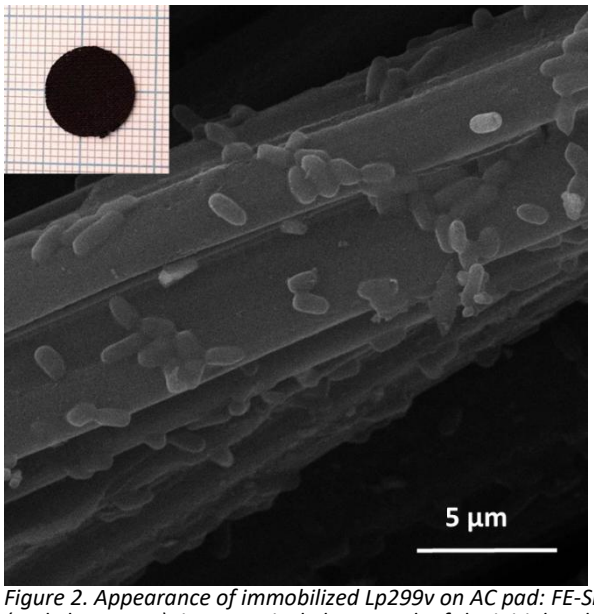

Figure 2. Appearance of immobilized Lp299v on AC pad: FE-SEM micrograph of the pad after lyophilization without any protectant (scale bar: 5 µm); inset: optical photograph of the initial pad

In our study, ACF has been chosen as a suitable carrier for freeze-drying of immobilized probiotics because carbon materials are shown to be excellent thermal conductors that secure proper thermal distribution into the samples, thus reducing the chance of damaging the cells [19].

In the first experimental series, non-activated probiotic cells were successfully immobilized on AC pads in a concentration of approximately 10^6 CFU/pad, and samples were freeze-dried for either 5 or 48 h. Skimmed milk and sucrose were used as protective agents, while the controls were R18 and NS. The resulting cell viabilities are shown in Figure 3.

Skimmed milk and R18 showed the highest protective capacity with approximately 87 % probiotic viability after the first time point in comparison to approximately 62 and 77 % for samples without protectant and the ones with sucrose, respectively. However, prolongation of freeze-drying up to 48 h adversely affected viability of the immobilized bacteria in all tested samples except in the ones containing R18. *Oluwatosin et al*. also demonstrated that skimmed milk exhibited the highest protective effect on *L. plantarum* during freeze-drying compared to various saccharides. Specifically, 10 % (m/v) skimmed milk, inulin, maltodextrin, and sucrose were evaluated as protective agents, and among the saccharides tested, inulin provided the highest protective capacity [20].

The standard protocol for lyophilization of cells in a vial implies a duration of the process of 18 h [17]. However, lyophilization is a very energy-consuming process and one of the ways to freeze-dry faster is to increase the surface area of the frozen sample by spreading out the sample and pre-freezing it in a thin layer thus allowing a larger contact for heat input as well as shorter distances in which the drying front has to move through the sample.

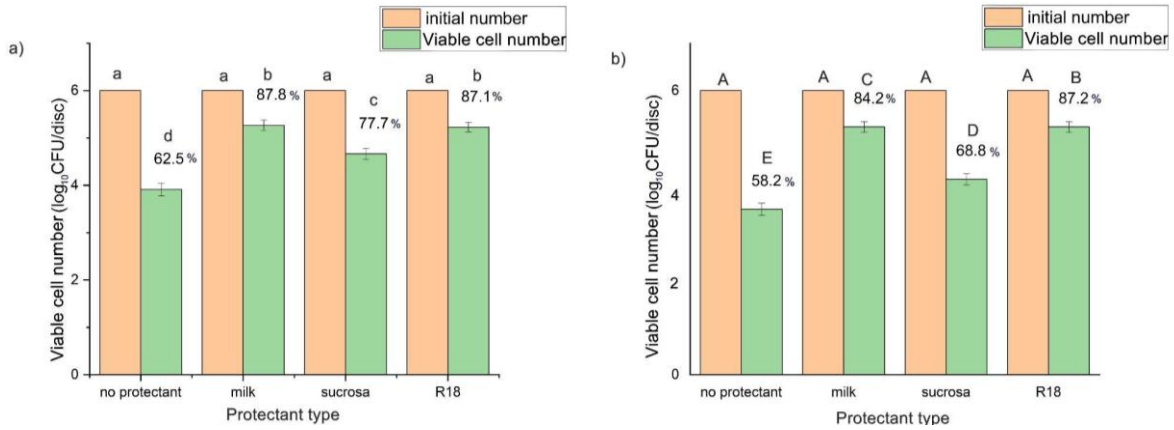

Figure 3. Viable cell number before and after lyophilization of samples with or without a protective agent (milk, sucrose, and R18), frozen at -80 °C and lyophilized for: a) 5 h, b) 48 h (experimental values are mean ± standard deviation (SD < 2 %) of n=3). Statistically different groups are marked with different letters

Since our samples were in the form of thin discs with the external surface area of approximately 1 cm^2 (Fig. 2), reduction of freeze-drying time was suitable. This was confirmed by the obtained results, which showed that a lyophilization time of 5 h is more favorable than a longer period of 48 h. Furthermore, in this experimental series it was noticed that samples containing sucrose were very difficult to manipulate because of the stickiness and stiffness of the material. So, even though sucrose is the most commercially used protectant for freeze-drying probiotic cultures in pharmaceutical products, we had to substitute it with other disaccharides instead.

To enhance bacterial viability during the freeze-drying process, approximately 18 h-old bacterial cultures are usually used [17]. So, in the next step, we examined freeze-drying of the immobilized activated culture. Activated probiotic cells were successfully immobilized in a concentration of approximately 10^9 CFU/pad. Freezing sensitive and high-value materials such as biological formulations, vaccines, bacteria, viruses, *etc*., in liquid nitrogen is the best way to preserve materials that cannot withstand oxygen or heat. Since *Lactobacillus* spp. is microaerophilic, in this experimental series the samples were immediately frozen at an ultra-low temperature. Skimmed milk, trehalose, and maltose were used as protective agents while the controls were R18 and NS. Trehalose is an exceptional and extensively used protectant in the food, medical, pharmaceutical, and cosmetic industries. Even though modern advancements in enzyme production technology have significantly decreased the production costs of trehalose, it is still more costly than common sugars like glucose or sucrose. However, lower-priced maltose in a concentration of 30 % w/v was shown to be a good alternative to trehalose in lyophilizing sensitive biological materials [21]. The obtained results are shown in Figure 4.

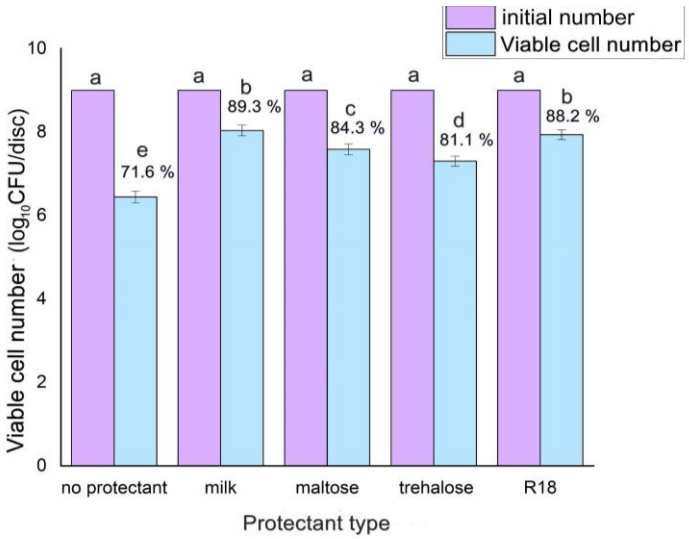

Figure 4. Viable cell numbers before and after 5 h of lyophilization for samples with or without a protective agent (milk, maltose, trehalose, and R18), frozen in liquid nitrogen (experimental values are mean ± standard deviation (SD < 2 %) of n = 3). Statistically different groups are marked with different letters

As expected, activation of probiotics (cultivation in MRS broth 2 times, consequently for 18 h) increased the total initial number of living bacteria and consequently the number of immobilized cells per pad (approximately 10^9 CFU/pad for activated culture *vs*. approximately 10^6 CFU/pad for non-activated ones). Effects of activation on the cell survival after the lyophilization process could be seen by comparing Figures 3a and 4. In specific, the largest increase in cell viability as a consequence of activation was achieved in samples without a protectant (from 62.5 to 71.6 %, *i.e.* ~10 % increase). In the case of skimmed milk and R18, the increase was negligible by 1 to 2 % (from 87.8 to 89.3 % for milk and from 87.1 to 88.2 % for R18). In the case of samples containing disaccharides, the increase in cell viability compared to non-activated cell samples in sucrose was modest, ranging from approximately 4% to 8%. The obtained results show that skimmed milk and R18 still had the highest level of protection, and that activation of probiotics as well as freezing in liquid nitrogen had only a minor beneficial influence with respect to cell viability (up to 2 %). However, the total initial number of immobilized cells is significantly higher as a result of activation, which enables the cells to have greater potential to exhibit their beneficial effect in later use. The use of trehalose and maltose with prior activation of the bacteria, as well as immediate freezing at ultra-low temperatures, resulted in much better survival compared to the use of sucrose as a protectant without cell activation. This increase can be attributed to the activation of bacteria and the use of liquid nitrogen rather than the protectant itself, since there was a significant viability increase of almost 10 % in the samples with cells alone without any protectant (Figure 3a and 4). In addition, maltose, similarly to sucrose, also showed undesirable properties, namely the stickiness and stiffness of the samples. Since the freezing step is critical in the lyophilization process due to potential cell damage, different freezing strategies are explored in the literature. For example, in a recent study the authors investigated the effects of pre-freezing at -80 *vs*. -196 °C in liquid nitrogen on the quality and storage stability of several probiotic cultures, including *L. plantarum* CN2018, and found that the latter pre-freezing did not cause cell death during the freezing phase [22]. However, in case of some probiotic strains (*e.g. B. breve* CCFM1025) liquid nitrogen pre-freezing increased the melting enthalpy of the cell suspension and consequently decreased the survival rate, which suggests that the impact of pre-freezing methods on probiotic viability following lyophilization is strain-dependent [22].

In the third experimental series, activated probiotic cells were successfully immobilized in a concentration of approximately 10^9 CFU/pad. The samples were first precooled at 7°C for either 2 h or 10 h, followed by freezing of the samples at -80 °C. This freezing temperature was chosen since freezing in liquid nitrogen did not show significant beneficial effects on cell survival in samples with milk and R18, and at the same time, it is economically very demanding. Skimmed milk was used as a protectant while NS was used as a control. The results of this experimental series are shown in Figure 5.

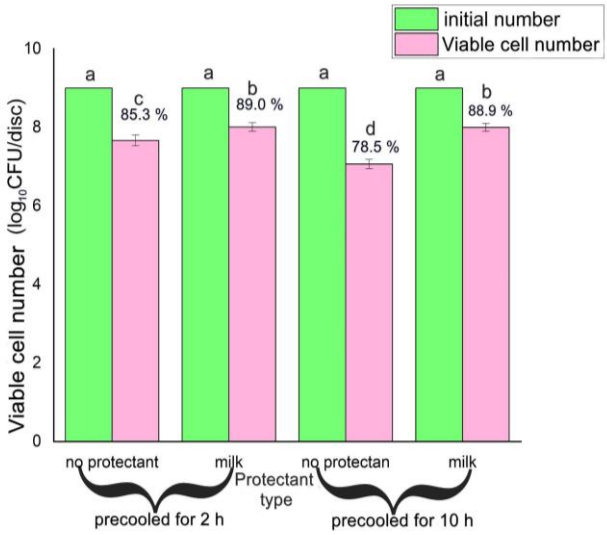

Figure 5. Viable cell numbers before and after 5h of lyophilization for samples with and without a protective agent (milk), precooled for 2 h or 10 h, at 7 °C before freezing at -80 °C (experimental values are mean ± standard deviation (SD < 2 %) of n = 3). Statistically different groups are marked with different letters

Precooling of the samples at 7 °C for both durations contributed significantly to the survival of the probiotics without a protectant added and resulted in even better survival than in the case of freezing in liquid nitrogen (85.3 and 78.5% *vs*. 71.6 % for precooling for 2 and 10 h *vs*. freezing in liquid nitrogen, respectively). These results are in accordance with literature data, which show that cryotolerance can be acquired after an adaptation period. Concretely, the viability of *Lactococcus lactis* subsp. *lactis* cultured at 37 °C improved significantly after it was cold shocked at 10 °C for 2 h prior to freezing at -20 °C [23,24]. It is well known that microorganisms can adapt to environmental stresses by the induction of proteins and other products. So, by modification of the cell environment, such as temperature, the composition of cells can be phenotypically altered in a number of ways, which can play a role in the resistance to freezing [25]. Although cooling prior to pre-freezing and lyophilization positively affects cell viability and the overall efficiency of the lyophilization process, the duration of exposure to low temperatures before freezing at -80 °C plays a critical role. In the experiment conducted, as shown in Figure 6, keeping the bacteria at 7 °C for 10 h proved to be too long, yielding poorer results compared to a 2 h cooling period.

Interestingly, survival of probiotics protected with milk was the same in the case of precooling and freezing at -80 °C as in the case of freezing in liquid nitrogen without the precooling step (Figs. 4 and 5), which confirms that precooling can be a very efficient and at the same time inexpensive strategy inducing cryoresistance in LAB.

4. CONCLUSION

This study investigated the influence of different pretreatment procedures, freeze-drying durations, freezing modes, and protective agents on the survival of immobilized probiotics. Pretreatments such as activation of *Lp*299v in MRS broth and precooling, as well as freezing at ultra-low temperatures, significantly affected the survival of immobilized cells without any protective agent. The activation of probiotics was shown to be an important pretreatment step because it increased the initial number of live bacteria and consequently the number of cells immobilized on the ACF. This study also showed that precooling is very beneficial in inducing cryo-resistance and that, in comparison to costly freezing in liquid nitrogen, it results in higher survival in the case of samples without any protectant. However, all these beneficial effects are not so pronounced in the samples protected with skimmed milk and formulation R18, which both exhibited very high protective ability. Furthermore, skimmed milk was shown to be equally efficient providing the same degree of protection for a short 5-hour freeze-drying time as the costly formulation R18. Since it is inexpensive and widely available, it is a better option for the protection of immobilized cells on ACF. To sum up, activation, short precooling treatment with skimmed milk as a protective agent, resulted in a very high total number of immobilized live cells after deep freezing and consequent 5 h freeze-drying. Thus, this process enables a greater capacity of microbial cells to exhibit their positive effects in potential pharmaceutical and medical applications.

Acknowledgement: *This research was supported by the Science Fund of the Republic of Serbia, Grant No 9802, Activated Charcoal as a Carrier of Probiotics: A New Approach for Pathogen Elimination in Wounds-ProHealingAC.*

REFERENCES

[1] Malik KA. Survival and stability of microorganisms during freeze-drying. *Cryobiology.* 1988; 25(6): 517-518. https://doi.org/10.1016/0011-2240(88)90324-0

[2] Champagne CP, Gardner N., Brochu E., Beaulieu Y. The freeze-drying of lactic acid bacteria. *Can Inst Food Technol J.* 1991; 24: 118-128. https://doi.org/10.1016/S0315-5463(91)70034-5

[3] Hubálek Z. Protectants used in the cryopreservation of microorganisms. *Cryobiology.* 2003; 2003; 46: 205-229. https://doi.org/10.1016/S0011-2240(03)00046-4

[4] Alonso S. Novel Preservation Techniques for Microbial Cultures. in Ojha K, Tiwari B, eds. *Novel Food Fermentation Technologies. Food Engineering Series*. Springer; 2016: 8-33. https://doi.org/10.1007/978-3-319-42457-6_2

[5] Carvalho AS, Silva J, Ho P, Teixeira P, Malcata FX, Gibbs P. Relevant factors for the preparation of freeze-dried lactic acid bacteria. *Int Dairy J*. 2004; 14: 835-847. https://doi.org/10.1016/j.idairyj.2004.02.001

[6] Carvalho AS, Silva J, Ho P, Teixeira P, Malcata FX, Gibbs P. Survival of freeze-dried *Lactobacillus plantarum* and *Lactobacillus rhamnosus* during storage in the presence of protectants. *Biotechnol Lett.* 2002; 24: 1587-1591. https://link.springer.com/article/10.1023/A:1020301614728

[7] Morgan CA, Herman N, White PA, Vesey G. Preservation of micro-organisms by drying. *J Microbiol Methods*. 2006; 66: 183-193. https://doi.org/10.1016/j.mimet.2006.02.017
[8] Bouabidi ZB, El-Naas MH, Zhang Z. Immobilization of microbial cells for the biotreatment of wastewater. *Environ Chem Lett*. 2019; 17: 241-257. https://doi.org/10.1007/s10311-018-0795-7
[9] Wu P, Wang Z, Bhatnagar A, Jeyakumar P, Wang H, Wang Y, Li X, Microorganisms-carbonaceous materials immobilized complexes: Synthesis, adaptability and environmental applications. *J Hazard Mater*. 2021; 416: 125915. https://doi.org/10.1016/j.jhazmat.2021.125915
[10] Partovinia A, Rasekh B. Review of the immobilized microbial cell systems for bioremediation of petroleum hydrocarbons polluted environments. *Crit Rev Environ Sci Technol.* 2018; 48 (1): 1-38. https://doi.org/10.1080/10643389.2018.1439652
[11] Gong W, Fan Y, Xie B, Tang X, Guo T, Luo L, Liang H. Immobilizing Microcystis aeruginosa and powdered activated carbon for the anaerobic digestate effluent treatment. *Chemosphere* 2020; 244: 125420. https://doi.org/10.1016/j.chemosphere.2019.125420
[12] Lin Q, Donghui W, Jianlong W. Biodegradation of pyridine by Paracoccus sp. KT-5 immobilized on bamboo-based activated carbon. *Bioresour Technol*. 2010; 101: 5229-5234. https://doi.org/10.1016/j.biortech.2010.02.059
[13] Chen B, Yuan M, Qian L. Enhanced bioremediation of PAH-contaminated soil by immobilized bacteria with plant residue and biochar as carriers. *J Soil Sediments.* 2012; 12: 1350-1359. https://link.springer.com/article/10.1007/s11368-012-0554-5
[14] Shen Y, Li H, Zhu W, Ho SH, Yuan W, Chen J, Xie Y. Microalgal-BC 16. immobilized complex: a novel efficient biosorbent for cadmium removal from aqueous solution. *Bioresour Technol*. 2017; 244: 1031-1038. https://doi.org/10.1016/j.biortech.2017.08.085
[15] Peñalver Jl, linares-Fernández Jl, de Araujo Farías V, lópez-Ramón MV, Tassi M, Oliver FJ, Moreno-Castilla C, de Almodóvar JMR. Activated carbon cloth as support for mesenchymal stem cell growth and differentiation to osteocytes. *Carbon*, 2008; 47:3574-3577. https://doi.org/10.1016/j.carbon.2009.08.016
[16] Osmokrovic A, Jancic I, Vunduk J, Petrovic P, Milenkovic M, Obradovic B. Achieving high antimicrobial activity: Composite alginate hydrogel beads releasing activated charcoal with an immobilized active agent. *Carb Pol*. 2018; 196: 279-288. https://doi.org/10.1016/j.carbpol.2018.05.045
[17] ATCC Bacteriology Culture Guide. https://www.atcc.org/resources/culture-guides/bacteriology-culture-guide#preservation. Accessed February 1, 2025
[18] Tukey JW. Comparing individual means in the analysis of variance. *Biometrics* 1949; 5(2): 99–114. https://doi.org/10.2307/3001913
[19] Malik KA. A simplified liquid-drying method for the preservation of microorganisms sensitive to freezing and freeze-drying. *J Microbiol Methods*. 1990; 12: 125-132. https://doi.org/10.1016/0167-7012(90)90022-X
[20] Oluwatosin SO, Tai SL, Fagan-Endres MA. Sucrose, maltodextrin and inulin efficacy as cryoprotectant, preservative and prebiotic - towards a freeze dried *Lactobacillus plantarum* topical probiotic. *Biotechnol Rep (Amst)*. 2021; 33: e00696. https://doi.org/10.1016/j.btre.2021.e00696
[21] Drvenica I, Stancic A, Kalusevic A, Markovic S, Dragisic Maksimovic J, Nedovic V, Bugarski B, Ilic V. Maltose-mediated, long-term stabilization of freeze- and spray-dried forms of bovine and porcine haemoglobin. *J Serb Chem Soc*. 2019; 84(10): 1105-1117. https://doi.org/10.2298/JSC190513067D
[22] Fan X, Shi Y, Li R, Yang R, Yang X, Hang F, Chen W. Preliminary study on the effect of pre-freezing methods on lyophilization quality and storage stability of probiotics. *Dry Technol.* 2024; 42(9): 1480-1492. https://doi.org/10.1080/07373937.2024.2361351
[23] Hartke A, Bouche S, Giard J-Ch, Benachour A, Boutibonnes Ph, Auffray Y. The lactic acid stress response of *Lc. lactis* subsp. *lactis*. *Curr. Microbiol*. 1996; 33: 194-199. https://link.springer.com/article/10.1007/s002849900099
[24] Kim WS, Dunn NW. Identification of a cold shock gene in lactic acid bacteria and the effect of cold shock on cryotolerance. *Curr Microbiol*. 1997; 35: 59-63. https://link.springer.com/article/10.1007/s002849900212
[25] Bâati L, Fabre-Gea C, Auriol D, Blanc PJ. Study of the cryotolerance of *Lactobacillus acidophilus*: effect of culture and freezing conditions on the viability and cellular protein levels. *Int J Food Microbiol*. 2000; 59 (3): 241-247. https://doi.org/10.1016/S0168-1605(00)00361-5

Uticaj predtretmana, parametara liofilizacije, korišćenja različitih krioprotektanata na preživljavanje imobilisanih probiotika tokom postupka liofilizacije

Tanja Ž. Krunić[1] i Andrea M. Osmokrović[2]

[1]Inovacioni centar Tehnološko-metalurškog fakulteta, Beograd, Srbija
[2]Univerzitet Beogradu, Tehnološko-metalurški fakultet Beograd, Srbija

(Naučni rad)

Izvod

Liofilizacija je odlična metoda koja omogućavo produženje roka trajanja prehrambenih proizvoda kao i očuvanje probiotskih kultura. Žive ćelije preferiraju blage uslove i svako odstupanje (npr. vakuum, visoka ili niska temperatura) dovodi do oštećenja ćelija. U ovom radu je ispitan uticaj različitih parametara kao što su predtretmani, trajanje liofilizacije, tip smrzavanja, primena krioprotektanata na preživljavanje probiotika imobilisanih na tkaninu od aktivnog uglja tokom procesa liofilizacije. Aktivacija *L. plantarum* u De Man, Rogosa and Sharpe (MRS) bujonu pre imobilizacije značajno povećava broj živih ćelija, ali i njihovo preživljavanje tokom liofilizacije. Zamrzavanje imobilisanih ćelija tečnim azotom nije dalo željeno povećanje procenta preživelih probiotskih ćelija nakon liofilizacije u poređenju sa dubokim smrzavanjem na -80 °C, dok je inkubacija ćelija 2 h u frizideru pre dubokog smrzavanja doprinela povećanju broja ćelija koje prežive liofilizaciju. Dužina trajanja (5 i 48 h) samog procesa sušenja imala je blagi uticaj na stepen preživljavanja probiotika. Upotreba mleka kao krioprotektanta značajno je povećala stepen preživljavanja, dok su saharoza, maltoza i trehaloza pokazale dobru zaštitnu moć, ali znatno manju u poređenju sa mlekom. Najviši stepen preživljavanja *L. plantarum* obezbeđuje procedura koja podrazumeva inkubaciju ćelija u MRS bujonu, korišćenje mleka kao krioprotektanta, inkubaciju 2h u frizideru, duboko smrzavanje i liofilizaciju u trajanju od 5 h.

Ključne reči: Lactobacillus plantarum; preživljavanje; mleko; tečni azot; prezervacija

Prediction of functional characteristics of interlock and rib knitted fabrics by the use of 3D computational modelling and analysis

Hassan Ali, Salma Farooq, Muhammad Owais Raza Siddiqui, Muhammad Dawood Husain and Saira Faisal

Department of Textile Engineering, NED University of Engineering and Technology, University Road, Karachi, Pakistan

Abstract

In this work, a computational model of interlock and rib knitted structures is developed to predict the air permeability and thermal properties of the fabric. Repeatable unit cells of interlock and rib structures are developed in COMSOL Multiphysics® software by using actual fabric parameters, extracted with the help of an image analysis technique. The obtained modeling results are then compared with the actual experimental values for the fabric. Furthermore, the validated computational model is utilized to analyze the effect of stitch length and fabric thickness on the thermal properties and air permeability of the fabric. It is found that stitch length has a direct relation with air permeability and an inverse relation with effective thermal conductivity. The fabric thickness influences directly the effective thermal conductivity and has an inverse relation with air permeability of the fabric.

Keywords: Air permeability; effective thermal conductivity; weft knitting; computational fluid dynamics; repeating unit cell.

Available on-line at the Journal web address: http://www.ache.org.rs/HI/

ORIGINAL SCIENTIFIC PAPER

UDC: 677.075.44: 519.67

Hem. Ind. **79(3)** 167-178 (2025)

1. INTRODUCTION

Weft knitted fabrics are widely used in multiple application areas, and now with the help of knitted fabric simulation technology, manufacturers can easily distinguish the intuitive fabric simulation images that will shorten the trial-and-error process as well as improve the efficiency of work by shortening the development cycle of a product [1].

A loop is formed by bending the yarn from three points and these loops are entangled into one another and make the basic unit of the knitted fabric. The geometrical model of a single loop should be established, and the geometrical structure of the knitted fabric is obtained by the loop [2]. Numerous models have been developed for weft knitted fabrics starting from 2D (two-dimensional) to 3D (three-dimensional) loop models, which were used to investigate fabric properties, simulate geometric structures, and explore mechanical aspects, production, and design, while 3D simulation is more important than 2D loop models [1].

Analyses using geometrical models of knitted fabrics were performed in many studies (*e.g.* [3-9]). In the Kurbak's model, the loop was divided into 8 sections that described the orientation of yarn, and this model can establish tuck, purl, and rib stitches [9]. Demiroz *et al.* [10] have presented the mathematical approach to develop 3D models of plain weft-knitted structure. Choi and Lo [11] have also worked on a plain weft-knitted structure and analyzed the mechanical and dimensional properties of the structure. This approach was later extended by Kyosev *et al.* [12] who developed the models of the same structure and further considered the elliptical yarn cross-section. In the weft knitted fabric simulation, the piecewise function of the loop model was applied to enhance the 3D construction.

To determine the geometry of knitted spacer fabrics, a more accurate mathematical model was developed with the use of simulation in Abaqus software [13] and by numerical analysis mechanical properties of composite materials were predicted. The yarn path was also derived through equations and geometry of 1x1 rib knitted fabric was developed. The predicted geometry and compression modulus results showed the overall 4.0 and 4.2 % error, respectively [13].

Corresponding author: Muhammad Owais Raza Siddiqui, Department of Textile Engineering, NED University of Engineering and Technology, University Road, 75270, Karachi, Pakistan

E-mail: orazas@neduet.edu.pk

Paper received: 24 July 2024; Paper accepted: 30 July 2025; Paper published: 10 September 2025.

https://doi.org/10.2298/HEMIND240619012A

Another study aimed to enhance the joint strength in composite pipes integrated with the plain weft knitted structure for which mathematical modelling and fabric simulations were performed. The curved shaped models were created for the joint composites with curved surfaces and the results revealed maximum of 10 % error in structural parameter predictions [14].

ABAQUS plugins were developed for the analysis of mechanical parameters of weft knitted composites including strength, stiffness and the mechanism of failure. It is reported that the maximum of 7 % error was observed in predicting the tensile modulus in both directions [15].

An algorithm was developed, which can forecast the pore size of weft knitted structures without the input parameters of machine and yarn combination. Although it has some inherent limitations, the model provides customization of the fabric as per the required end application, thus helping to manufacture customized structures more efficiently [16].

In a nutshell, the geometry of plain knitted structures is studied extensively, but interlock and rib structures have not yet been investigated much despite their importance. This research aims to build 3D computational models of interlock and rib knitted structures using the actual construction parameters of the fabric to predict the air permeability and thermal properties of the fabric. To validate the model, we kept the other fabric and knitting parameters constant and analyzed the effects of stitch length and fabric thickness on these properties.

2. MATERIALS AND METHOD

2. 1. Material

Samples were developed using 100 % polyester drawn textured (DTY) 75/72 multifilament semi-intermingle yarn from Suzhou Nextile fiber Technology, China. Table 1 shows experimentally determined specifications of the interlock and rib structure developed fabrics. The wales and course density were evaluated according to the BS EN 14971:2006 standard, the stitch length according to the EN 14970:2006 standard, thickness was measured according to the ISO 5084 standard, and the areal density of the fabric was calculated as per the standard EN 12127:1997. Thermal resistance was determined as per standard ISO 11092 and used for calculation of the thermal conductivity. Air permeability of the fabrics was tested according to the method specified by the ISO 9237 standard and the permeability value, k, was calculated by the Darcy's law, Equation (1) [23]:

$$V = -\frac{kA\Delta P}{\mu L} \tag{1}$$

where V is the total volumetric discharge per unit time, A is the cross-sectional area of wales a porous medium, $\Delta P/L$ ratio is the pressure gradient, μ is the fluid viscosity, and k represents the air permeability.

Table 1. Specifications of the weft knitted fabric samples, yarn 8.33 tex, yarn diameter 0.14 mm

Type of fabric	Wales per mm	Courses per mm	Stitch length, mm	Fabric thickness, mm	Areal density, g m^{-2}
Interlock Fabric	15.75[a]	18.11[b]	2.82	0.54	125
Rib fabric	10.24[c]	17.32[d]	2.70	0.36	65

[a]40 per inch; [b]46 per inch; [c]26 per inch, [d]44 per inch

Moreover, the interlock fabric was manufactured by using a Dragan double-bed circular knitting machine of 28-gauge, consisting of 2976 needles and 68 feeders (producer, country). The diameter of this circular knitting machine was 34 in. The needles used in the dial and cylinder of the machine have a length of 74 mm, thickness of 0.41 mm and latch size of 8 mm.

Similarly, the rib fabric was manufactured by using a Dragan double-bed circular knitting machine of 18-gauge, consisting of 1920 needles and 68 feeders (producer, country). The diameter of this circular knitting machine was 34 in. The needles used in the dial and cylinder have a length of 90 mm, thickness of 0.41 mm and latch size of 8 mm.

2. 2. Methodology

The methodology implemented to develop the 3D models of interlock and rib structures included: (i) development of parametric 3D unit cell of interlock and rib knitted structures; (ii) calculating the air permeability and effective thermal

conductivity by using the developed unit cells; (iii) parametric analysis to predict and analyze the effect of stitch length and fabric thickness on air permeability and effective thermal conductivity to validate the models.

2. 2. 1. Development of 3D models of interlock and rib structures

The interlock and rib structures consist of the face of a plain loop on both sides of the fabric. In the case of interlock fabric, the wales are interlocked and opposite to each other while in the rib fabric single yarn is used to create the loops on technical front and the back. In the case of interlock, sinker loops of two 1×1 rib courses cross over each other alternately, to produce an interlock fabric. Majorly, the structure can be segmented into two including the arms and the needle loops, obtained by mathematical equations, while the second segment is the sinker loop or linking bottom part of the loop which connects the front and the back loop in case of interlock structure [18].

The 3D model of plain loop is also explained in literature [19] by using a second continuous cubic non-uniform rational B-splines (NURBs). Some key points include (i) the plain loop is the space curve, easily identified by using data points and weight factor, which bends in all 3 dimensions; (ii) assumption that the yarn is continuous during bending and its cross-section is uniform and circular; (iii) the structure of a single loop is determined by using the data points from $P_0 = (X_0+Y_0+Z_0)$ to $P_8 = (X_8+Y_8+Z_8)$. Practically, the NURBs curve must follow the path obtained from these data points. The parameters for calculating the points include the width of head and sinker loop, height of the loop, space between adjacent sinker loops, thickness of fabric, adjacent loop distance in wale direction and coefficient of inter-meshed points represented by γ, Equation (2):

$$\gamma = C / H, \quad 0 < \gamma < 1 \tag{2}$$

where C is the distance of two adjacent loops in the wale direction and H is the height of the loop.

The single loop consists of 9 interpolation points, as shown in Figure 1(a), which were then calculated. It is assumed that the points P_2 and P_6 are the mid points with respect to P_1 and P_3 and P_5 and P_7, respectively [19].

Figure 1 shows the development steps of 3D computational model of interlock structure while Figure 2 shows the development steps of 3D computational model of rib structure. Both structures are created by using similar methodology as discussed above.

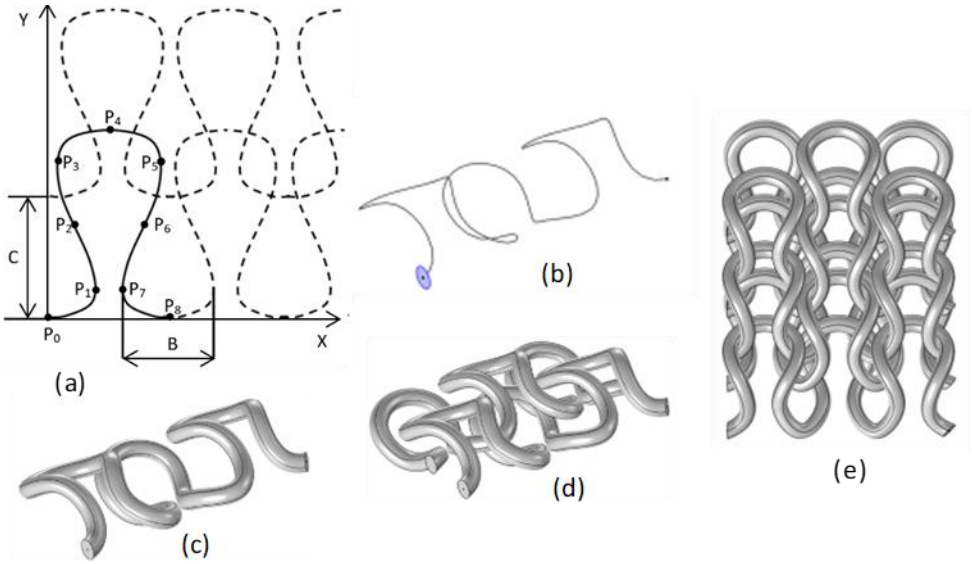

Figure 1. Development of a 3D computational model of interlock structure: (a) plain weft knitted loop geometry, (b) interpolation curve with yarn circular cross-section, (c) 3D loops of the 1st yarn, (d) interlocking of the 2nd yarn to complete the structure

Image analysis was performed by using the actual images of the fabric to extract the parameters of the unit cell described earlier. The 3D computational model of structures is developed by using similar assumption that the loops on technical back are the mirror image of technical front loops and are similar to the technical front of the plain weft knitted structure. The center line of the created interpolation curve lies in the three-dimensional space. By using the sweeping tool, circular cross-section of yarn is created and then the loops were mirrored.

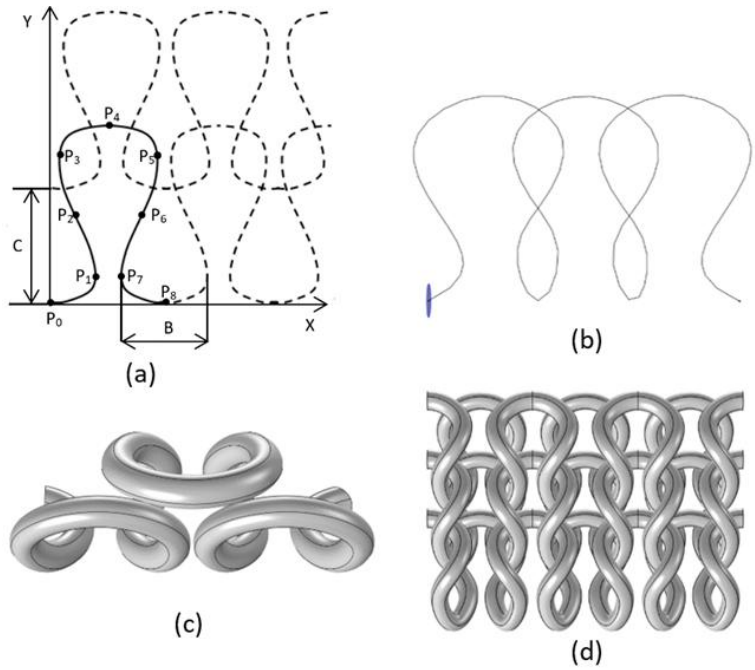

Figure 2. Development of the 3D computational model of rib structure: (a) plain weft knitted loop geometry, (b) interpolation curve with yarn circular cross-section, (c) top view of rib structure, (d) computational model of rib structure

The 3D loop geometrical models of weft knitted Interlock and rib structures were developed based on the improved model of plain loop and their central axes as some 3D space curves were achieved by using non-uniform rational B-splines (NURBS). Figure 3 shows the top view of the ideal and the developed interlock structure. Here, the central axis of yarn is determined by the data points of yarn path. The equations for calculating the points are obtained with the relation between the actual parameters of fabric, calculated by using image analysis techniques, and the data points.

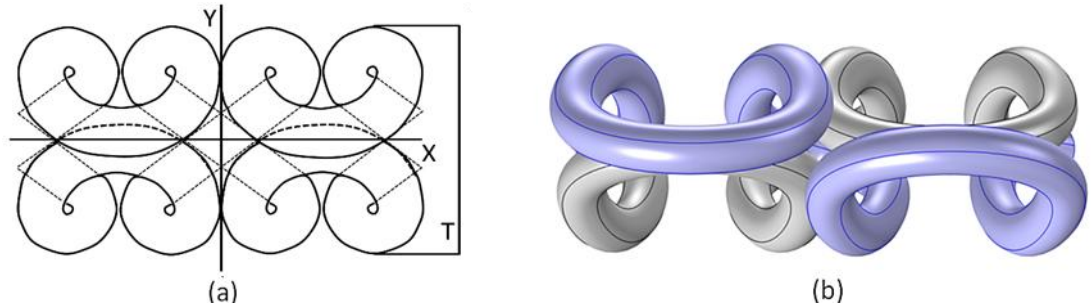

Figure 3: Top view of interlock structure: (a) ideal structure and (b) developed 3D model

2. 3. Analysis

2. 3. 1. Air permeability

Stitch length, also known as loop length, is one of the most critical parameters in the knitted fabric production process which influences dimensional and physical properties of the end product. These include air permeability and thickness of a fabric, which are mainly influenced by the loop length [20].

The air flow rate which passes perpendicularly through a unit area is defined as the air permeability. The air permeability of a fabric is directly proportional to the stitch length so that the increment in loop length will increase the air flow rate through the structure of the fabric [21].

Similarly, the stitch length has an inverse relation with the areal density and thickness of the fabric. As the loop length decreases, the fabric's stitch density increases, so the overall areal density and thickness of the fabric increase [22].

The air permeability (k) of the yarn used in the interlock and rib fabric in the traverse direction is calculated using the Gebart model [23], Equation (3):

$$k = \frac{16R_f^2}{9\pi\sqrt{6}}\left(\sqrt{\frac{V_{max}}{V_f}} - 1\right)^{\frac{5}{2}} \quad (3)$$

where V_{max} is the maximum fiber fraction volume which is $\pi/2\sqrt{3}$ of hexagonal fiber array, R_f is the fiber radius which is 0.01 µm and V_f is fiber volume fraction

Similarly, the fiber volume fraction, and porosity of the yarn ϵ_p, can be calculated by using the Equations (4) and (5):

$$V_f = \frac{4T_y}{d^2 10^3 P_f} \quad (4)$$

where T_y is the count of yarn, tex and P_f / g cm^{-3} is the fiber density.

$$\epsilon_p = 1 - V_f \quad (5)$$

Figure 4 shows the methodology to predict air permeability of interlock structure while Figure 5 shows the methodology to predict air permeability of rib structure. The unit cell of interlock and rib structure is placed inside the air domain which is then extruded to 2 mm at the inlet and 6 mm at the outlet. The pressure difference is then created at the front and back side of the structure by applying the inlet pressure of 300 Pa and outlet pressure of 0 Pa. The geometry is then discretized by using tetrahedral elements. The outward volume flow rate across the geometry is then calculated by the developed geometrical models.

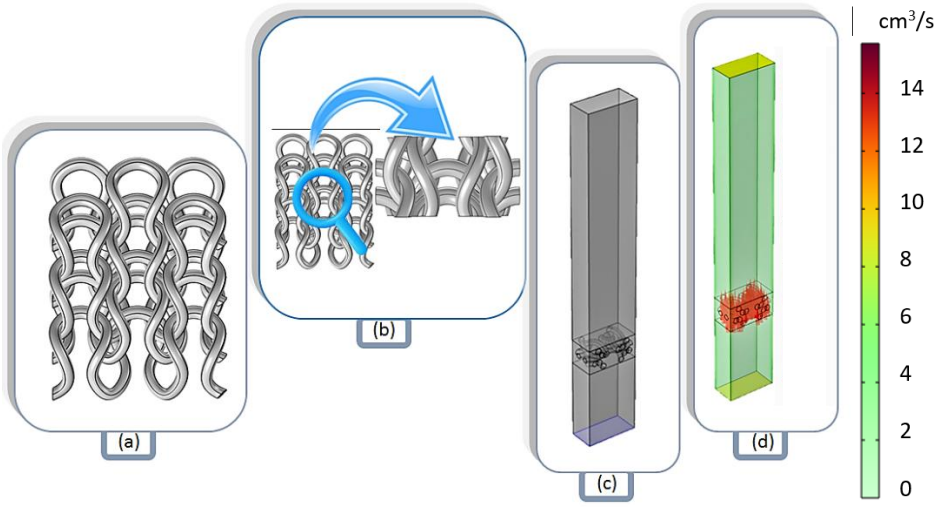

Figure 4. Methodology for prediction of the air permeability of interlock fabric: (a) interlock structure, (b) unit cell, (c) unit cell with extruded geometry, (d) predicted outward volume flow rate through the geometry

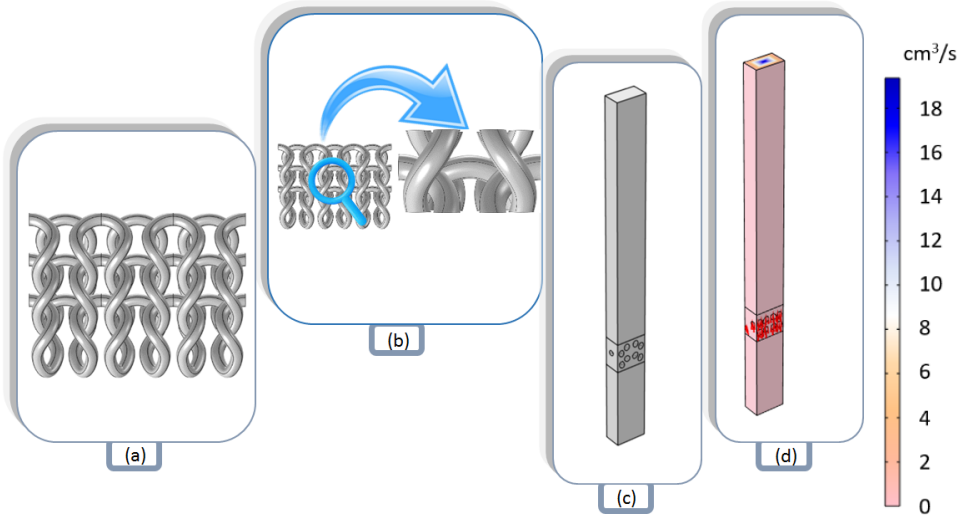

Figure 5: Methodology for prediction of the air permeability of rib fabric: (a) rib structure, (b) unit cell, (c) unit cell with extruded geometry, (d) predicted outward volume flow rate through the geometry

2. 3. 2. Thermal conductivity

Thermal resistance directly correlates with thermal insulation and is inversely proportional to the thermal transmittance. Thermal resistance is also directly related to the stitch length. As the stitch length is reduced, the thermal resistance decreases due to the increment in thickness of the fabric, and the thermal conductivity and absorptivity increase due to the increased stitch density of the fabric and the less porous structure. Also, the thermal conductivity is directly proportional to the areal density of fabric and thermal absorptivity is inversely proportional to the thermal resistance. The increase in the areal density of fabric results in the increment of contact points due to which the conductivity increases [24].

Thermal resistance and thermal insulation are directly proportional to fabric thickness. As the loop length increases, the thickness of the fabric decreases, and the structure of fabric becomes more porous due to which the thermal absorptivity is decreased.

Effective thermal conductivity of the structures, K_{eff}, is predicted by using the Fourier's law of conduction, Equation (6):

$$K_{eff} = \frac{Qt}{S\Delta T} \tag{6}$$

where Q represents the heat flux, S is the surface area, t is the thickness of fabric and ΔT is the temperature difference.

By using effective thermal conductivity, thermal resistance of the structures (R), can also be calculated by using the thickness of the fabric, Equation (7).

$$R = \frac{t}{K_{eff}} \tag{7}$$

Similarly, the thermal conductivity of the yarn in axial direction, which is 0.50648 w $m^{-1}K^{-1}$, and in the traverse direction, which is 0.038696 W m^{-1} K^{-1}, can be calculated by using Equations (8) and (9) [25]:

$$Kya = Kfl Vfy + Kair\ (1 - Vfy) \tag{8}$$

$$K_{yt} = \frac{K_{ft}K_{air}}{V_{fy}K_{air} + \left(1\text{-}V_{fy}\right)K_{ft}} \tag{9}$$

where K_{ya} represents Yarn axial thermal conductivity, K_{yt} is yarn tranverse thermal conductivity, K_{fl} and K_{ft} are Fiber thermal conductivity in longitudinal and traverse direction, respectively, V_{fy} is fiber volume fraction of yarn and K_{air} is thermal conductivity of air.

The unit cell of the interlock structure is placed inside the box which acts as an air domain so that the temperature difference can be created at the front and back sides of the fabric to predict thermal conductivity, as shown in Figure 6.

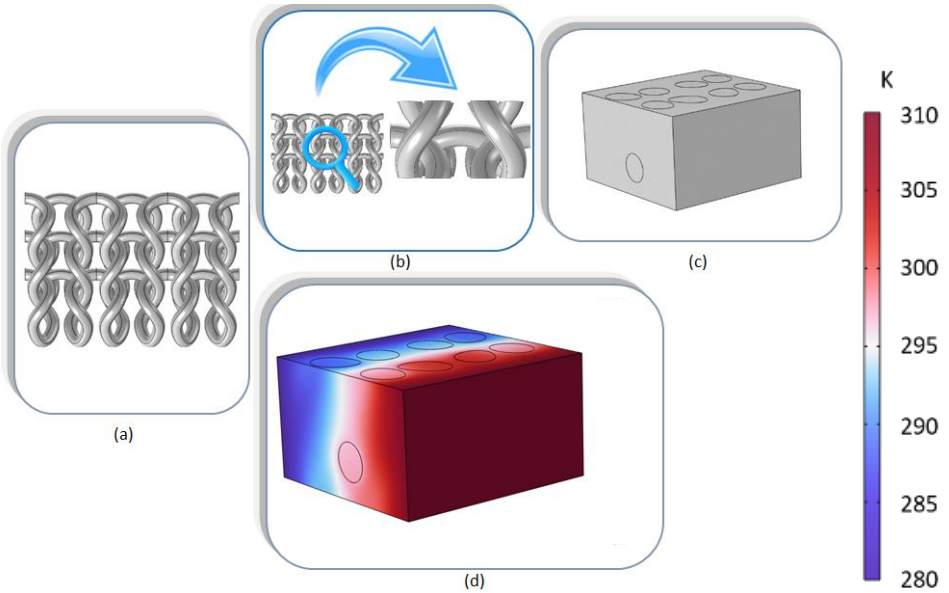

Figure 6. Methodology for prediction of the thermal conductivity of interlock fabric: (a) interlock structure, (b) unit cell, (c) unit cell with air domain, (d) predicted temperature profile

Similar methodology is opted for the Rib structure which is shown in Figure 7. Heat is transferred from the hot surface towards the cold surface. The hot surface temperature is 310 K while that of the cold surface is about 280 K. The whole geometry is then meshed by using the tetrahedral geometry, and the total net energy rate is calculated.

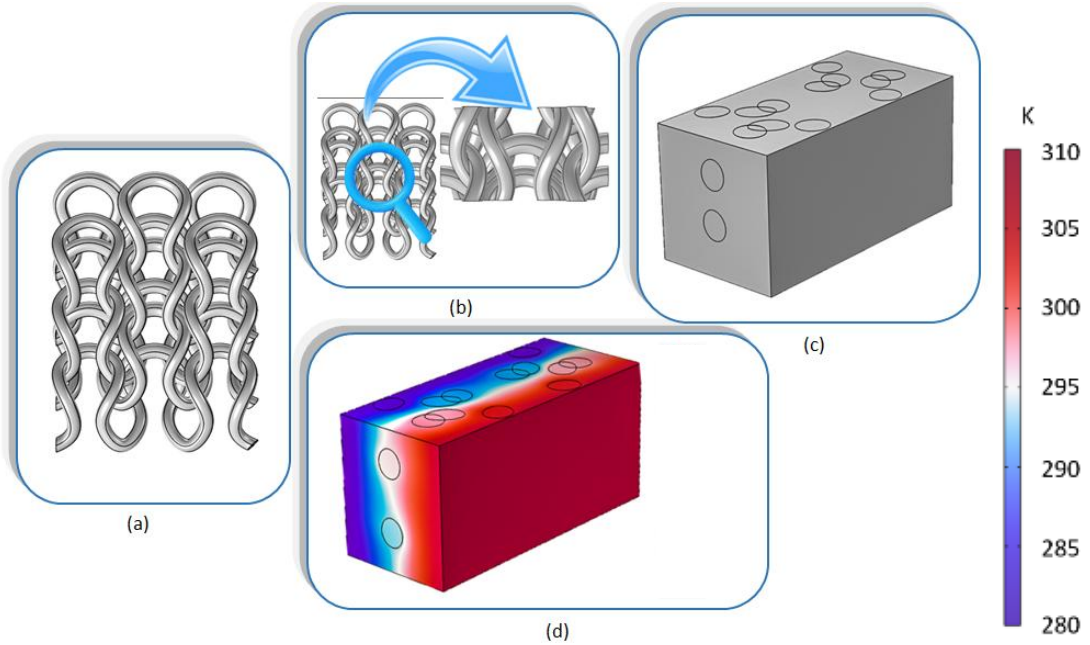

Figure 7: Methodology for prediction of the thermal conductivity of rib fabric: (a) rib structure, (b) unit cell, (c) unit cell with air domain, (d) predicted temperature profile

3. RESULTS AND DISCUSSION

3. 1. Model validation

Air permeability of the interlock and rib knitted fabrics is analyzed by using the unit cell, the image analysis and numerical modelling, as shown in Table 2.

Table 2: Air permeability of interlock and rib structures, yarn - 100 % polyester

Type of fabric	Fiber diameter, mm	Fiber volume fraction	Porosity	Air permeability, μm²		Absolute error of model, %
				Actual	Predicted	
Interlock fabric	0.01	0.3893	0.6107	4.642	4.795	3.2
Rib Fabric	0.01	0.275	0.725	4.902	5.33	8

By using the unit cell, the thermal conductivity of the interlock and rib fabric are analyzed, and the obtained results are shown in Table 3.

Table 3: Thermal Conductivity of Interlock and rib structures, yarn – 100 % polyester

Type of fabric	Specific heat, J kg^{-1} K^{-1}		Thermal conductivity, W m^{-1} k^{-1}		Absolute error of model, %
	Yarn	Air	Actual	Predicted	
Interlock fabric	1030	1006.96	0.04112	0.0430	4.57
Rib Fabric	1030	1006.96	0.0395	0.0378	4.3

3. 2. Model utilization for parametric analysis

By using the developed validated models for interlock and rib knitted structures, the parametric analysis is then performed by gradually increasing the stitch length and decreasing the thickness of the structures to predict and analyze the effects on air permeability and effective thermal conductivity of the fabric. The results are shown in Tables 4 and 5.

Table 4: Impact of the stitch length and fabric thickness in the air permeability and thermal conductivity of the interlock structure

Fabric code	Stitch length, mm	Fabric thickness, mm	Air permeability, μm^2	Thermal conductivity, W m^{-1} K^{-1}
A1	2.76	0.60	4.770	0.04920
A2	2.82	0.54	4.795	0.04300
A3	2.86	0.48	4.850	0.04000
A4	2.90	0.44	4.863	0.03635
A5	2.95	0.40	4.891	0.03481

Table 5: Impact of the stitch length and fabric thickness on the air permeability and thermal conductivity of the rib structure

Fabric code	Stitch length, mm	Fabric thickness, mm	Air permeability μm^2	Thermal conductivity, W m^{-1} K^{-1}
B1	1.38	0.6	4.68	0.04
B2	1.43	0.58	4.752	0.0392
B3	1.68	0.54	4.955	0.03906
B4	1.89	0.5	5.33	0.0378
B5	2.3	0.46	5.45	0.037

Change in the stitch length results in the change in geometry of the overall structure and its properties which results in the change in air flow through the fabric. Air flow through the interlock and rib fabric structures are simulated in Figures 8 and 9, respectively. The velocity magnitude is shown by using the arrow lines, parallel to the air flow through the free and porous air domains. Hence, the variation in volumetric flow rate across the geometry is observed with the change of stitch length and fabric thickness.

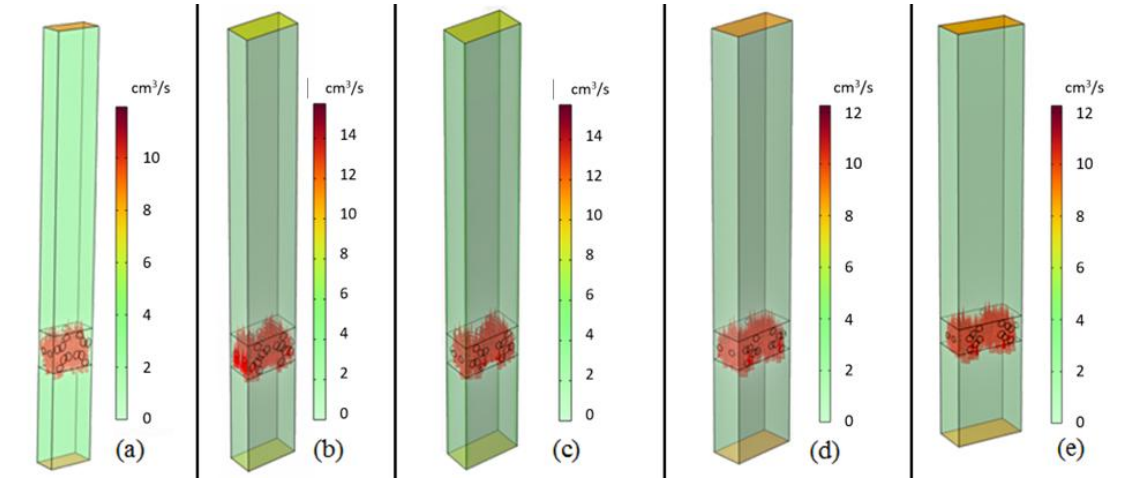

Figure 8: Simulation results of velocity magnitude in the interlock knitted structure in the free and porous air domains: (a) fabric A1, (b) fabric A2, (c) fabric A3, (d) fabric A4, (e) fabric A5

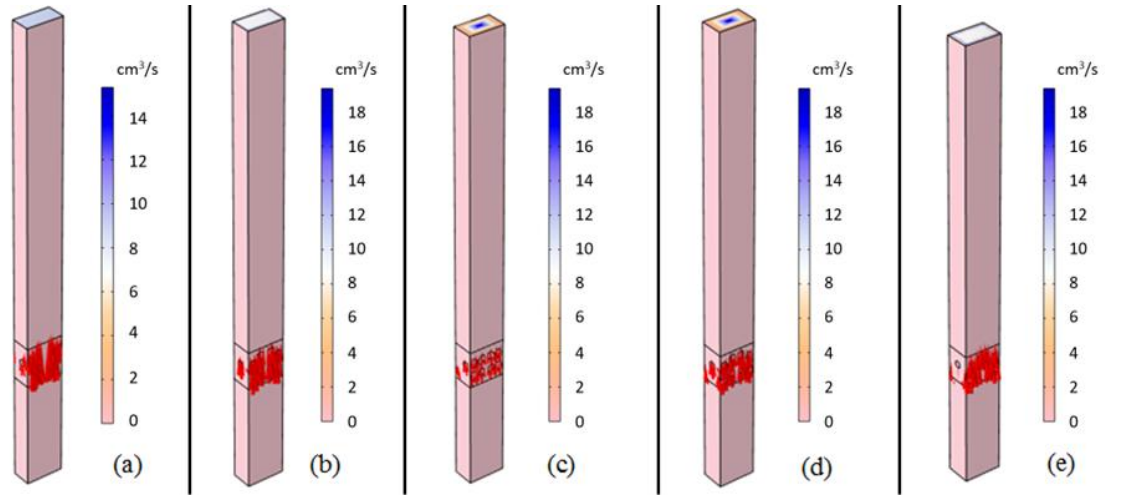

Figure 9. Simulation results of velocity magnitude in the rib knitted structures in the free and porous air domains: (a) fabric B1, (b) fabric B2, (c) fabric B3, (d) fabric B4, (e) fabric B5

Similarly, the change in the structure geometry by changing the stitch length and fabric thickness also results in the change in overall effective thermal conductivity of the fabric. The major reason behind is the change in the fiber volume fraction in the overall fabric by changing the fabric parameters. Due to the change in heat transfer the total net energy rate also varies, which results in the variation in thermal properties of the fabric. The simulation results of the heat transfer through Interlock fabric are shown in Figure 10, while the simulation results for the rib fabric are shown in Figure 11.

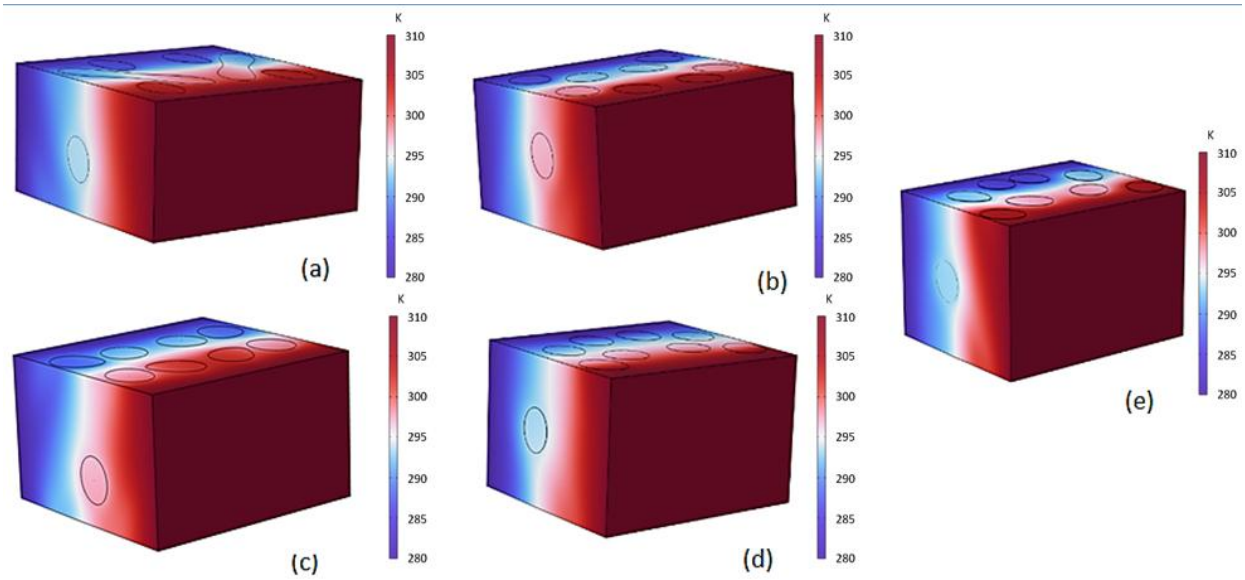

Figure 10. Simulation results of heat transfer through the unit cell of interlock fabric: (a) fabric A1, (b) fabric A2, (c) fabric A3, (d) fabric A4, (e) fabric A5

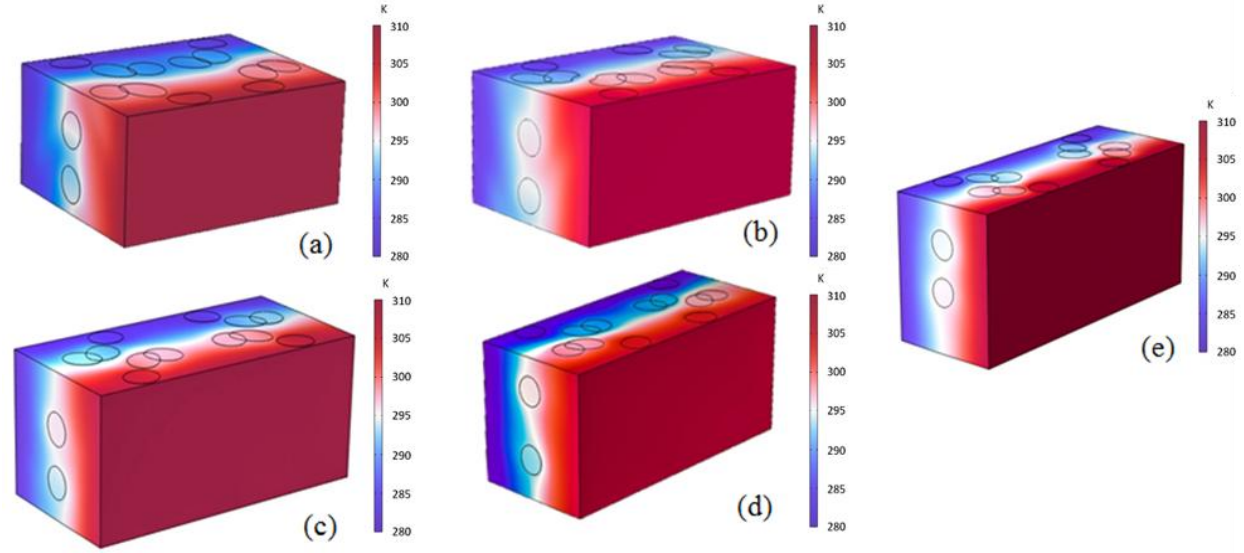

Figure 11: Simulation results of heat transfer through the unit cell of rib fabric: (a) fabric B1, (b) fabric B2, (c) fabric B3, (d) fabric B4, (e) fabric B5

Figures 12 and 13 directly show the general relationships of the air permeability and effective thermal conductivity with the fabric parameters, stitch length and fabric thickness. The following could be concluded:

a) By increasing the stitch length, the air permeability of the knitted fabrics also increases due to the decrement in stitch density and the increment in porosity.
b) Increasing the fabric thickness by keeping the yarn count and yarn diameter constant, the fabric's air permeability decreases. Hence, air permeability is directly related to the stitch length whereas inversely proportional to the fabric thickness.
c) Similarly, if the stitch length of the fabric increases, it will reduce the effective thermal conductivity of the fabric.
d) By increasing the fabric thickness, the effective thermal conductivity of the fabric also increases. Hence, the thermal conductivity is directly proportional to the fabric thickness and inversely proportional to the stitch length of the fabric.

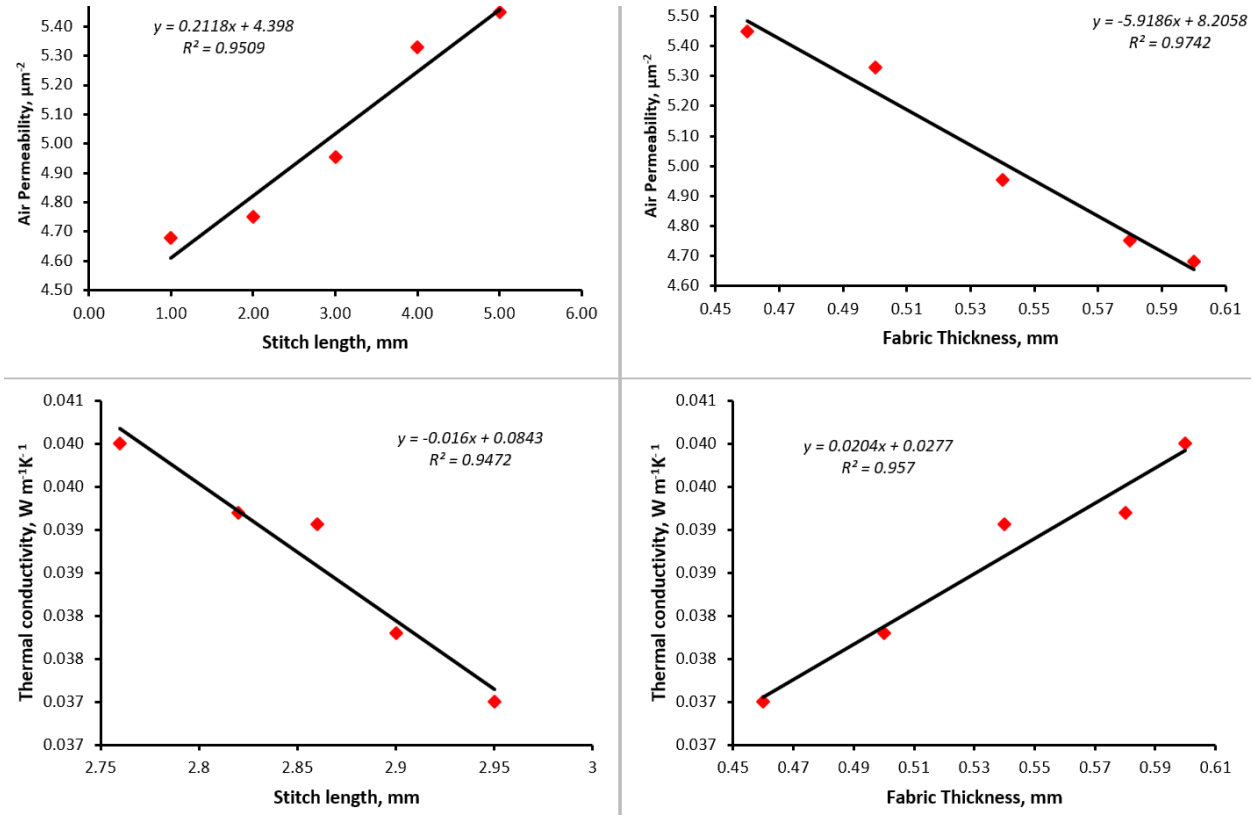

Figure 12. Relation between the air permeability and thermal conductivity predicted through interlock model with the stitch length and fabric thickness

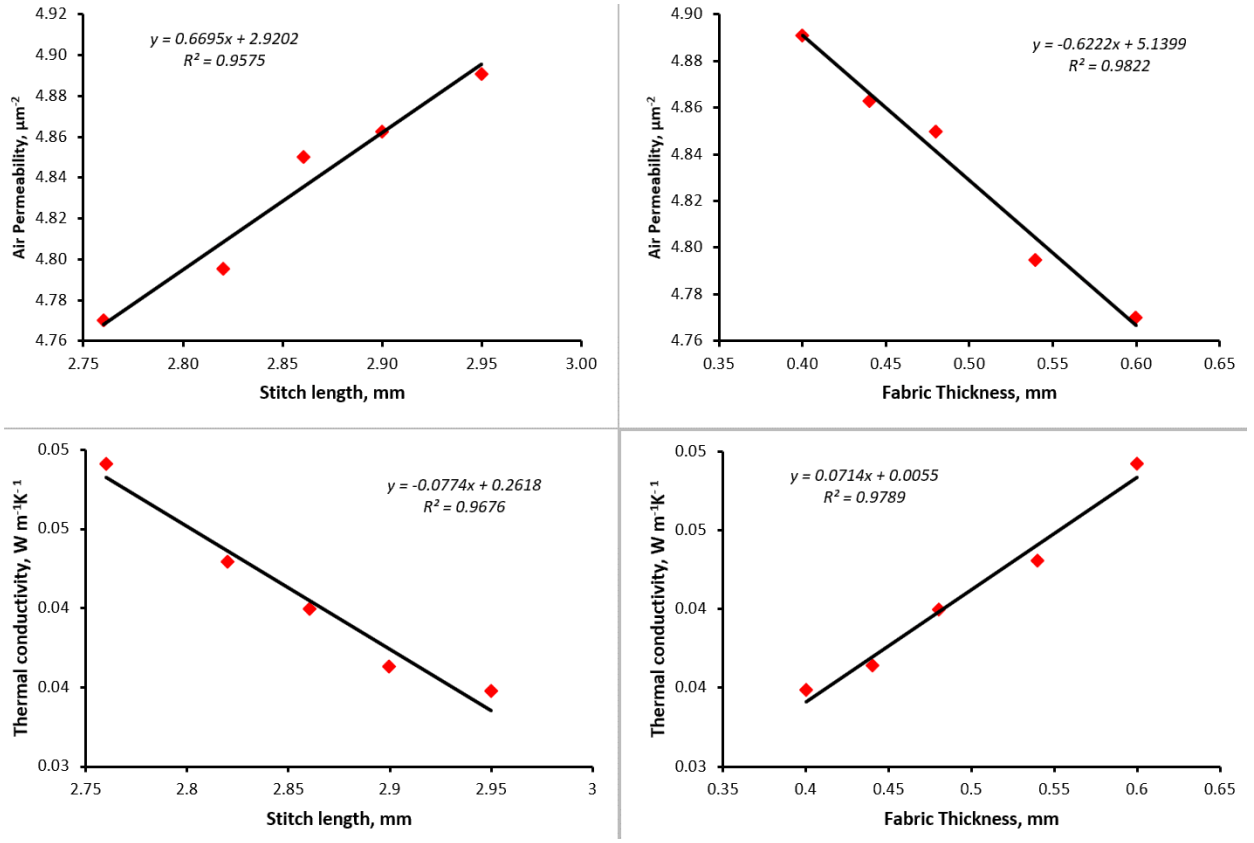

Figure 13. Relation between the air permeability and thermal conductivity predicted through rib model with the stitch length and fabric thickness

4. CONCLUSION

Functional and computational 3D models of interlock and rib knitted structures are developed by extracting the actual constructional parameters of the fabric, by using the image analysis technique, to develop a parametric 3D unit cell of the structures. The air permeability and effective thermal conductivity of the fabrics are then predicted and compared with the actual values to validate a model. The absolute error is less than 8 % between the predicted and actual value of both air permeability and effective thermal conductivity for both the structures. The parametric analysis is then conducted by changing the stitch length and thickness of the fabrics to analyze the trend and its effect on the air permeability and effective thermal conductivity. It is found that as the stitch length increases, the air permeability also increases while the effective thermal conductivity is reduced. Similarly, as the thickness of the fabric increases, by keeping the yarn diameter and yarn count constant, the air permeability is reduced, while the effective thermal conductivity is increased.

This approach and the developed models offer a powerful tool for accurately predicting and analyzing the performance of knitted fabrics, enabling more efficient and informed design processes in the textile industry, particularly for applications requiring specific thermal and comfort properties.

Acknowledgement: Authors are thankful to the Higher Education Commission of Pakistan for funding this research work under the Grand Challenge Fund (GCF-063).

REFERENCES

[1] Li YL, Chen SY, Yang LH, Cao LH. Study on three-dimension computer simulation of plain knitted fabrics. *Adv Mat Res.* 2011; 213: 595–599 https://doi.org/10.4028/www.scientific.net/AMR.213.595

[2] Sha S, Geng A, Gao Y, Li B, Jiang X, Tao H, Luo L, Yuan X, Ke H, Hu X. Review on the 3D simulation for weft knitted fabric. *J Eng Fiber Fabr.* 2021; 16: 1-10 https://doi.org/10.1177/15589250211012527

[3] Peirce FT. Geometrical principles applicable to the design of functional fabrics. *Text Res J*. 1947; 17(3): 123-147. https://doi.org/10.1177/004051754701700301

[4] Hurd JCH, Doyle, PJ. Fundamental aspects of the design of knitted fabrics. *J Text Inst* Proc. 1953; 44(8): 561-578. https://doi.org/10.1080/19447015308687861

[5] Shinn WE. An engineering approach to jersey fabric construction. *Text Res J.* 1953; 25(3): 270-277. https://doi.org/10.1177/004051755502500314

[6] Leaf GAV, Glaskin A. 43—The geometry of a plain knitted loop. *J Text Inst Trans.* 1955; 46(9): T587-T605. https://doi.org/10.1080/19447027.1955.10750345

[7] Munden D L. 26—The geometry and dimensional properties of plain-knit fabrics. *J Text Inst Trans.* 1959; 50(7): T448-T471. https://doi.org/10.1080/19447025908659923

[8] Postle R. 6—Dimensional stability of plain-knitted fabrics. *J Text Inst.* 1968; 59(2): 65-77. https://doi.org/10.1080/00405006808659967

[9] Kurbak A. Plain knitted fabric dimensions (Part II). *Text A.* 1998; 78: 36-44.

[10] Demiroz A, Dias T. A study of the graphical representation of plain-knitted structures part I: Stitch model for the graphical representation of plain-knitted structures. *J Text Inst.* 2000; 91(4): 463-480. https://doi.org/10.1080/00405000008659121

[11] Choi KF, Lo TY, An energy model of plain knitted fabric. *Text Res J.* 2003; 73(8): 739-748. https://doi.org/10.1177/004051750307300813

[12] Kyosev Y, Angelova Y and Kovar R. 3D modeling of plain weft knitted structures of compressible yarn. *Res J Text Appar.* 2005; 9(1): 88-97. https://doi.org/10.1108/RJTA-09-01-2005-B009

[13] Delavari K, Dabiryan H. Mathematical and numerical simulation of geometry and mechanical behavior of sandwich composites reinforced with 1× 1-Rib-Gaiting weft-knitted spacer fabric; compressional behavior. Compos Struct. 2021; 268: 113952. https://doi.org/10.1016/j.compstruct.2021.113952

[14] Ghatrenabi MH, Dabiryan H, Nosraty H. Modeling the Geometry of Weft-knitted Integrated Preforms as Reinforcement of Composite Joints. *Fibers Polym.* 2021; 22(9): 2572-2580. https://doi.org/10.1007/s12221-021-1180-x

[15] Omrani E, Dibajian SH, Hasani H. Development of ABAQUS Plugin Predicting the Mechanical Behavior and Failure Modes of Weft knitted-Reinforced Composites. *Fibers Polym*. 2025; 26: 883-907. http://dx.doi.org/10.1007/s12221-025-00850-2

[16] Huang R. Characterization and Modeling of Pores in Weft-Knitted Fabrics. PhD Dissertation, North Carolina State University; 2023. https://www.lib.ncsu.edu/resolver/1840.20/40816

[17] Ogulata RT. Air permeability of woven fabrics. *J Text Appar Tech and Manag.* 2006; 5(2): 1–10. https://www.researchgate.net/publication/283451342_Air_Permeability_of_Woven_Fabrics

[18] Jeddi AAA, Dabiryan H. Ideal stitch model for interlock-knitted fabric. *J Text Inst.* 2008; 99(4): 369–374. https://doi.org/10.1080/00405000701584444
[19] Li Y L, Yang L H, Chen S Y, Yuan J, Li N-N. 3D modeling and simulation of fancy fabrics in weft knitting. *J DongHua Uni*. 2012; 29(4): 351-358. https://doi.org/10.19884/j.1672-5220.2012.04.013
[20] Kejkar VKV, Tjprc. An Effect of Stitch Length. Lycra Percentage on Comfort Properties of Knitted Sport Wear. *Int J Text Fash Tech.* 2019; 9(3): 1-10. https://paper.researchbib.com/view/paper/225864
[21] Chakroun M G, Benltoufa S, Fayala F. The effect of fabric's structure on the breathability and the drying rate properties. *Comm Develop Assem Text Prod.* 2021; 2(1): 61–69. https://doi.org/10.25367/cdatp.2021.2.p61-69
[22] Megeid ZMA, Al-Bakry M, Ezzat M. The influence of stitch length of weft knitted fabrics on the sewability. *J Amer Sci.* 2011; 7(8): 610–617. https://www.jofamericanscience.org/journals/am-sci/am0708/068_6200am0708_610_617.pdf
[23] Gebart BR. Permeability of unidirectional reinforcements for RTM. *J Compos Mater* 1992; 26(8): 1100–1133. https://doi.org/10.1177/002199839202600802
[24] Afzal A, Ahmad S, Rasheed A, Ahmad F, Iftikhar F, Nawab Y. Influence of fabric parameters on thermal comfort performance of double layer knitted interlock fabrics. *Autex Res J.* 2017; 17(1): 20–26. https://doi.org/10.1515/aut-2015-0037
[25] Kaviany M. *Principles of Heat Transfer in Porous Media.* 2nd ed., Springer, New York, USA; 1995. https://doi.org/10.1016/S0017-9310(05)80083-3

Predviđanje funkcionalnih karakteristika interlok i rebrastih pletiva korišćenjem 3D računarskog modelovanja i analize

Hassan Ali, Salma Farooq, Muhammad Owais Raza Siddiqui, Muhammad Dawood Husain i Saira Faisal

Department of Textile Engineering, NED University of Engineering and Technology, University Road, Karachi, Pakistan

(Naučni rad)

Izvod

U ovom radu je razvijen računarski model interlok i rebrastih pletiva kako bi se predvideli propustljivost vazduha i termička svojstva tkanine. Ponavljajuće jedinične ćelije interlok i rebrastih pletenih struktura razvijene su u COMSOL Multiphysics® softveru, korišćenjem stvarnih parametara tkanine ekstrahovanih uz pomoć tehnike analize slike. Dobijeni rezultati modelovanja s zatim upoređena sa stvarnim eksperimentalnim vrednostima za tkaninu. Pored toga, validirani računarski model je korišćen za analizu uticaja dužine boda i debljine tkanine na termička svojstva i vazdušnu propustljivost tkanine. Utvrđeno je da dužina boda direktno proporcionalna vazdušnoj propustljivosti i obrnuto proporcionalna efektivnoj toplotnoj provodljivosti tkanine. Debljina tkanine direktno utiče na efektivnu toplotnu provodljivost, a obrnuto proporcionalno na vazdušnu propustljivost tkanine.

Ključne reči: Propustljivost vazduha; efektivna toplotna provodljivost; pletenje potke; računarska dinamika fluida; ponavljajuća jedinična ćelija

Co-pyrolysis of corn stalks and plastic waste: Chemical composition of the pyrolyzates as a base for producing environmentally sustainable fuels

Ivana Jovančićević[1], Vesna Antić[2] and Jan Schwarzbauer[1]

[1]*Institute of Organic Biogeochemistry in Geo-Systems, RWTH Aachen University, Aachen, Germany*
[2]*University of Belgrade, Faculty of Agriculture, Belgrade, Serbia*

Abstract

In this study pyrolysis and co-pyrolysis experiments involving lignocellulosic corn stalks (CS) samples and selected plastic waste fractions (high density polyethylene (HDPE) and polystyrene (PS)) were conducted at various mixing ratios. The main objective was to evaluate how the composition of the feedstock affects the yield and composition of the resulting pyrolysis products, by developing a sustainable method for the management of both biomass and plastic waste through the production of valuable oils and chemicals. This study contributes to a transitional approach for plastic waste management, given the anticipated reduction in the usage of plastic materials in the future. The co-pyrolysis mixtures demonstrated synergistic effects between the feedstocks, with plastic waste serving as hydrogen donors and enhancing the yield of CS pyrolysis products. Moreover, the products from plastic waste exhibited a significant predominance over those from CS, constituting ca. 66.6 and 85.6 % in the 1:1 CS/HDPE and CS/PS mixtures, respectively. This is particularly beneficial considering the elevated oxygen content in the CS products, which can contribute to heightened acidity and corrosion in the resulting synthetic bio-oil. This study reveals valuable insights into the formation of synthetic bio-oils by designing the chemical composition and optimising the pyrolysis yield.

Keywords: Biomass waste; high density polyethylene; polystyrene; synthetic bio-oil; gas chromatography-mass spectrometry.

Available on-line at the Journal web address: http://www.ache.org.rs/HI/

ORIGINAL SCIENTIFIC PAPER

UDC: 66.092-97-922: 62-665.9

Hem. Ind. **79(3)** 179-189 (2025)

1. INTRODUCTION

The extensive use of fossil fuels has given rise to a significant global environmental issue, characterized by the substantial emission of greenhouse gases such as carbon dioxide (CO_2), nitrogen oxides (NO_x), and sulfur oxides (SO_x) [1,2]. These emissions induce extensive consequences on the environment, climate, and human health. Therefore, there is a growing need to investigate alternative feedstocks to replace fossil fuels.

In recent decades, various forms of lignocellulosic biomass waste have been studied as a more sustainable and renewable alternative to fossil fuels [3-6]. Most studies have been carried out on woody residues; however, any form of biomass waste can be considered for bio-oil production [7,8]. Due to its abundance, renewable nature, and low price, lignocellulosic biomass stands as a promising resource for both the chemical industry and energy production. Thus, the context of using biomass waste such as agricultural residues as a raw material for fuel production to replace fossil fuels, hold a special significance. Furthermore, improper managing of biomass waste can lead to substantial environmental problems, since after harvesting, the remaining biomass is often treated only as discarded material. It is either left in fields, creating solid waste, or burned, resulting in substantial air pollution [9]. Therefore, the use of biomass waste as a replacement for fossil fuels can prevent environmental pollution from its discharge and contribute to sustainable environmental protection, as the resulting bio-oil and biochar have the potential to be used as fuels.

Corn holds paramount significance as an agricultural feedstock in Serbia. According to the Serbian Ministry of Agriculture, in year 2022 a record of 8 million metric tons of corn was produced [10]. The byproducts stemming from corn production are being improperly managed, often subjected to landfill disposal or incineration, thereby culminating

Corresponding author: Jan Schwarzbauer, Institute of Organic Biogeochemistry in Geo-Systems, RWTH Aachen University
E-mail: jan.schwarzbauer@emr.rwth-aachen.de
Paper received: 8 June 2024; Paper accepted: 24 June 2025; Paper published: 26 August 2025.
https://doi.org/10.2298/HEMIND240608010J

in pronounced atmospheric contamination. Hence, a more logical approach for corn waste management would be to use the lignocellulosic parts of the corn waste for energy production.

However, a prominent disadvantage of bio-oils is significant content of oxygen originating from the biomass source material [11]. This results in a reduced calorific value, coupled with challenges encompassing corrosion and instability [11]. To address these limitations in an effective manner, a promising approach could be co-pyrolysis of biomass with plastic wastes. Significantly, due to their substantial carbon and hydrogen contents, plastic materials such as polyethylene (PE) and polystyrene (PS) can play an important role as valuable substrates for generating synthetically derived bio-oils. Furthermore, the improper disposal of plastic waste stands as one of the foremost environmental problems of our time. Therefore, co-pyrolysis of biomass with plastic waste introduces a sustainable approach for waste recycling, leading to the creation of valuable oils and chemical compounds. Oils derived from plastic waste are not considered bio-oils as they are produced from synthetic materials. However, for reasons of practicability, oils derived from co-pyrolysis of biomass and plastic waste will be referred to as synthetic bio-oils in this paper.

Some research has been already conducted to explore co-pyrolysis of diverse forms of biomass waste in combination with plastic waste. It was demonstrated that co-gasification of polyethylene and woodchips using high-temperature steam in a semi-batch reactor exhibited synergistic effects, leading to superior syngas yield, hydrogen yield, and apparent thermal efficiency compared to the weighted average properties of individual components [12]. In another study co-pyrolysis of agricultural biomass and plastic wastes, specifically polyethylene terephthalate (PET), polypropylene (PP), and polyvinyl chloride (PVC) was investigated showing that rapeseed stalk and PP exhibited a synergistic effect, enhancing the production of aliphatic hydrocarbons and alcohols [13]. Furthermore, Liu *et al.* [14] systematically investigated the synergistic effects during co-pyrolysis of pinewood and PP in a fixed-bed reactor. Their results revealed significant improvements in syngas yield, hydrogen yield, and carbon monoxide yield, with the increases of 27, 80 and 63 %, respectively, compared to the weighted averages obtained by pyrolysis of individual components. Also, in another study it was shown that the addition of PS to cellulose clearly improved the quality of the obtained oil, resulting in decreased acid number, pour point and density [15]. Furthermore, addition of PS to Sargassum macroalgae pyrolysis was reported to improve the oil potential heating value and decreased its potential for producing air pollution when combusted, by lowering its nitrogen content [16]. Co-pyrolysis of low-density polyethylene (LDPE) and biomass was investigated in another study reporting that the LDPE addition can effectively improve the selectivity for naphthalene family products (1-methylnaphthalene and 2-methylnaphthalene) in the catalytic pyrolysis of biomass and decrease the content of aromatic hydrocarbons larger than C_{10} [17].

However, systematic studies of co-pyrolysis regarding molecular compositions and their relevance for designing bio-oils are scarce. Therefore, in this study the general approach to copyrolyse plastic waste and agricultural residues has been tested for an optimal bio-fuel design. Therefore, pyrolysis and co-pyrolysis gas chromatography-mass spectrometry (GC/MS) experiments were conducted using corn stalks (CS) together with high density polyethylene (HDPE) and 'polystrene (PS) plastic waste at different ratios. The overall goal of this study was to investigate the influence of PS and HDPE addition to CS pyrolysis and the corresponding molecular compositions. Therefore, the specific goals of this study were: (i) to identify and quantify distinct pyrolysis products derived from these feedstocks, and (ii) to investigate potential interactions between these samples during the pyrolysis process. Additionally, the study aimed to assess whether specific waste ratios could induce synergistic effects, influence production of particular products or giving rise to the formation of novel compounds.

2. EXPERIMENTAL

2. 1. Chemicals and reference compounds

Standard reference materials for the natural and synthetic polymers comprising cellulose, lignin, PE, and PS were purchased from Geyer Th. GmbH & Co. KG, Germany. Organic solvents required for the pyrolysis and fractionation experiments, namely acetone, dichloromethane (DCM), and methanol, were also obtained from Geyer Th. GmbH & Co. KG, Germany. Corn stalks were gathered in the vicinity of the city of Šabac in Serbia. Plastic waste materials such as food

packaging, containers for food and cosmetics, plastic furniture, plastic bottles, *etc.*, were collected from multiple households in Aachen, Germany.

2. 2. Sample preparation

2. 2. 1. Agricultural waste samples

Corn stalks with leaves were cut off about 5-10 cm above the ground. They were then coarsely chopped with a knife and air dried. The samples were then ground and sieved to a specific particle size of approx. 1-2 mm suitable for pyrolysis experiments.

2. 2. 2. Plastic waste samples

After collecting the plastic waste, the material was washed with water and left to dry in air. The material was then cut into smaller particles (about 2 cm) by using scissors and shredded into particles smaller than 5 mm. The shredding was carried out under a flow of nitrogen, which was used to cool the samples and prevent melting and thermal degradation.

2. 3. Continuous flow off-line pyrolysis experiments

The pyrolysis and co-pyrolysis experiments were carried out in a model MTF 10/15/130 tube furnace (Carbolite, UK). The samples were placed in an aluminium foil vessel located in the middle of a quartz tube 150 mm long and 15 mm in diameter. The quartz tube was connected at one end to a continuous nitrogen stream, while the other end was connected to a flask tube filled with acetone that was cooled with dry ice and ethanol. To minimize the risk of secondary reactions during the heating process, the samples were placed directly into a preheated oven, consequently, the experiments were carried out without heating rate at a constant temperature of 450 °C for 30 min. The temperature of 450 °C was selected based on the optimization of experimental conditions. Experiments were conducted at the following temperatures: 400, 450, 500 and 550 °C. Based on the semi-quantitative evaluation of the pyrograms in terms of yield, 450 °C was determined to be the most efficient temperature for the thermal degradation of the samples as also suggested in a former study [18].

The co-pyrolysis experiments using corn stalk CS with one of the synsthetic polymers HDPE or PS, respectively, were carried out with the following ratios of pyrolysis educts: 4:1 (100 mg CS : 25 mg HDPE or PS); 4:2 (100 mg CS : 50 mg HDPE or PS); 4:3 (100 mg CS : 75 mg HDPE or PS); 1:1 (100 mg CS : 100 mg HDPE or PS); 3:4 (75 mg CS : 100 mg HDPE or PS); 2:4 (50 mg CS : 100 mg HDPE or PS); 1:4 (25 mg CS : 100 mg HDPE or PS). All experiments were carried out in duplicates.

The resulting pyrolyzates were left to evaporate until they reached about 2 mL and were then dried with anhydrous Na_2SO_4. Then, the samples were subjected to fractionation by liquid chromatography with a micro glass column with 2 g of activated silica gel (Baker, UK). Elution was performed by 8 mL of DCM (1st fraction), followed by 8 mL of methanol (2nd fraction). To both fractions 50 µL of surrogate standard containing fluoracetophenone (5.8 ng/µL), d20-benzophenone (6.3 ng µL^{-1}), and d_{34}-hexadecane (6.0 ng µL^{-1}) were added. The volume was reduced to approx. 200 µL prior to the GC/MS analysis.

2. 4. Gas chromatography-mass spectrometry analysis

Qualitative and quantitative analysis of all pyrolyzates was performed on a Finnigan Trace MS single quadrupole mass spectrometer (ThermoElectron, Egelsbach, Germany) coupled to a HRGC 5160 gas chromatograph (CarloErba, Milano, Italy). The gas chromatograph was equipped with a ZB-5 (Phenomenex, Aschaffenburg, Germany) capillary column (30 m length × 0.25 mm inner diammeter × 0.25 µm film). The chromatographic conditions were the following: aliquots of ca. 0.2 to 1 µL injected splitless (injector temperature 270 °C) at an initial temperature of 60 °C, isothermal time 3 min, followed by a ramp of 3 °C min^{-1} up to 240 °C, and a subsequent increase of 10 °C min^{-1} up to 310 °C. Helium was used as the carrier gas, with a flow rate set at 1.5 mL min^{-1}. The mass spectrometer measured in electron impact ionisation mode (EI+, 70 eV) with a source temperature of 200 °C, an interface temperature of 270 °C and by full scan from 35 to 500 *m*/*z*. The scan rate was set to 0.67 scans per second.

2. 5. Identification and quantification of the pyrolysis products

Pyrolysis products were identified based on the comparison of the obtained mass spectra with the NIST 14/Wiley registry mass spectral data bases [19], detailed interpretation of the mass spectra, comparison with reference material as well as published literature data. The relative quantification of the obtained degradation products was based on the integration of specific ion chromatograms and corresponding peak areas, corrected using the surrogate standard.

3. RESULTS AND DISCUSSION

3. 1. Pyrolysis experiments

To evaluate the initial composition of the pyrolysis oils and to relate it to the products, pyrolysis experiments were conducted using individual samples of the synthetic polymer waste, and reference materials of cellulose and lignin, as well as the CS sample. The specific pyrolysis products for HDPE and PS have been previously identified and are presented in detail in our former study [18]. Briefly, pyrolysis experiments on HDPE revealed a distinct pattern, characterized by a sequence of triplets. Each triplet consists of alkadienes, *n*-alkenes, and *n*-alkanes, with a systematic increase in the carbon number as given by the homologues series [18]. Contrary, pyrolysis of PS produced only aromatic products, with styrene dimer and styrene trimer having the highest abundance [18].

Pyrolysis of CS produced dark oil as the predominant pyrolysis product. The GC/MS analysis of the resultant pyrolyzate revealed a complex mixture of oxygenated compounds, including phenols, aldehydes, fatty acids, furans, and alcohols. This spectrum of degradation products is characteristic for lignocellulosic materials, highlighting the contribution of components coming from the thermal degradation of both lignin and cellulose [20]. The pyrolysis products were identified and assigned to their specific compound group (see Table 1). All identified pyrolysis products were quantified. However, the quantification represents only a fraction of all peaks observed in the chromatogram obtained. As listed in Table 1, the predominant group of degradation products observed are phenolic compounds derived from the lignin content present in CS. Phenols comprised 44.6 % of the obtained pyrolizate. The most abundant compound is methoxy-vinylphenol, constituting 13.5 % of the total pyrolizate, followed by methoxyphenol at 8 %, and dimethoxyphenol, representing up to 7.8 % of the composition. The cellulose derived compounds in CS were determined at 18.8 %, including compounds such as furanone, furyl methyl ketone, methylfurfural, ethenylfuran, methyl-cyclopentanedione and 1,4:3,6-dianhydro-α-d-glucopyranose. The given compounds were also identified in corn stalk samples in literature [20].

Table 1. Identified degradation products obtained in the pyrolysis experiments using CS samples

Compound group	Content, %
Phenolyc compounds	
2-Methoxyphenol	8
4-Ethyl phenol	6.3
2-Methoxy-6-methylphenol	2.3
4-Ethyl-3-methylphenol	0.7
4-Ethyl-2-methoxyphenol	4.2
2-Methoxy-4-vinylphenol	13.5
2,6-Dimethoxyphenol	7.8
2-Methoxy-4-allylphenol	0.6
1-(4-Hydroxy-3-methoxyphenyl)-2-propanone	0.9
2,6-Dimethoxy-4-(2-propenylphenol)	0.3
Aldehydes	
3-Methoxy-4-hydroxybenzaldehyde	2.4
4-Hydroxy-3,5-dimethoxy-benzaldehyde	0.7
5-Methylfurfural	0.9
Acidic compounds	
4-Hydroxy-3-methoxybenzoic acid (Vanillic acid)	1.3
Hexadecanoic acid	0.2
Oleic acid	0.1
Octadecanoic acid	0.1

Compound group	Content, %
Ketones	
Furanone	4.8
2-Furyl methyl ketone	0.8
Methyl-cyclopentanone	9.6
3-Methyl-1,2-cyclopentanedione	6.3
Alcohols	
3-Methoxy-1,2-benzenediol	< 0.1
1-(2,4,6-Trihydroxyphenyl)-2-pentanone	0.9
Others	
3-Ethyl-2-hydroxycyclopent-2-en-1-one	2.1
1,4:3,6-Dianhydro-α-d-glucopyranose	3.4
Unknown	14.6
Unknown	4.0
2-Ethenylfuran	2.6
2.3-Dihydroinden-1-one	0.6
Isopropyl myristate	<0.1

3. 2. Co-pyrolysis experiments

Co-pyrolysis experiments involving mixtures in different ratios of CS and HDPE resulted in a blend of the distinct degradation products from both feedstocks (Fig. 1). Subsequent fractionation of the pyrolyzates effectively separated these products.

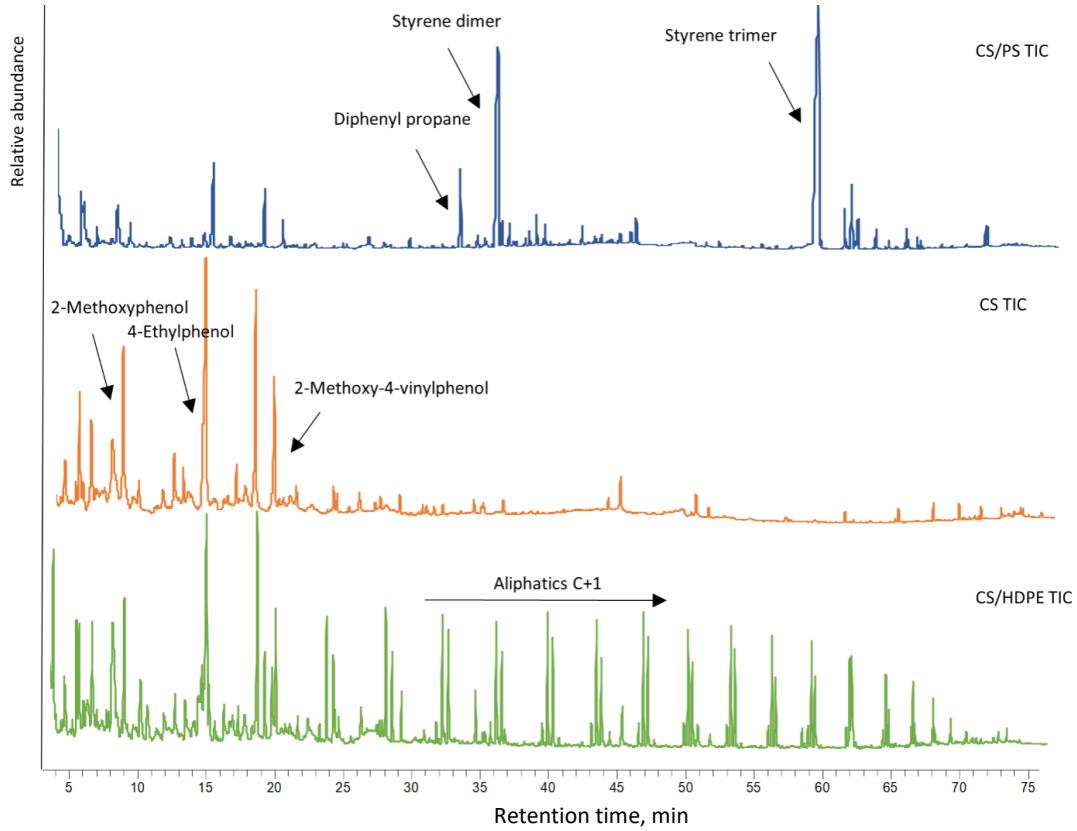

Figure 1. total ion chromatograms (TIC) obtained from the pyrolysis of CS samples and co-pyrolysis experiments on CS/PS and CS/HDPE mixtures in the 1:1 ratio

GC/MS analysis of the fractions revealed that, in contrast to the methanol fraction containing only CS degradation products, DCM fractions contained predominantly products derived from HDPE degradation, with only trace amounts of CS-derived products.

Co-pyrolysis of the CS/PS mixture resulted in a mixture of specific products as already observed in the CS/HDPE experiments. In contrary to the CS/HDPE experiments, in the DCM fraction, in all the observed ratios, products from the CS degradation were not identified, and only products coming from PS thermal degradation were observed. Consequently, the CS pyrolysis products were identified in the methanol fraction.

3. 2. 1. Co-pyrolysis of corn stalks / high density polyethylene mixtures

The effects of CS/HDPE ratios, ranging from 4:1 to 1:4 in the co-pyrolysis experiments were evaluated by the composition pattern based on calculated percentages of CS and HDPE products in the total products (as illustrated in Figure 2). According to Figure 2a, thermal degradation of both CS and HDPE was inhibited during CS/HDPE co-pyrolysis, resulting in significantly lower product yields compared to those obtained from individual pyrolysis processes. Already a very low amount of 25 mg of HDPE addition to CS pyrolysis has influenced the degradation process of CS. The fact that co-pyrolysis of biomass with different plastics differs from the individual pyrolysis of biomass was already proven in the literature [21,22].

However, further addition of the polymer into the mixture led to a linear increase in the amount of the obtained CS degradation products. Figure 2b demonstrates a linear correlation between the specific pyrolysis products and the amount of CS and HDPE in the pyrolysis mixtures. The respective pyrolysis product groups exhibited a yield increase from the CS/HDPE ratio of 4:1, reaching their maximum at the 1:1 ratio, followed by a decrease in ratios from 1:1 to 1:4. Only glucose derivatives reached their maximum at the 4:3 ratio (Table 2). In the 1:4 mixture, CS products constituted only 2.6 % of the resulting pyrolysis liquids (Figure 2b). This is in line with the study of Fan *et al.* investigating pyrolysis of lignin and PE mixtures in different ratios [22]. They reported that the addition of PE to lignin pyrolysis experiments led to the production of higher yields of lignin products, reaching the maximum at the ratio of 1:1 [23].

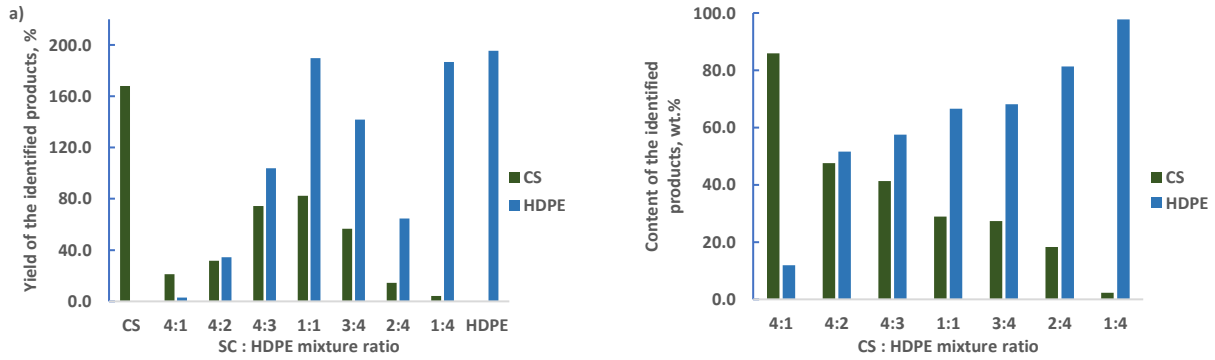

Figure 2. Co-pyrolysis of CS/HDPE mixtures: a) yields of the total identified CS and HDPE products; b) content of the total identified CS and HDPE products in the overall co-pyrolysis products

Table 2. Composition of the CS/HDPE co-pyrolysis products expressed as content of the compound groups for different CS/HDPE mass ratios

Compound group	CS/HDPE mass ratio						
	4:1	4:2	4:3	1:1	3:4	2:4	1:4
	Content, %						
Phenols	32.8	14.5	19.4	16.5	16.7	7.7	0.2
Aldehydes	1.7	2.9	1.6	0.8	0.8	2.2	0.3
Acids	0.3	0.2	0.7	0.7	0.7	0.2	0.0
Ketones	11.2	8.4	8.9	7.3	7.1	7.8	1.8
Diols and triols	0.7	0.8	1.3	0.9	1.1	0.2	0.0
Glucose derivatives	39.2	20.6	9.4	2.7	0.8	0.1	0.0
Alkadienes	0.0	3.1	3.4	7.6	7.7	6.1	9.0
n-Alkenes	0.0	14.0	22.2	30.4	32.8	31.7	43.5
n-Alkanes	11.9	34.5	31.9	28.6	27.7	43.5	45.3
Others	2.2	0.9	1.2	4.5	4.6	0.4	

Furthermore, in the CS/HDPE = 4:1 ratio (see subchapter 2.3), alkadienes and alkenes were not observed, and only alkanes from C_{13} to C_{31} were identified, constituting 11.9 % of all pyrolysis products for this experiment (Figure 2b).

However, as the proportion of HDPE in the feedstock increased, a linear increase in the amount of detected HDPE products occurred, including alkadienes, *n*-alkenes, and *n*-alkanes. *n*-Alkenes and *n*-alkanes dominated the pyrolizates in the ratios from 4:3 to 1:4, indicating a pronounced prevalence over CS products.

The 1:4 ratio resulted in a substantial production of HDPE products reaching 97.7 % (Figure 2b). The introduction of lower amounts of CS (25 mg) during HDPE pyrolysis suppressed the generation of n-alkanes. However, it resulted in increased production of n-alkenes and alkadienes (see Table 2). Moreover, the CS/HDPE ratio of 2:4 led to a noteworthy reduction in the total generated aliphatic products compared to 1:4 ratio (Figure 2a). However, with the further addition of CS in the feedstock, HDPE products experienced an increase starting from the 2:4 ratio and reaching their maximum at the 1:1 ratio.

The ratio of CS to HDPE was observed to significantly influence the composition of the pyrolytic liquids (Table 2). Co-pyrolysis of HDPE and CS resulted in the production of synthetic bio-oils characterized by lower oxygen content compared to the bio-oils obtained from the CS degradation, and a significant aliphatic contribution particularly those ranging from 4:3 to 2:4. These ratios revealed chemical compositions of the obtained oils beneficial for synthetic bio-oil production exhibiting a favourable balance of aliphatic and oxygen-aromatic compounds with content of 57.5 to 81.3 % of the aliphatic compounds (sum of alkanes, alkenes and alkadienes; see Table 2) within the specified range. This aliphatic composition is comparable to that found in commercial fuels like diesel, indicating substantial promise for future applications.

Table 2. Composition of the CS/HDPE co-pyrolysis products expressed as content of the compound groups for different CS/HDPE mass ratios

Compound group	CS/HDPE mass ratio						
	4:1	4:2	4:3	1:1	3:4	2:4	1:4
	Content, %						
Phenols	32.8	14.5	19.4	16.5	16.7	7.7	0.2
Aldehydes	1.7	2.9	1.6	0.8	0.8	2.2	0.3
Acids	0.3	0.2	0.7	0.7	0.7	0.2	0.0
Ketones	11.2	8.4	8.9	7.3	7.1	7.8	1.8
Diols and triols	0.7	0.8	1.3	0.9	1.1	0.2	0.0
Glucose derivatives	39.2	20.6	9.4	2.7	0.8	0.1	0.0
Alkadienes	0.0	3.1	3.4	7.6	7.7	6.1	9.0
n-Alkenes	0.0	14.0	22.2	30.4	32.8	31.7	43.5
n-Alkanes	11.9	34.5	31.9	28.6	27.7	43.5	45.3
Others	2.2	0.9	1.2	4.5	4.6	0.4	

3. 2. 2. Co-pyrolysis of corn stalks /polystyrene mixtures

As noticed above in Figure 1, in the CS/HDPE co-pyrolysis experiments the CS products were identified in the methanol fraction. Moreover, the comprehensive outcomes from the CS/PS pyrolysis experiments demonstrated a significant predominance of PS products over CS degradation (Figure 3a). The most abundant group of pyrolysis products in all co-pyrolysis experiments were benzene derivatives coming from the PS degradation, followed by phenols, glucose derivatives and ketones.

The relative proportions of the identified products given as content of the respective compound groups are given in Table 3. In the 1:1 ratio, acids, aldehydes and alcohols were detected at a minimal level of 0.4, 0.8 and 0.3 %, respectively. Ketones and glucose derivatives appeared at a range of 2.2 and 1.3 % respectively. The phenol formation decreased from 44.6 % in the individual CS pyrolysis to 8.4 % in the CS/PS 1:1 ratio. Moreover, at the 1:1 ratio benzene derivative dominated the pyrolizate with 85.6 %. Here, benzene derivatives include compounds like styrene oligomers, cyclopropyl benzene, biphenyl, diphenylmethane, diphenylethylene, diphenyl propane and diphenyl hexadiene. Styrene oligomers, styrene dimer and styrene trimer were identified as the most abundant pyrolysis products. Even at the 4:2 ratio, PS products showed overall prevalence over the products from CS degradation comprising 69.4 % of the obtained pyrolizate (Fig. 3b). It is suggested that lignocellulosic biomass sources typically exhibit a low hydrogen content, reflected in an H/C ratio ranging from 0 to 0.3. In contrast, plastic waste possesses a significantly higher H/C value when compared to biomass sources, resulting in higher yields of products with petrochemical characteristics [24].

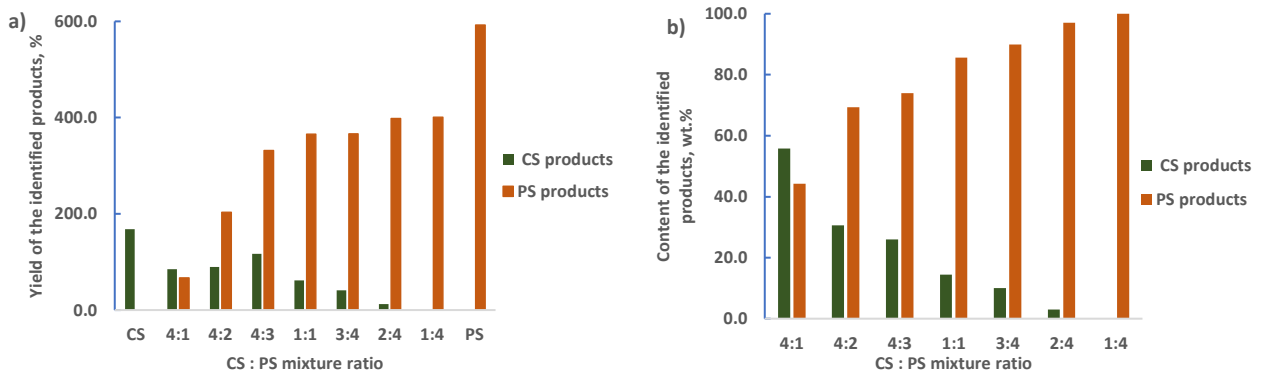

Figure 3. a) yield of the total identified CS and PS products; b) content of the total identified CS and PS products in the obtained pyrolizates

Table 3. Relative composition of the compound groups in the CS/PS co-pyrolysis experiments. Given ratios of co-pyrolysis educts correspond to subchapter 2.3

Compound classes / Co-pyrolysis experiments	Ratio of co-pyrolysis educts						
	4:1	4:2	4:3	1:1	3:4	2:4	1:4
	Relative content, %						
Phenols	13.4	16.4	10.9	8.4	6.2	0.7	0.0
Aldehydes	6.7	1.5	2.2	0.8	0.8	0.7	0.0
Acids	0.2	0.5	0.5	0.4	0.3	0.0	0.0
Ketones	4.6	5.1	8.7	2.2	1.5	0.6	0.0
Alcohols	0.9	0.7	0.3	0.3	0.5	0.1	0.0
Glucose derivatives	28.1	4.6	2.0	1.3	0.0	0.8	0.0
Benzene derivatives	44.2	69.4	74.0	85.6	89.9	97.0	100.0
Others	2.0	1.8	1.4	1.0	0.7	0.1	0.0

Furthermore, yields for both CS and PS samples were suppressed during the co-pyrolysis process as compared to the individual pyrolysis experiments. However, higher amounts of PS in the pyrolysis mixture did once again lead to higher amounts of the total CS products starting from the 4:1 ratio and reaching their maximum at the 4:3 ratio. For the 1:4 ratio, CS products were not identified. This can be explained by the prevalence of products derived from the PS degradation process, particularly styrene dimer and styrene trimer. The high abundance of these compounds might mask the presence of CS products in the chromatogram, making their detection challenging. Furthermore, the introduction of CS into PS pyrolysis resulted in reduced quantities of PS products compared to the individual PS pyrolysis. This pattern persists as the CS amount in the pyrolysis mixture increases. However, the 1:4 ratio demonstrated the most significant decrease in product yields, with subsequent additions showing only small changes in the obtained products.

3. 3. Comparison of co-pyrolysis processes of CS/HDPE and CS/PS mixtures

The co-pyrolysis of CS with different plastic wastes—HDPE and PS—demonstrated divergent pathways, both in product distribution and in the nature of biomass-plastic interactions. While both systems aimed to improve bio-oil quality by reducing oxygenated species, the underlying mechanisms and product outcomes differed.

In CS/HDPE mixtures, the co-pyrolysis resulted in liquid products with a marked aliphatic character, indicating effective hydrogen transfer and synergistic interaction. The formation of diesel-like compounds in HDPE-rich systems supports previous findings that polyolefins can enhance the deoxygenation of lignocellulosic biomass via radical neutralization and hydrogen donation [24]. Conversely, in CS/PS mixtures, the pyrolysates were dominated by compounds originating from PS degradation. The obtained CS product yields in the CS/PS mixture were much higher compared to the yields obtained in the CS/HDPE mixture. This could be due to the formation of wax, that is being produced as a solid product of the pyrolysis process during the thermal degradation of HDPE. This is a residual product that partly remains in the pyrolysis container and can thus compress the degradation of the biomass, which is not the case with PS degradation.

These contrasting behaviors suggest that plastic type plays a decisive role in directing co-pyrolysis pathways. HDPE serves primarily as a hydrogen source, enabling improved fragmentation and volatilization of biomass-derived species while PS contributes predominantly through its own decomposition, producing high-value aromatics but offering limited synergy with the lignocellulosic matrix. From an application standpoint, CS/HDPE systems are more aligned with fuel-oriented outcomes, while CS/PS may be more suited for producing specialty chemicals. Therefore, the choice of plastic co-feedstock should be aligned with the desired product spectrum.

Achieving economically feasible production of high-quality bio-oil requires careful process optimization to ensure satisfactory yields. One viable upgrading strategy focuses on in situ catalytic deoxygenation during pyrolysis. Zeolite-based catalysts, particularly ZSM-5, are widely used for this purpose due to their efficiency in facilitating dehydration reactions [25,26]. Other catalysts, such as basic metal oxides (e.g., CaO and MgO), have also been explored [26], though their application may lead to increased coke formation and a decline in oil yield [26].

4. CONCLUSION

In this study, pyrolysis and co-pyrolysis experiments on corn stalk samples and HDPE and PS plastic waste samples were conducted at various ratios. The objective was to explore the influence of the feedstock composition on the obtained product yields and the selectivity of the obtained products. Synergistic effects were observed in both CS/HDPE and CS/PS mixtures. The plastic samples acted as hydrogen donors during CS degradation, resulting in increased yields of CS products as the proportion of plastic waste in the pyrolysis mixture varied from 4:1 to 1:1. Notably, both HDPE and PS products exhibited a pronounced prevalence over CS products, which is particularly advantageous given the high oxygen content in CS products. In CS/HDPE experiments, aliphatic compounds, specifically *n*-alkenes and *n*-alkanes, constituted the most abundant compounds. The total aliphatic content in the obtained pyrolyzates ranged from 57.5 % to 81.3 % for ratios ranging from 4:3 to 2:4. This range of aliphatic compounds closely resembles diesel fuel, highlighting the potential of these co-pyrolysis products for synthetic bio-oil production. In contrast, CS/PS experiments showed that benzene derivatives were the predominant compounds, constituting 85.6 % in the 1:1 ratio. This resulted in a reduction in the phenolic structures originating from the pyrolysis of CS, as opposed to the individual pyrolysis of CS.

It is important to highlight that this method signifies a transitional approach for managing plastic waste, as the utilization of plastic materials is expected to phase out in the anticipated future. However, this investigation presents insights into the behaviors of lignocellulosic biomass waste and plastic materials, revealing valuable understandings into the chemical composition of the bio oils obtained from co-pyrolysis experiments. The results represent important and general aspects as base for designing bio fuels from different waste fractions.

Acknowledgement: The authors acknowledge the financial support by the German Federal Ministry of Education and Research (Bundesministerium für Bildung und Forschung)

REFERENCES

[1] Ryu HW, Kim DH, Jae J, Lam SS, Park ED, Park Y-K. Recent advances in catalytic co-pyrolysis of biomass and plastic waste for the production of petroleum-like hydrocarbons. *Bioresour Technol.* 2020; 310: 123473. https://doi.org/10.1016/j.biortech.2020.123473

[2] Wang G, Dai Y, Yang H, Xiong Q, Wang K, Zhou J, Li Y, Wang S. A review of recent advances in biomasspyrolysis. *Energ Fuel.* 2020; 34(12): 15557-15578. https://doi.org/10.1021/acs.energyfuels.0c03107

[3] Chen H, Lin G, Chen Y, Chen W, Yang H. Biomass pyrolytic polygeneration of tobacco waste: product characteristics and nitrogen transformation. *Energ Fuel.* 2015; 30(3): 1579-1588. https://doi.org/10.1021/acs.energyfuels.5b02255.

[4] Munawer ME. Human health and environmental impacts of coal combustion and post-combustion wastes. *J Sustain Min.* 2018; 17(2): 87-96. https://doi.org/10.1016/j.jsm.2017.12.007.

[5] Martín JVG, González JF, Martínez G. Energetic use of the tomato plant waste. *Fuel Process Technol.* 2008; 89(11): 1193-1200. https://doi.org/10.1016/j.fuproc.2008.05.011.

[6] Tsai W, Lee MK, Chang Y-F. Fast pyrolysis of rice husk: Product yields and compositions. *Bioresour Technol.* 2007; 98(1): 22-28. https://doi.org/10.1016/j.biortech.2005.12.005 .

[7] Mohan D, Pittman ACU, Steele PH. Pyrolysis of Wood/Biomass for Bio-oil: A Critical review. *Energ Fuel.* 2006; 20(3): 848-889. https://doi.org/10.1021/ef0502397.

[8] Bridgwater AV. Renewable fuels and chemicals by thermal processing of biomass. *J Chem Eng.* 2003; 91(2-3): 87-102. https://doi.org/10.1016/s1385-8947(02)00142-0.

[9] Koul B, Yakoob MY, Shah MP. Agricultural waste management strategies for environmental sustainability. *Environ Res.* 2022; 206: 112285. https://doi.org/10.1016/j.envres.2021.112285.

[10] Maslac T. Grain and Feed Annual Report (Serbia). United States Department of Agriculture - Foreign Agricultural Service, 2021. https://apps.fas.usda.gov/newgainapi/api/Report/DownloadReportByFileName?fileName=Grain%20and%20Feed%20Annual_Belgrade_Serbia_04-01-2021

[11] Omais B, Crépier J, Charon N, Courtiade M, Quignard A, Thiébaut D. Oxygen speciation in upgraded fast pyrolysis bio-oils by comprehensive two-dimensional gas chromatography. *Analyst* 2013; 138(8): 2258. https://doi.org/10.1039/c2an35597c

[12] Ahmed I, Nipattummakul N, & Gupta A, Characteristics of syngas from co-gasification of polyethylene and woodchips. *Appl Energy*, 2010; 88(1): 165-174. https://doi.org/10.1016/j.apenergy.2010.07.007

[13] Wu M, Wang Z, Chen G, Zhang M, Sun T, Wang Q, Zhu H, Guo S, Chen Y, Zhu Y, Lei T, Burra K, G & Gupta AK, Synergistic effects and products distribution during Co-pyrolysis of biomass and plastics. *J Energy Inst.* 2023; 111, 101392. https://doi.org/10.1016/j.joei.2023.101392

[14] Liu X, Burra KG, Wang Z, Li J, Che D, & Gupta AK, On deconvolution for understanding synergistic effects in co-pyrolysis of pinewood and polypropylene. *Appl Energy* 2020; 279: 115811. https://doi.org/10.1016/j.apenergy.2020.115811

[15] Rutkowski P, Kubacki A. Influence of polystyrene addition to cellulose on chemical structure and properties of bio-oil obtained during pyrolysis. *Energy Convers Manag.* 2006; 47(6): 716-731. https://doi.org/10.1016/j.enconman.2005.05.017

[16] KositkanawuthK, Bhatt A, Sattler M, & Dennis, Renewable Energy from Waste: Investigation of Co-pyrolysis between Sargassum Macroalgae and Polystyrene. *Energy Fuels.* 2017; 31(5): 5088-5096. https://doi.org/10.1021/acs.energyfuels.6b03397

[17] Zheng Y, Tao L, Yang X, Huang Y, Liu C, Zheng Z. Study of the thermal behavior, kinetics, and product characterization of biomass and low-density polyethylene co-pyrolysis by thermogravimetric analysis and pyrolysis-GC/MS. *J Anal Appl Pyrol.* 2018; 133: 185-197. https://doi.org/10.1016/j.jaap.2018.04.001

[18] Jovancicevic I, Antić M, Gajica G, Schwarzbauer J. Co-pyrolysis of various plastic waste components as an environmentally sustainable source of alternative fuels. *J Serb Chem Soc.* 2024; 89(7-8): 1053-1066. https://doi.org/10.2298/jsc240207046j

[19] Wiley Registry/NIST Mass Spectral Library 2023. https://sciencesolutions.wiley.com/solutions/technique/gc-ms/wiley-registry-nist-mass-spectral-library/ (Accessed July 31, 2025)

[20] Pittman CU, Mohan D, Eseyin AE, Li Q, Ingram LL, Hassan EB, Mitchell B, Guo H, Steele PH. Characterization of Bio-oils Produced from Fast Pyrolysis of Corn Stalks in an Auger Reactor. *Energ Fuel.* 2012; 26(6): 3816-3825. https://doi.org/10.1021/ef3003922.

[21] Wang S, Lin X, Li Z, Yi W, Bai X. Thermal and kinetic behaviors of corn stover and polyethylene in catalytic co-pyrolysis. *Bioresour.* 2018; 13(2): 4102-4117. https://doi.org/10.15376/biores.13.2.4102-4117.

[22] Fan Y, Liu C, Kong X, Yue-Hong H, Lei M, Xiao R. A new perspective on polyethylene-promoted lignin pyrolysis with mass transfer and radical explanation. *Green Energy Environ.* 2022; 7(6): 1318-1326. https://doi.org/10.1016/j.gee.2021.02.004.

[23] Chu SY, Subrahmanyam AV, Huber GW. The pyrolysis chemistry of a β-O-4 type oligomeric lignin model compound. *Green Chem.* 2013; 15(1): 125-136. https://doi.org/10.1039/c2gc36332a.

[24] Chattopadhyay J, Pathak TS, Srivastava R, Singh A. Catalytic co-pyrolysis of paper biomass and plastic mixtures (HDPE (high density polyethylene), PP (polypropylene) and PET (polyethylene terephthalate)) and product analysis. *Energy* 2016; 103: 513-521. https://doi.org/10.1016/j.energy.2016.03.015.

[25] Nishu, Liu R, Rahman MdM, Sarker M, Chai M, Li C, Cai J. A review on the catalytic pyrolysis of biomass for the bio-oil production with ZSM-5: Focus on structure. *Fuel Proc Technol.* 2020; (199): 106301. https://doi.org/10.1016/j.fuproc.2019.106301

[26] Zadeh ZE, Abdulkhani A, Aboelazayem O, Saha B. Recent Insights into Lignocellulosic Biomass Pyrolysis: A Critical Review on Pretreatment, Characterization, and Products Upgrading. *Processes.* 2020; 8(7): 799. https://doi.org/10.3390/pr8070799

Hemijski sastav pirolizata dobijenih ko-pirolizom ostataka kukuruznih stabljika i plastičnog otpada kao osnova za proizvodnju ekološki održivih goriva

Ivana Jovančićević[1], Vesna Antić[2] i Jan Schwarzbauer[1]

[1]Institut za organsku biogeohemiju u organskim geosistemima, RWTH Univerzitet u Ahenu, Ahen, Nemačka
[2]Univerzitet u Beogradu, Poljoprivredni Fakultet, Beograd-Zemun, Srbija

(Naučni rad)

Izvod

U ovom istraživanju izvršeni su eksperimenti pirolize i ko-pirolize uzoraka otpada lignoceluloznih kukuruznih stabljika (KS) i odabranih frakcija plastičnog otpada (polietilen velike gustine (engl. high density polyethylene, HDPE) i polistiren (PS)) u različitim masenim odnosima. Glavni cilj bio je procena uticaja sastava sirovine na prinos i sastav rezultujućih piroliznih proizvoda, razvijajući održivu metodu za upravljanje kako otpadom biomase tako i plastičnim otpadom kroz proizvodnju ulja i hemikalija. Reakcije ko-pirolize dokazale su sinergističke efekte između sirovina, pri čemu se plastični otpad pokazao kao donor vodonika poboljšavanjem prinosa proizvoda KS. Osim toga, proizvodi od plastičnog otpada su pokazali značajnu premoć nad onima od KS, čineći oko 66,6 i 85,6 % u odnosu 1:1 smeša KS/HDPE i KS/PS, redom. Ovo istraživanje pruža važne uvide u formiranje sintetičkih bio-ulja kroz dizajn hemijskog sastava i optimizaciju prinosa pirolize, što je posebno značajno zbog povećanog sadržaja kiseonika u proizvodima dobijenim pirolizom KS koji može povećati kiselost i korozivnu aktivnost bio-ulja.

Ključne reči: Plastični otpad; polietilen velike gustine; polistiren; gasna hromatografija-masena spektrometrija; sintetička bio-ulja; održivi razvoj